Analysis of Production Process of Fine Dry Ice Particles and Application for Surface Cleaning

Yi-Hung Liu

2012

Contents

List of Symbols **iv**

Chapter 1 **1**

General Introduction **1**

1.1 Introductory remarks 1

1.2 Manufacturing of dry ice and its thermodynamics 2

1.3 Industrial surface cleaning 4

1.3.1 Wet cleaning 4

1.3.2 Dry cleaning 6

1.4 Dry ice blasting 8

1.5 Nozzle design and system characterization for dry ice blasting 9

1.5.1 Particle size control in the dry ice blasting device 9

1.5.2 Additional functions in dry ice blasting device 11

1.6 Removal mechanisms in dry ice blasting 12

1.6.1 Removal mechanisms for particulate contaminants 13

1.6.2 Removal of filmy contaminants 14

1.7 Objective of this work 17

Chapter 2 **20**

Agglomeration Process of Dry Ice Particles **20**

2.1 Introduction 20

2.2 Experimental apparatus and procedures 21

2.3 Results and discussion 23

2.3.1 Effect of temperature of jet flow on producing dry ice particles 23

2.3.1.1 Experiment using expansion nozzle 23

2.3.1.2 Experiment using expansion nozzle with glass tube 23

2.3.2 Effect of glass tube size 26

2.3.3 Interparticle collisions on the agglomeration of dry ice particles in the

glass tube 32
2.3.4 Effect of particle deposition and reentrainment on the agglomeration of dry ice particles in the glass tube 35
2.4 Conclusions 39

Chapter 3 40

Size Measurement of Dry Ice Particles by Laser Diffraction 40

3.1 Introduction 40
3.2 Experimental apparatus and procedures 40
3.3 Results and discussion 43
3.3.1 Effect of nozzle diameter on production of dry ice particles 43
3.3.2 Agglomeration of dry ice particles in the ABS tubes 50
3.3.3 Effect of interparticle collision on agglomeration 54
3.3.4 Flow velocity in a tube 56
3.3.5 Distribution of particles in the jet flow 57
3.4 Conclusions 60

Chapter 4 62

Effect of Particle Impact on Surface Cleaning Using Dry Ice Jet 62

4.1 Introduction 62
4.1.1 Dry ice blasting for removing fine particles 62
4.1.2 Theoretical particle removal model 62
4.2 Experimental apparatus and procedure 65
4.3 Results and discussion 68
4.3.1 Local pressure on surface 68
4.3.2 Effective cleaning area 68
4.3.3 Time-dependent particle removal efficiency 70
4.3.4 Temperature of the dry ice jet 74
4.3.5 Particle removal rate 77
4.3.6 Effect of the impact of dry ice particles on particulate contaminant

removal 79
4.4 Conclusions 86

Chapter 5 87
Particle Removal Process during Impinging Dry Ice Jet Application 87
5.1 Introduction 87
5.2 Material and methods 88
5.2.1 Deposition of particulate contaminants 88
5.2.2 Removal of particulate contaminants 88
5.2.3 Analysis method 91
5.3 Results and discussion 91
5.3.1 Visualization of the particle impact caused by the dry ice jet 91
5.3.2 Particle removal efficiency 92
5.3.3 Theoretical analysis for slow removal stage 96
5.3.4 Temperature dependence of dry ice jet 97
5.3.5 Removal area and frequency at rapid removal stage 102
5.3.6 Evaluation of particle removal by dry ice jets 105
5.4 Conclusions 109

Chapter 6 110
General Conclusions 110

Appendix 114

References 116

Acknowledgements 125

List of Publications 127

List of Symbols

a_s	contact radius at separation	[m]
C_c	Cunningham slip correction factor	[–]
D	reduced particle diameter ($=D_{p1}\,D_{p2}\,/\,(D_{p1}+D_{p2})$)	[m]
D_{p1}	diameter of dry ice particle	[m]
D_{p2}	diameter of particulate contaminant	[m]
E	Young's modulus	[Pa]
F_a	adhesion force	[N]
F_c	impact force	[N]
F_d	drag force	[N]
f	dimensionless coefficient of force	[–]
g	dimensionless coefficient of moment	[–]
k_{12}	elastic characteristic $(=(1-\nu_1^2)/E_1+(1-\nu_2^2)/E_2)$	[Pa^{-1}]
k_{23}	elastic characteristic $(=(1-\nu_2^2)/E_2+(1-\nu_3^2)/E_3)$	[Pa^{-1}]
M_a	moment caused by adhesion force	[N m]
M_c	moment caused by impact force	[N m]
M_d	moment caused by drag force	[N m]
M_t	moment about center of mass of particulate contaminant	[N m]
m	reduced mass $(= m_1\,m_2\,/\,(m_1+m_2))$	[kg]
m_1	mass of dry ice particle	[kg]
m_2	mass of particulate contaminant	[kg]
N_0	initial number of particulate contaminants	[m^{-2}]
N_r	number of residual particulate contaminants	[m^{-2}]
Re_{p2}	particle Reynolds number	[–]
r^*	moment ratio of impact force to drag force	[–]
u	fluid velocity pointing to the center of a particulate contaminant	[m s^{-1}]
u_0	core velocity of dry ice jet	[m s^{-1}]
v	impact velocity	[m s^{-1}]
W_{23}	surface energy per unit area	[J m^{-2}]
x	horizontal position on the test plate surface	[m]

Greek Letters

γ	solid-to-gas mass flow ratio	[–]
η	particle removal efficiency	[–]
θ	contact angle of the particulate contaminant adhering to surface	[rad]
λ	mean free path of gaseous CO_2	[m]
μ	fluid viscosity	[Pa s]
ν	Poisson's ratio	[–]
ρ	density of fluid	[kg m^{-3}]
ρ_1	density of dry ice	[kg m^{-3}]
ρ_2	density of polystyrene	[kg m^{-3}]
ϕ	impact angle	[rad]

Subscripts

1	particle (dry ice)
2	particulate contaminant adhering to wall (polystyrene)
3	wall (glass)

Chapter 1
General Introduction

1.1 Introductory remarks

Dry ice is a well known material that can be applied in many industrial fields. The most common usage of dry ice is refrigeration of foods, beverages, and laboratory biological samples. Oxidation or other reactions of the organic compounds can also be prevented during refrigeration because CO_2 is chemically stable. To continuously use its refrigeration effect, a cyclic refrigeration system using CO_2 as a working fluid has been demonstrated [Lorentzen and Petterson, 1993; Liao and Zhao, 2002; Kim *et al.*, 2004; Zhang and Yamaguchi, 2007, 2011; Yamaguchi *et al.*, 2008, 2009, 2011; Niu *et al.*, 2011]. This system is expected to replace the old one using CFC (Chlorofluorocarbon) fluids, which causes the ozone depletion problem. It is also considered a good way of relieving the greenhouse effect by recycling CO_2 and using it as a refrigerant, which can be regarded as a kind of CO_2 capture and storage.

Another application which attracts the attention of people in medical field is for drug granulation. Nanosized fine drug particles produced by rapid expansion of supercritical solution (RESS) [Matson *et al.*, 1989; Jung and Perrut, 2001] can be agglomerated by dry ice particles produced during the expansion process [Arieda *et al.*, 2006; Sonoda *et al.*, 2009; Watano, 2009]. The particle diameter, particle size distribution, porosity, and sphericity of the drug agglomerates can be controlled by the state of the produced dry ice to improve drug delivery and processing.

These specific features of dry ice, such as sublimation and soft property, enable dry ice to overcome many industrial cleaning problems. Contaminants can be removed by the blasting method using dry ice as abrasive blast media (dry ice blasting). Since dry ice will eventually sublimate after dry ice blasting, the problem of secondary contamination, i.e. the contamination caused by the abrasive media, can be avoided.

Among these applications, the size, structure, and concentration of dry ice particles are thought to be important because these physical properties will have a great influence

on its application. For example, higher concentrations of dry ice particles with sufficient inertia are more effective to remove contaminants. Therefore, a fundamental study on the physical properties of dry ice particles, particularly the behaviors in a jet flow is necessary for the control and optimization of dry ice application systems.

1.2 Manufacturing of dry ice and its thermodynamics

Dry ice is the solid state of CO_2 with density in the range of 1400 to 1600 kg m^{-3}, and it cannot permanently exist at room conditions, i.e. 1 atm and 25 °C. Figure 1.1 shows the phase diagram of CO_2. When the conditions are below the triple point (−56.4 °C, and 5.13 atm), CO_2 changes from a solid to a gas without intervening liquid state; this process is known as sublimation. On the other hand, the process where CO_2 changes from the gas to solid state is called deposition. These features are particularly different from most of other materials whose gas state intervening liquid state before changing into solid state. This phase change, i.e. sublimation or deposition will occur at −78.5 °C at 1 atm, enabling its application of gas–solid two phase flow for many industrial purposes. Since dry ice exists only at low temperature, it can be applied as a kind of cryogenic particles.

In addition, CO_2 is generally stored as liquid state in the cylinder for easy transport in the industry. Therefore, the generation and manufacturing of dry ice is basically from the liquid CO_2. Dry ice production efficiency will depend on the process where CO_2 changes from liquid state to solid state.

Dry ice can be produced by rapidly expanding liquid CO_2 through a nozzle based on the Joule-Thomson effect. The Joule-Thomson process is a constant–enthalpy process. In this process, the pressure will rapidly decrease and cause the vaporization of some liquid CO_2. Accordingly, rapid reduction of temperature occurs, resulting in the solidification of the remaining liquid CO_2. The CO_2 gas–solid two phase flow is therefore produced by the expansion. Dry ice snow, the expanded CO_2 two phase flow, can be further compressed and extruded to form dry ice pellets or nuggets. The percentage of dry ice snow produced can be obtained according to the

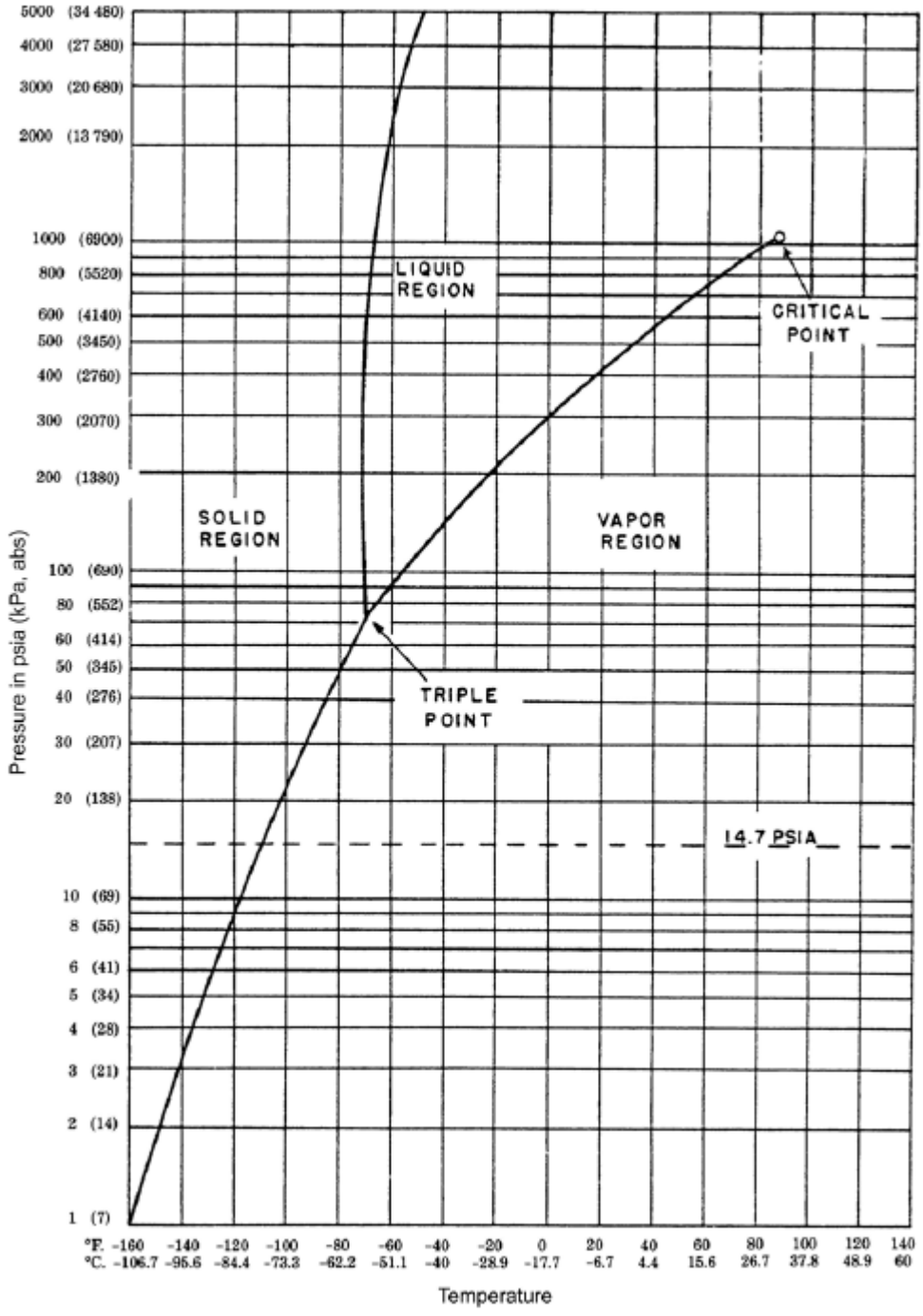

Figure 1.1 Pressure–temperature phase diagram of CO_2

(from Asia Industrial Gases Association, 2009).

pressure–enthalpy phase diagram of CO_2, as shown in Fig. 1.2. In general, the pressure of the cylinder filled with liquid CO_2 is about 6.5 Mpa at 25 ℃, which is indicated at point A in Fig.1.2 b. When expanding the liquid CO_2 through the nozzle under insulation, the pressure will considerably decrease without enthalpy change to point B, where CO_2 presents in equilibrium of gas and solid state. The percentage of dry ice snow can therefore be determined according to the final state of CO_2 at point B. In other words, the percentage varies with the initial state of the liquid CO_2 or the manner of the expansion. For example, the percentage of dry ice snow will be smaller through an expansion process using a non–adiabatic nozzle, i.e. the final state will be on the right of point B in the solid–gas region. The expansion nozzle design is therefore considered an important issue to achieve efficient dry ice snow production.

1.3 Industrial surface cleaning

In industrial manufacturing, surface cleaning is imperative because contaminants on the surfaces of products lead to low production quality and yields; for example, defects in electronic devices are generally caused by fine particles that are deposited during the manufacturing process. However, surface cleaning is not easy in the case of fine particles because the adhesion force tends to be larger than the separation force, therefore making their removal difficult. Nevertheless, today's technical innovations are rapidly progressing, and the development of high–efficiency cleaning methods is accelerated to meet the requirements of pioneering industries; in addition, such cleaning methods must also satisfy the increasing environmental concerns related to industrial processes.

1.3.1 Wet cleaning

Cleaning methods can be primarily divided into two categories—wet cleaning employs liquid media and dry cleaning employs gaseous media. Wet cleaning has good cleaning performance and is popular in industries. Wet cleaning technology has been extensively studied for the surface cleaning of wafer. Solutions composed of alkaline

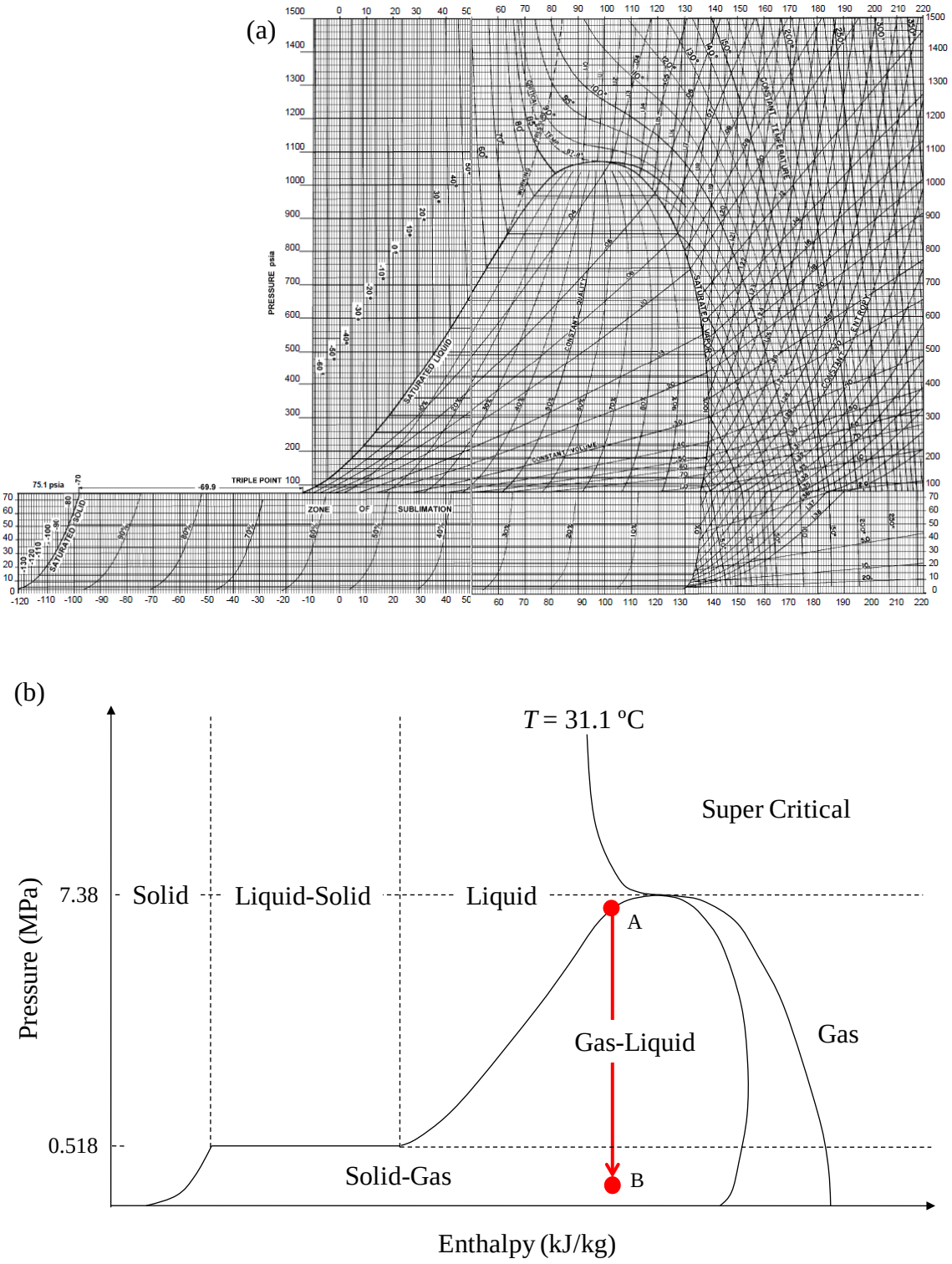

Figure 1.2 Pressure–enthalpy phase diagram of CO_2

((a) is from Asia Industrial Gases Association, 2009).

and acidic hydrogen peroxide are used in a process known as “RCA Standard Clean” to remove surface contaminants based on reaction chemistry [Kern, 1990]. The mechanisms for the chemical wet cleaning methods were reported as well [Niida *et al.*, 1989; Itano *et al.*, 1993; Qin and Li, 2003]. For removing fine particles, several physical wet cleaning technologies have been developed: for example, Brush scrubbing [Hymes and Malik, 1996], high pressure fluid jets [Kuo and Matijevic, 1980; Kally and Matijevic, 1981; Yamamoto *et al.*, 1994], and ultrasonic/megasonic techniques [Itano *et al.*, 1995; Shwartzman *et al.*, 1985; Menon *et al.*, 1989; Ohmi, 1996; Busnaina and Dai, 1997]. However, drying processes are required after the wet cleaning and water processing is unavoidable before discharging or recycling wastewater, thereby increasing the energy and cost consumptions. Hence, alternative effectively, environment-friendly, and economical cleaning methods need to be established.

1.3.2 Dry cleaning

Dry cleaning was developed to avoid excessive usage of water and the environmentally harmful chemical additives such as acids in cleaning. Many studies on dry cleaning have been reported and several dry cleaning techniques are categorized in Table 1.1.

Among these dry cleaning methods, air jet cleaning is the easiest one to access because the equipments and procedures are relatively simple. Many studies on particle removal by employing the aerodynamic effect have been previously reported. Further, in order to explain the time course of particle removal efficiency, Masuda et al. [1994] proposed a model that assumed that the removal flux is proportional to the number of particles whose adhesion force is smaller than the separation force. Otani et al. [1993, 1995] showed that consecutive pulse air jets are effective for particle removal. The removal efficiency was analyzed by taking into account the ratio of drag force to adhesion. Gotoh et al. [1994a, 1994b, 1995] discussed the effects of surface material, contaminant particle sizes, and relative humidity on the removal efficiency. To improve the removal efficiency, electrostatic pre-charging and vibrating air jets were also investigated [Gotoh *et al.*, 1996]. In addition to the above cleaning systems,

Table 1.1 Typical dry cleaning methods.

Cleaning method	Cleaning Objects	Mechanism	Reference
Thermal enhanced cleaning	Organics, metals, particles	Chemical reaction between high energy gas and contaminants	Busnaina and Dai [1997]; Ghidini and Smith [1984]; Donahue and Reif [1985]; Meyerson *et al.* [1986]; Moslehi and Davis [1990]; Silvestri *et al.* [1990]
Vapor–gas cleaning	Organics, metals, particles	Chemical reaction between reactive gas and contaminants	Sanganeria *et al.* [1994]; Cleavelin [1987]; Wong *et al.* [1991]
Plasma cleaning	Organics, metals, particles	Chemical reaction between free radical and contaminants	Mcintosh *et al.* [1992]; Rudder *et al.* [1986]; Zhou *et al.* [1993]
Photochemi-cally enhanced cleaning	Organics, metals, particles	Chemical reaction between free radical and contaminants (free radicals are caused by irradiation of UV light to gas)	Lao *et al.* [1997]; Tabe [1984]; Norström *et al.* [1985]; Ruzyllo *et al.* [1987]; Ishikawa *et al.* [1989]; Kasi and Liehr [1990]
Laser–assist ed cleaning	Particles	Thermal expansion of surfaces or contaminants by laser energy transfer	Lippert *et al.* [1995]; Magee and Leung [1991]; Tam *et al.* [1992]; Lee *et al.* [1993]; Kelly and Hovis [1993]; Allen [1991]; Imen *et al.* [1991]; Lee *et al.* [1992]
Air jet cleaning	Particles	Aerodynamic force	Heloux *et al.* [1996]; Masuda *et al.* [1994]; Otani *et al.* [1995]; Gotoh *et al.* [1996]; Smedley *et al.* [1999a, 1999b]; Phares *et al.* [2000]
Cryogenic aerosol cleaning	Organics, particles	Aerodynamic and impact force	Smedley *et al.* [2001]; Yoon *et al.* [1999]; Narayanswami [1999]; Banerjee and Campbell [2005]; Dangwal and Müller [2007]; Hoenig [1986]; Hills [1995]; Jackson and Carver [1999]; Sherman and Whitlock [1990]; Sherman *et al.* [1991]; Sherman *et al.* [1994]; Sherman [2007]; Toscano and Ahmadi [2003]; Layden and Wadlow [1990]; Yang *et al.* [2007]; Spur et al. [1999]

Smedley *et al.* [1999a, 2001] slowly translated a sample under a steady jet to avoid the transient effects associated with jet startup. The translating gas jet produces a long clean path that provides very good statistics for exploring the effect of jet parameters. Smedley *et al.*, [1999b] also performed experiments using impinging shock waves, which effectively cleaned a large surface area.

1.4 Dry ice blasting

In order to improve the cleaning effect, fine particles are added into the gas jet to act as abrasive media; this process is known as abrasive blasting. Metal, oxide, as well as organic compounds can be used as the abrasive media. However, the hard abrasive media will cause damage after impact on the friable surface of the cleaning object. It should be avoided, particularly, for the precise cleaning. Hoenig [1986] demonstrated that a cleaning system using the flow of a soft material over the surface is required to remove smaller particles. Carbon dioxide is the most suitable soft material because it is available under exceptionally clean conditions and is less costly and toxic.

A jet flow containing dry ice particles can be produced by two kinds of methods. One method is to supply pre-made dry ice particles in an individual production process; then add them to the compressed air stream. The mixed flow can be further accelerated with a nozzle. The other method is to directly expand liquid carbon dioxide through a nozzle. The latter one is simpler and more convenient to access; thus, it is generally adopted for industrial application. When cleaning a surface, the aerodynamic drag forces are generally weak in the stagnant regions in impinging jet flows and the particles adhering to the surface cannot be removed easily. However, they can be effectively removed by the collision of dry ice particles since it provides sufficient momentum transfer. Dry ice blasting, i.e. the gas–solid two phase jet flows of gaseous carbon dioxide and dry ice particles, is capable of the removal of particulate contaminants and organic residues [Hoenig, 1986]. Since dry ice particles will eventually sublimate into carbon dioxide gas after impact, there is no deposition of the dry ice particles; however, impurities in the carbon dioxide should be taken into consideration [Sherman *et al.*,

1994; Sherman, 2007]. To evaluate the cleaning effect of dry ice blasting, the pumpdown curves showing the relationship between pressure and time, have been used for cleaning the vacuum components. [Layden and Wadlow, 1990]. Comparisons between the initial number density of the particles adhering to the surface and the number density of the residue particles after cleaning were usually employed to directly evaluate the cleaning effect for particulate contaminants. Dangwal *et al.* [2007] utilized field emission scanning microscopy (FESM) combined with high–resolution secondary electron microscopy (SEM) and energy dispersive x–ray analysis (EDX) for studying the field emission properties of Cu and Nb surfaces after dry ice blasting.

To evaluate the cleaning effect for organic contaminants, X-ray photoelectron spectroscopy [Sherman *et al.*, 1994; Sherman, 2007], and infrared spectroscopy [Hills, 1995] have been employed to analyze the composition of organic contaminants before and after cleaning. Hills showed that the removal efficiency of filmy organic contaminants strongly depends on the solubility of the organic film in liquid CO_2.

Recently, the dry ice blasting has also been introduced into atmospheric plasma spraying and shown to be effective for improving the properties of metallic, alloy and ceramic coatings [Dong *et al.*, 2011]. Unlike most studies focusing on the cleaning effect of consecutive dry ice blasting, Yang *et al.* [2007] demonstrated the optimization of a pulsed dry ice blasting system for the removal of particles on the surface of complementary metal oxide semiconductor (CMOS) image sensors by using the Taguchi method, a statistical method for optimal system design. As a result, less CO_2 consumption in the dry ice blasting system can be achieved. In this optimization, the physical properties of liquid CO_2 were not taken into consideration; however, Sherman [2007] mentioned that the input pressure of liquid CO_2 source may affect the cleaning result.

1.5 Nozzle design and system characterization for dry ice blasting

1.5.1 Particle size control in the dry ice blasting device

As described in Section1.1, the size and concentration of dry ice particles will have a great influence on the application. The formation of dry ice particles depends on temperature, pressure and the jet flow conditions. These factors are related to the design of the expansion instrument; thus the operation conditions must be precisely controlled to match the various application needs. The design of the expansion nozzle has been studied to effectively produce primary dry ice particles, Whitlock *et al.* [1989] proposed a special apparatus including a plurality of expansion nozzles where a coalescing chamber is connected between. The large droplets were thought to be the precursor of the minute dry ice particles; hence the coalescing chamber for producing large droplets before entering into the second orifice was important. Swain *et al*. [1992] expanded liquid CO_2 from an orifice into a thermally insulated chamber to form small dry ice particles and then retained the small particles in the chamber until the small particles agglomerated into large ones. In this process, formation of large dry ice particles is beneficial for cleaning a larger surface area per unit time than small dry ice particles. The large dry ice particles do not sublimate away as rapidly as small ones thereby surviving longer and removing more contaminants along a longer and wider path. Furthermore, each large, rapidly moving dry ice particles possesses more kinetic energy than small ones, and, therefore, more effectively removes contaminants clinging to the surface of substrates being cleaned.

However, as the cleaning object is very delicate, impact of large dry ice particles will damage the surface. To prevent the problem, Stratford [2003] proposed a dry ice blasting system which provides a useful, finely focused beam of dry ice particles whose size is less than 8.9 mm, with an order of magnitude less of air consumption and remarkably reduced noise. In addition, Broecker [2010] proposed a media blast nozzle comprising a media size changer to change a size of the dry ice particles for cleaning a surface. When the dry ice particles in an initial consistent size are introduced into the media blast nozzle, the particles impact with one or more media size changing members, creating more finer particles.

Momotsuka *et al.* [2005] found that the impact of fine dry ice particles can cool

down the cleaning objective, causing the decrease of adhesion between the contaminants and the surface due to the difference of coefficient of thermal expansion. On the other hand, the impact of large dry ice particles can directly remove the contaminants by their strong inertia. Basically, the ejection of the fine dry ice whose particle diameter is less than 5 μm together with the large dry ice whose particle diameter is between 0.3 and 1.0 mm can effectively clean contaminants with short cleaning time. As a concept of combing the two advantages, a particular ejection nozzle consists of an inner circular tube with a convergent-divergent orifice for ejecting the fine dry ice particles produced from the adiabatic expansion and a cylindrical annulus where large dry ice particles produced from the mechanical destruction of dry ice block flow through, was proposed.

1.5.2 Additional functions in dry ice blasting device

In addition to the specific nozzle design for controlling the dry ice particles, other issues related to the static charge and the bridging phenomenon have been focused by the group of Okazawa *et al.* [2002]. Their cleaning apparatus comprises an air supplying device and a charging device for supplying destaticizing air with a polarity opposite to the polarity of the charged dry ice pellets to the cleaning object to be cleaned by the blast nozzle. As a result of electrically neutralization, the redeposition of the contaminants blown off from the surface of the cleaning object due to the electrostatic force of charged dry ice pellets can be prevented. In addition, an agitating tool is installed in this apparatus to agitate the dry ice pellets reserved in the hopper. The bridging phenomenon that the dry ice pellets fuse with each other by sublimation of part of the dry ice pellets is therefore prevented.

Increasing the cleaning area of dry ice blasting is another important issue for the nozzle design. Taniguchi [2001] claimed that the jet flow can be extended through an additional cover installed after the nozzle outlet. The cover, with a hollow dimension, extends horizontally toward the flow direction and the cover outlet has a flat shape. Accordingly, the area of ejected dry ice particles from the cover outlet is increased; as a

result, the cleaning area is increased, enhancing the cleaning efficiency.

In some dry ice blasting systems, the carrier gas, such as compressed air or nitrogen is generally introduced for increasing the particle velocity of dry ice; thus, the cleaning effect can be enhanced by its strong impact. To expand the application of the carrier gas, Merritello [2008] introduced an ozonated dry ice jet by mixing the CO_2 source and the carrier gas formed by feeding an oxygen-containing gas to an ozone generator to removal surface contaminants. Therefore, the effect of chemical reaction between ozone and contaminants can be employed together with the physical cleaning effect of dry ice blasting, improving and expanding its applications. The dry ice blasting can be diversified by introducing other gas streams into the cleaning system; however, the introduced gas stream may affect the state of the dry ice particles in the jet flow. This should be taken into consideration as building up a specific dry ice blasting system.

1.6 Removal mechanisms in dry ice blasting

The contaminants adhering to the surface can be mainly divided into particulate and filmy contaminants. The removal mechanism for the particulate contaminants in dry ice blasting differs from the mechanism for the filmy contaminants. This is because the specific properties of dry ice, such as solid-state, low temperature, and sublimation diversify the removal mechanisms in the dry ice blasting. Jackson and Carver [1999] summarized several possible removal mechanisms of dry ice blasting as follows: (i) kinetic separation based on the momentum transfer from dry ice particles to contaminants, (ii) aerodynamic drag separation, (iii) chemical separation caused by the dissolution of residues into liquid carbon dioxide, and (iv) electrostatic separation caused by the movement of the contaminants combined with charged dry ice particles. The kinetic and aerodynamic drag separations are usually applied for explaining the removal of particulate contaminants; on the other hand, chemical separation caused by the dissolution is generally applied for explaining the removal of filmy contaminants composed of organic compound.

1.6.1 Removal mechanisms for particulate contaminants

In general, the particulate contaminant adhering to the surface will be removed once the separation force exceeds the adhesive force. In a flow region, the separation force is caused by the aerodynamic drag force of the fluid, and the adhesive force is mainly determined by the net force of the gravity force, van der Waals force, electrostatic force and liquid bridge force generated between the contaminant and the surface. The aerodynamic drag force F_d generated under a fluid of density ρ, with a flow velocity u can be expressed as:

$$F_d = C_d A_p \frac{\rho u^2}{2}, \tag{1.1}$$

where C_d is the drag coefficient and A_p is the project area of the particle along its movement direction. The value of C_d depends on the particle Reynolds number Re_p. C_d will be $24/Re_p$ when Re_p is much less than 2, namely under the Stokes region, while it will change to $10/(Re_p)^{0.5}$ under the Allen region for $2 \leq Re_p \leq 500$. As the blasting media is added into the flow, namely the solid–gas two phase flow, the impact force caused by the blasting media becomes important. The impact force F_c between two particles can be expressed as:

$$F_c = 1.12 k_{12}^{-2/5} m^{3/5} D^{1/5} v^{6/5}, \tag{1.2}$$

where, k_{12} is the elastic characteristic of two materials, m is the reduced mass ($=m_1 m_2/(m_1 + m_2)$), D is the reduced particle diameter ($=D_{p1} D_{p2}/(D_{p1} + D_{p2})$), and v is the impact velocity [Timoshenko and Goodier 1970]. Subscripts 1 and 2 used in the above equation mean the two particles made of different materials.

For removing micro-sized or submicron-sized particle, the gravity force is much smaller than the other adhesion force and thus can be neglected in most cases. van der Waals force F_v between a sphere of diameter D_p and the a flat plate at a separation distance h is represented as:

$$F_{\mathrm{v}} = -\frac{AD_{\mathrm{p}}}{12h^2}, \tag{1.3}$$

where A is the Hamaker constant varying with the material. If a particle is charged with surface charge density σ, then the electrostatic force F_{e} can be shown as:

$$F_{\mathrm{e}} = \frac{\pi\sigma^2 D_{\mathrm{p}}{}^2}{4\varepsilon_{\mathrm{r}}\varepsilon_0}, \tag{1.4}$$

where ε_{r} and ε_0 mean the relative permittivity and vacuum permittivity, respectively. When the humidity is high, the adhesion strength caused by the liquid bridge force should be taken into account. The liquid bridge force F_{l} generated by the liquid between the particle and the surface with surface tension of γ is represented as:

$$F_{\mathrm{l}} = 2\pi\gamma D_{\mathrm{p}}{}^2. \tag{1.5}$$

Many studies focused on the particle removal from the surface based on the above forces introduced and they are summarized in Table 1.2.

The rotational removal based on the balance of the moments of forces acting on the particulate contaminant and the slide removal based on the force balance, are usually applied to theoretically estimate the particle removal. As a conclusion of the studies introduced, the critical removal velocity for rotation removal is considerably lower than that necessary for slide removal. However, the slide removal can also be effective for the removal of irregular particles.

1.6.2 Removal of filmy contaminants

In the study of Hoenig [1986], it has been mentioned that the pressing of the dry ice snow against the contaminated surface will result in local melting of the dry ice and the formation of liquid CO_2. Since liquid CO_2 is known to be an excellent solvent for many

Table 1.2 Selected studies related to the particle removal from the surface.

Target object	Separation force	Focused model of removal	Reference
Colloid particles on a flat substrate	Aerodynamic lift force caused by turbulent burst	Unsteady sublayer model	Cleaver and Yates [1973]
Agglomerate of dust particles on a flat glass surface	Aerodynamic drag force	Bending stress model, shear stress model	Kousaka *et al.* [1980]
Single spherical particle on a surface	Elastic restoring force, mean aerodynamic lift force	RRH model based on energy balance	Reeks *et al.* [1988]
Latex particles on a surface	Aerodynamic drag force	Kinetic particle desorption model	Wen and Kasper [1989]
Single spherical particle on a rigid surface	Aerodynamic drag force, stored elastic force	Lift-off model, slide model, rotation model	Wang [1990]
Single spherical particle on a computer disk surface	Aerodynamic drag force	Critical-moment model	Tsai *et al.* [1991]
Monodispersed PSL and wax particles on a silicon wafer and a glass plate	Aerodynamic drag force (impulse jet flow)	rotation model	Otani *et al.* [1995]
Small agglomerate (Fly ash) on the surface of a powder layer	Aerodynamic drag force, turbulent burst	Bending stress model, shear stress model	Matsusaka and Masuda [1996]
Monodispersed spheres (ammonium fluorescein and polystyrene) on glass substrates	Aerodynamic drag force	Dynamic resuspension model based on crack propagation kinetics	Phares *et al.* [2000]
Agglomerate (alumina) on the surface of a metal plate (brass, copper, aluminum, stainless steel)	Aerodynamic drag force, impact force	Rotation model	Adhiwidjaja *et al.* [2000]
Alumina spheres and graphite particles on a polished stainless-steel flat plate	Aerodynamic lift force, drag force	RRH model based on energy balance, Rotation model	Reeks and Hall [2001]
Agglomerate (alumina) on the wall surface of a glass tube	Aerodynamic drag force, impact force, force caused by wall vibration	Rotation model	Theerachai-supakij *et al.* [2002]
Agglomerate (alumina) on the wall surface of a glass tube	Aerodynamic drag force, impact force	Rotation model	Theerachai-supakij *et al.* [2003]

Single spherical particle (silicon) on a silicon wafer substrate	Aerodynamic drag force, impact force, lift force	Slide model, rotation model	Toscano and Ahmadi [2003]
Single irregular particle (silicon nitride and alumina) on a silicon wafer substrate	Aerodynamic drag force, impact force	Slide model	Banerjee and Campbell [2005]
Single spherical particle (copper, glass, polystyrene, calcium carbonate, aluminum oxide) on a substrate (copper, glass, steel, polystyrene, calcium carbonate, aluminum oxide)	Aerodynamic drag force, lift force	Slide model, rotation model	Ahmadi *et al.* [2007]

organics, the dry ice can also be used for the removal of organic deposits. In addition to that, Sherman [1991] mentioned that the dry ice snow particles rebound off the surface after impacting, resolidify, and carry the dissolved organics with them. Moreover, Hills [1995] claimed that the removal of filmy contaminants mainly occurs in two steps. First, a portion of the film is removed physically by either thermal shock or abrasion caused by the dry ice blasting. Second, the residual film is removed by solvation into a transiently formed liquid CO_2 film. In particular, the initial physical removal mechanisms will be important for the removal of thick films with lower solubilities in liquid CO_2.

1.7 Objective of this work

As mentioned above, many applications of dry ice jet have been carried out and new techniques are still under developing. From the viewpoint of recycling and reusing CO_2, the potential of dry ice jet for industrial application purpose is greatly desired, especially for replacing conventional cleaning method. However, the fundamental knowledge about the formation of dry ice particles in the expanded jet flow is still not sufficient. Also, the investigation of its cleaning effect still stopped at the stage of comparing the final state with the initial state of the cleaning object without noticing the dynamic phenomena during the cleaning process. Unlike other particles, the state of dry ice particles changes with time at room conditions; therefore, the dynamic analysis of the particle production and is significant

The present study aims to utilize in-situ observations and measurements 1) to clarify the particle growth, agglomeration, and sublimation occurring in the dry ice jet produced from liquid CO_2; 2) to evaluate the impact effect of dry ice particles and elucidate the removal mechanism in dry ice blasting for removing particles adhering to the surface. The nonsteady-state (dynamic) processes of the dry ice particle production and the dry ice blasting for particle removal are particularly focused to make clear each physical phenomenon about dry ice particles in detail.

This thesis consists of six chapters. In Chapter 1, the general introduction including

the research background, motivation and purpose is presented, following a basic understanding of dry ice properties.

In Chapter 2, the in-situ microscopic observations of dry ice jet were carried out to understand the formation of dry ice particles and their agglomeration process, by varying the flow types of dry ice jet. A tube attached to the expansion nozzle was used as an agglomeration chamber. The temperature of dry ice jet was also measured as a reference data to predict the state of dry ice particles. Through the discussion on the particle size and particle velocity of dry ice, the contribution of interparticle collisions on the agglomeration process is almost negligible; instead, the phenomenon of particle deposition and reentrainment. In example, primary particles are deposited on the tube wall and form a deposition layer; then, agglomerates are reentrained from the layer into the jet flow dominates.

In Chapter 3, an in-situ size measurement based on the laser diffraction method was applied for dry ice particles flowing in the jet flow. The size distributions of primary dry ice particles and their agglomerates were obtained to explain the phenomena of particle growth, agglomeration, and sublimation occurring in the jet flow. From the relationship between the median particle diameter of agglomerates and its corresponding flow velocity, dominance of particle deposition and reentrainment in the agglomeration process was quantitatively verified. The profiles of particle size and attenuation as a function of radial distance changed with the flowing distance, providing the information of the effective work distance for applying dry ice jet.

In Chapter 4, the removal of monosized particulate contaminants adhering to a surface was investigated using a dry ice blasting system. The removal of the contaminants was observed in-situ using a high speed microscope camera and the time course of removal efficiency was obtained from the digital image analysis. A relationship between the removal efficiency and the jet temperature was ascertained. This can be used to explain the difference in the profiles of removal efficiency between the micro-sized and submicron-sized contaminants. In addition, a theoretical analysis of the moments of the forces caused by particle impact and aerodynamic drag showed that

particle impact is particularly responsible for the removal of submicron-sized contaminants.

In Chapter 5, the particle removal efficiency, removal area, and frequency were focused to make clear the particle removal process of multi-dispersed fine particles covering a surface by using dry ice blasting. Two removal processes caused by the impacts of primary dry ice particles together with aerodynamic drag and dry ice agglomerates were found according to the analysis on the jet temperature. The effects of the jet flow rate on the removal areas and frequency were studied and a system parameter was proposed to determine the optimum jet flow rate for the efficient particle removal.

In Chapter 6, the conclusions of the study were summarized in detail. In addition, the perspectives for extending the investigations of dry ice jet on surface cleaning were given.

Chapter 2
Agglomeration Process of Dry Ice Particles

2.1 Introduction

Dry ice jet can be produced from the expansion of liquid CO_2 based on the Joule-Thomson effect, as mentioned in Chapter 1. Dry ice jet can be applied as a kind of dry cleaning method to remove surface contaminants; this concept was firstly proposed by Hoenig [1986]. In the dry ice blasting system, the produced dry ice particles can penetrate through the boundary layer to reach the contaminants and their mechanical impact can remove the fine particles strongly adhering to the surfaces. Conventional air jet uses aerodynamic drag to remove contaminants, whereas dry ice jet uses both mechanic impact of dry ice particles and aerodynamic drag to remove contaminants, the combination of the two mechanisms substantially enhance removal efficiency. The particle size of dry ice is an important factor that greatly affects the contaminant removal efficiency. Large dry ice particles with strong inertia and kinetic energies are therefore in favor of removing fine particles with strong adhesive force. In addition, large dry ice particles do not sublimate as rapidly as small ones; thus the large particles can last longer and impact on more contaminants. However, large dry ice particles may be limited to remove fine particles due to a geometry restriction [Toscano and Ahmadi, 2003]. Other than for cleaning applications, the particle size of dry ice has great influence on its refrigeration effect or pharmaceutical granulation effect. Small dry ice particles under several micrometer in diameter is generally called dry ice snow and can be agglomerated to big ones which are known as dry ice pellet or dry ice block. A nozzle comprising two coalescing chambers was designed to effectively produce the dry ice particles for removing fine particles [Whitlock et al. 1989]. Further, Swain et al. [1992] installed a thermally insulated chamber at the end of an expansion nozzle to produce agglomerates, improving the production efficiency of dry ice particles. However, the production, size and state of the dry ice particles, and the agglomeration process have not been studied in detail.

In this chapter, the production of dry ice particles by expanding liquid CO_2, and their agglomeration process in a tube chamber have been studied experimentally. The jet temperature, which has great influence on the state of dry ice, is investigated. To confirm the state of dry ice produced, its particle velocity and size are analyzed through microscopic observation under different experimental conditions. The agglomeration process of the dry ice particles is discussed through the particle deposition and reentrainment theory, i.e. primary particles are deposited on the tube wall to form a deposition layer; then, agglomerates are reentrained from the layer into the jet flow, as well as interparticle collision theory.

2.2 Experimental apparatus and procedures

Dry ice particles were produced from liquid carbon dioxide with purity of 99.5%. A flexible thermally insulated hose, 2 m long and 15 mm in inner diameter, was connected to a carbon dioxide cylinder and an expansion nozzle was installed at the end of the hose, as shown in Fig. 2.1. In order to change the conditions of the expanded flow, a glass tube was placed at the outlet of the expansion nozzle. The primary pressure of the carbon dioxide was measured at the entrance of the expansion nozzle.

Figure 2.2 shows the details of the test section, which consists of the expansion nozzle and the glass tube. The expansion nozzle has an inner diameter of 0.2 mm and a length of 6 mm, while the glass tube was 2, 4, or 6 mm in inner diameter and 50 mm in length (L), and was installed onto the outlet of the nozzle. The temperatures of the dry ice jet ejecting from the expansion nozzle and of the glass tube wall were measured by a K-type thermocouple connected to a temperature recorder (NR-1000, KEYENCE Corp.). A high speed camera (Fastcam-Max, Photron Ltd.) with a zoom lens was used to observe the state of agglomerated dry ice particles in the jet flow.

To investigate the formation of a deposition layer of dry ice particles, a glass plate instead of the glass tube was placed at the outlet of the expansion nozzle. The structures of the dry ice particles deposited on the plate were observed by an optical microscope (DS-3040L, Olympus Corp.). All the experiments were conducted under room

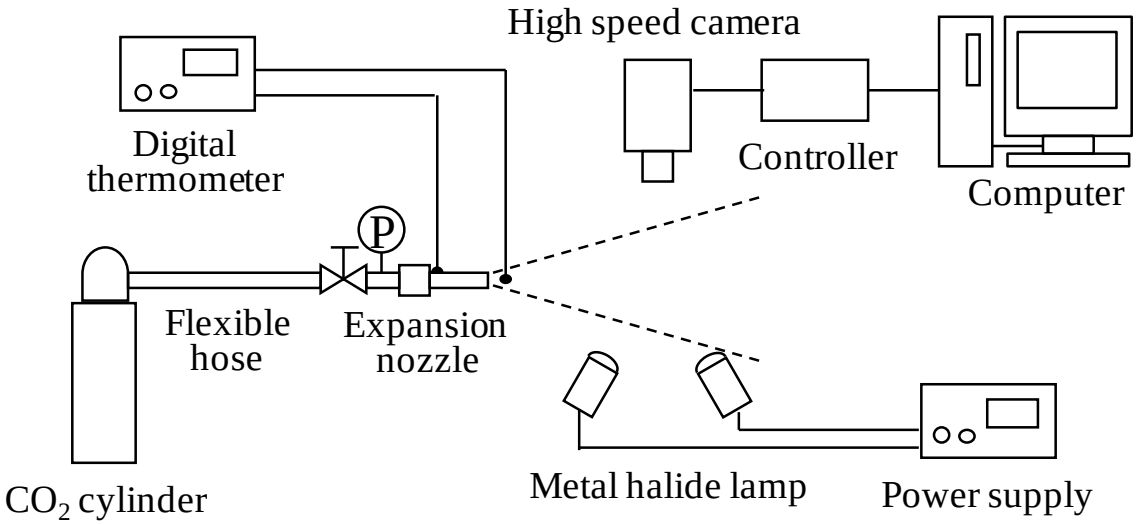

Figure 2.1 Schematic diagram of experimental apparatus.

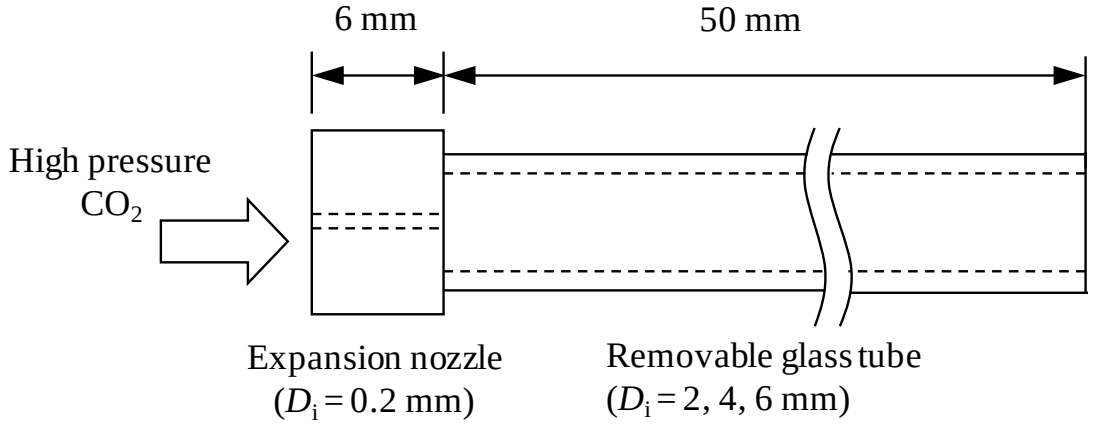

Figure 2.2 Test section.

temperature and pressure (25 ± 2 ºC; 1 atm).

2.3 Results and discussion

2.3.1 Effect of temperature of jet flow on producing dry ice particles

2.3.1.1 Experiment using expansion nozzle

Carbon dioxide was expanded from the nozzle at a primary pressure of 6.5 ± 0.2 MPa to atmospheric pressure. The expanded gas flow was cooled by rapid expansion. Figure 2.3 shows the temperature measured at the center of the expanded flow along the flow axis. The measurement position x is the distance from the nozzle outlet. The temperature measured at x = 1 mm was about −80 °C; however, it increased to −10 °C at x = 50 mm and closed to room temperature at x > 100 mm. The temperature of the flow increased sharply after ejecting from the expansion nozzle. According to a phase diagram of carbon dioxide, dry ice could be formed at −78.5 °C and 1 atm, which indicates that most of dry ice produced from the expansion nozzle sublimate to the atmosphere due to the temperature increase. Consequently, dry ice particles were not observed visually.

2.3.1.2 Experiment using expansion nozzle with glass tube

In order to avoid the direct contact of the expanded flow and the surrounding air, a glass tube was installed at the outlet of the nozzle, and an experiment was carried out under the same conditions as above. The dry ice particles were observed visually in the jet flow from the glass tube. Figure 2.4 shows the temperature variation of the outer tube wall as a function of time elapsed. The room temperature was 25 °C. For x = 5 mm (Fig. 2.4 a), the temperature decreased and approached about −30 °C after 300 s had elapsed. As for x = 48 mm (Fig. 2.4 b), the decrease of the temperature was relatively slow, and the stable temperature after 300 s was slightly higher than that for x = 5 mm, due to the heat transfer between the jet flow and the surrounding air through the tube

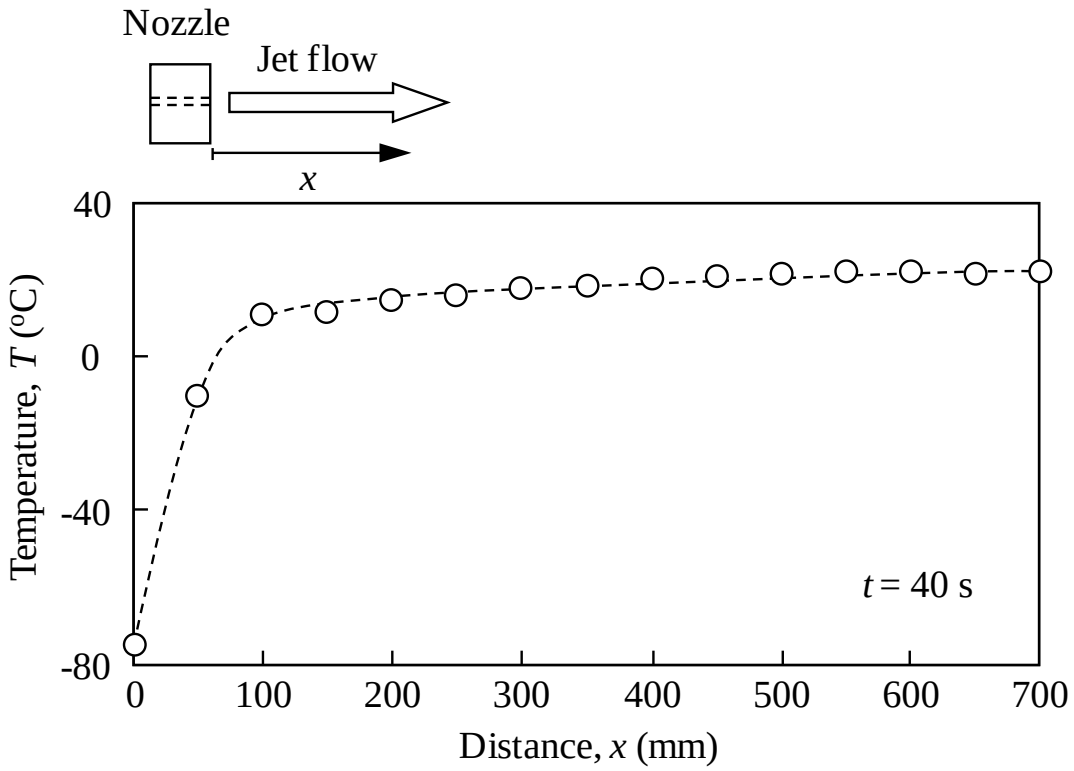

Figure 2.3 Temperature variation with distance from expansion nozzle.

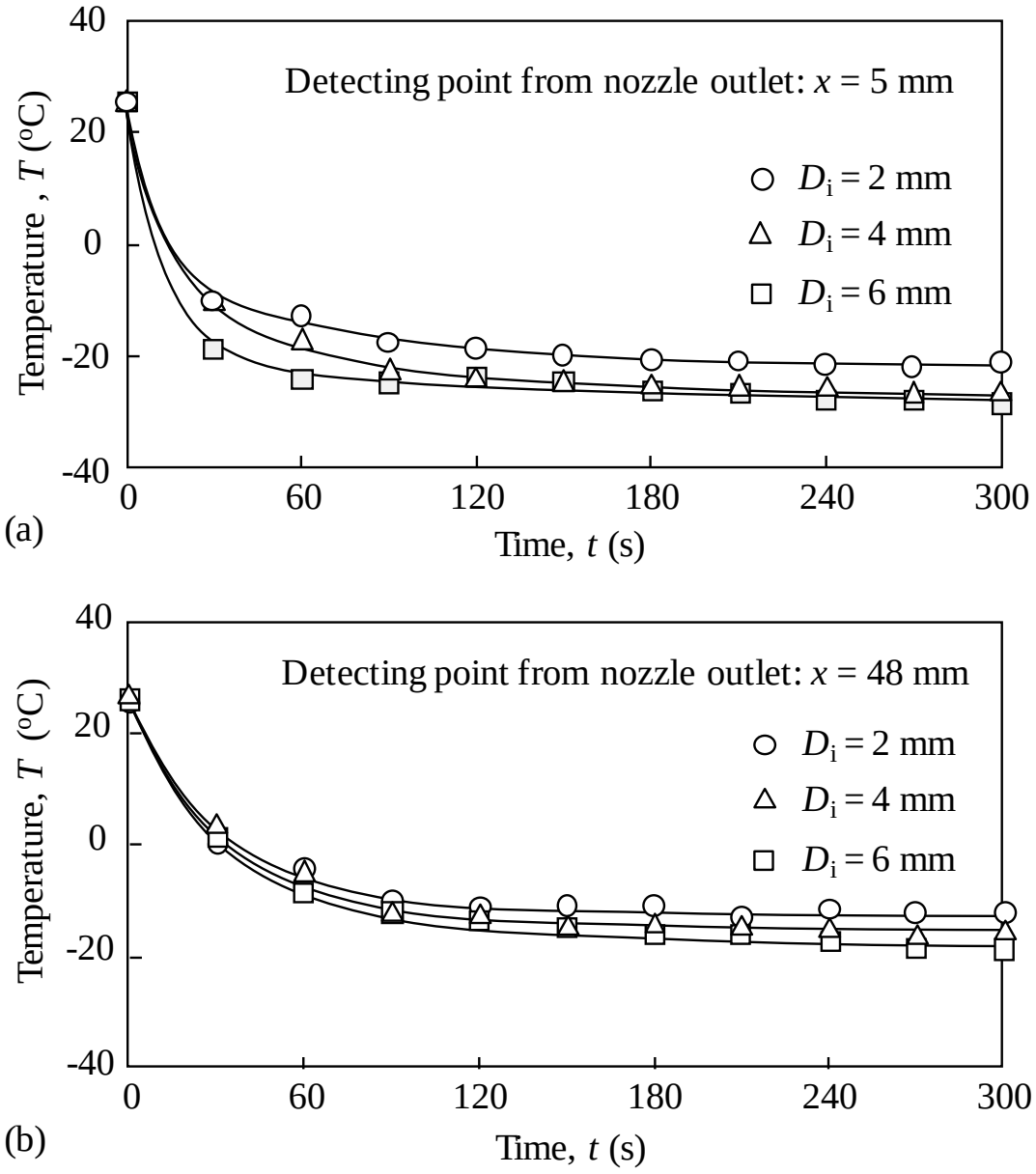

Figure 2.4 Temperature variation of outer tube wall.

wall. It is worth noting that the temperature at x = 48 mm was still kept at sub-zero temperature, i.e. the thermal insulation of the tube wall was effective; thus the sublimation of the dry ice particles produced by expanding liquid carbon dioxide was reduced. As a result, the dry ice particles were observed visually in the jet flow from the glass tube. In this experiment, glass tubes with different diameters were also used. Although there were small differences in the results, the temperature variations were almost the same as each other. Next, the time course of the temperature in the jet flow was measured. As shown in Fig. 2.5, the temperature decreased from room temperature as time elapsed and approached a stable temperature of -55 ± 5 °C, and then began to decrease further. The secondary stable temperature was -65 °C, i.e. there were two stages of temperature decrease in the jet flow. After the secondary temperature decrease, dry ice particles were observed visually in the jet flow from the glass tube, as shown in the image (c). Thus, the secondary temperature decrease is very important in the occurrence of this phenomenon. Dry ice particles ejected from the nozzle are thought to sublimate initially to cool down the tube. As the temperature of the tube decreases, the rate of heat exchange decreases and the jet temperature approaches to be stable. Once the visualized dry ice particles appear and contact with the thermocouple, the jet temperate decreases again.

For larger size glass tubes, the temperature was higher in the first stage, and the difference of the stable temperature between 2 mm and 6 mm in inner diameter was about 10 °C. Since larger glass tubes have a larger surface area; thus, the heat transfer through the tube wall is enhanced. Consequently, the stable temperature in the first stage is higher. Further discussion is mentioned in Section 2.3.4.

2.3.2 Effect of glass tube size

Since the temperature measurement implies that the glass tube size affects the state of the jet flow, we studied the formation and behavior of the dry ice particles produced in the flow using a high speed camera with a zoom lens. Figure 2.6 shows some typical images of the dry ice particles produced in the jet flow from the glass tube. Since the

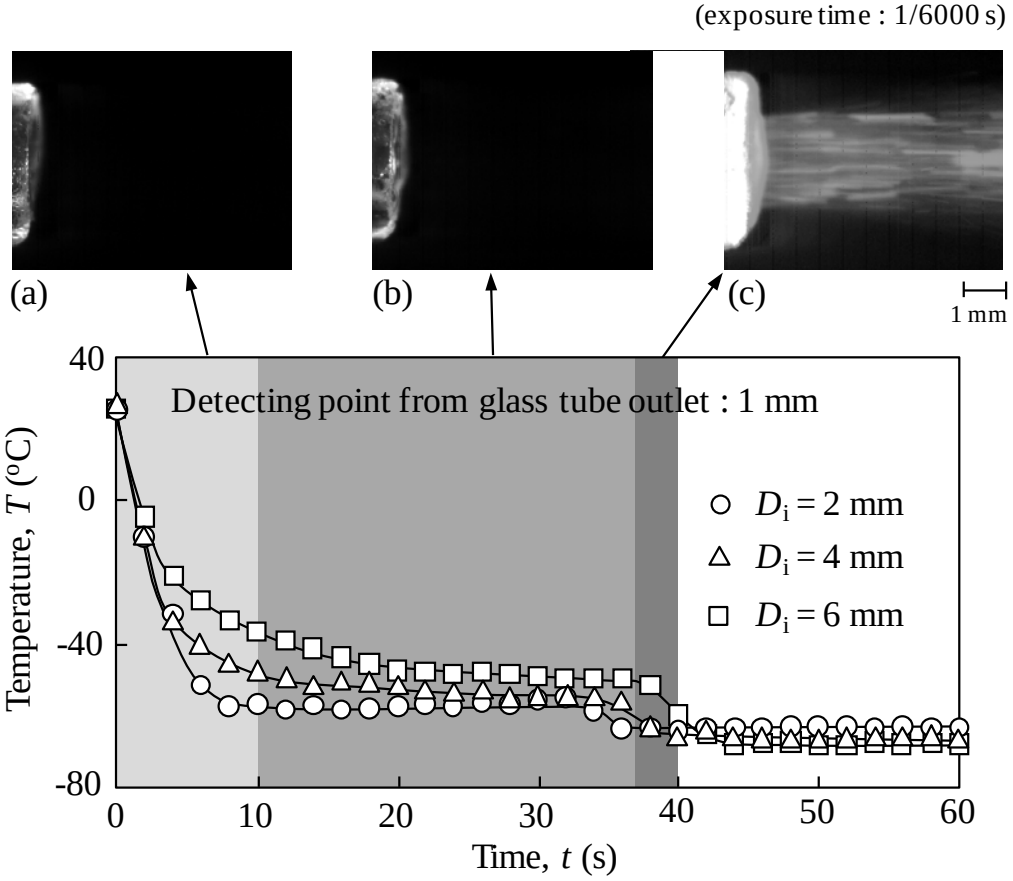

Figure 2.5 Temperature variation of dry ice jet.

exposure time in these images is known (1/6000 s), particle velocity can be calculated from the length of the trajectories of the dry ice particles. The velocity of the dry ice particles decreased and the size increased with increasing tube diameter. For larger dry ice particles (Fig. 2.6 c), the particles are more irregular in shape and seems to be agglomerated.

The particle velocity distributions are shown in Fig. 2.7 a. The data seem to be symmetrical distributions; as a trial, they are plotted on a normal graph. As shown in Fig. 2.7 b. each distribution is in a line; thus they are expressed as normal distributions. The median values for D_i = 2, 4, and 6 mm are 13.8, 6.9, and 3.4 m/s, respectively. The standard deviations for each tube diameter (from small to large) are 1.8, 1.7, and 1.4 m/s, and the coefficients of variation (standard deviation/mean value) are 0.13, 0.25, and 0.41, respectively.

If the mass flow rate of the carbon dioxide is constant, the flow velocity ratio may be proportional to the inverse ratio of the cross section area of the glass tube. As the ratio of inner tube diameter is 1:2:3, the flow velocity ratio is 9:2.25:1. The velocity ratio obtained experimentally was 9:4.5:2.2. Although the experimental results agree roughly with the theoretical values, the experimental results for larger tube diameter are relatively greater. This is probably because dry ice particles highly sublimated due to the heat transfer, and the amount of gas increased.

The particle size and shape is difficult to be determined from the image of the side view since the particles are moving with high velocities and there are many particles out of focus. The images should be taken from behind a glass plate set in the front of the jet flow. The flowing dry ice particles are trapped on the surface of the glass plate for a very short period and thus the particles in the focus depth can be easily observed.

Figure 2.8 shows the images of dry ice particles taken from behind this glass plate. The size and shape was able to be estimated from the images. The size of dry ice particles increased with the tube diameter, and many agglomerates in Fig. 2.8 c were several hundred micron meters in equivalent circle diameter based on projected area. The visible particles were agglomerated and the shape was irregular. The large

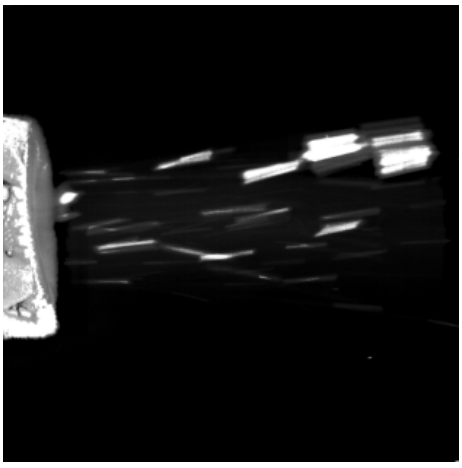

(a) D_i = 2 mm

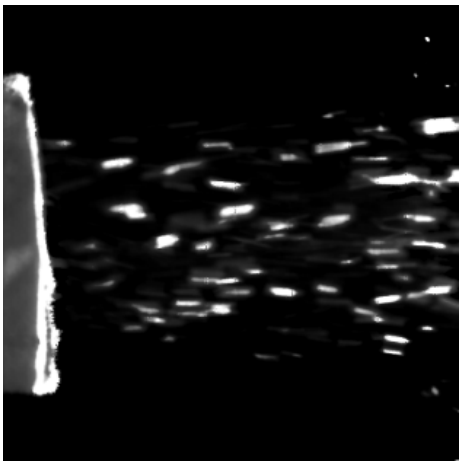

(b) D_i = 4 mm

(c) D_i = 6 mm

1 mm

Figure 2.6 Dry ice particles flowing out of the tube (L: 50 mm, exposure time: 1/6000 s).

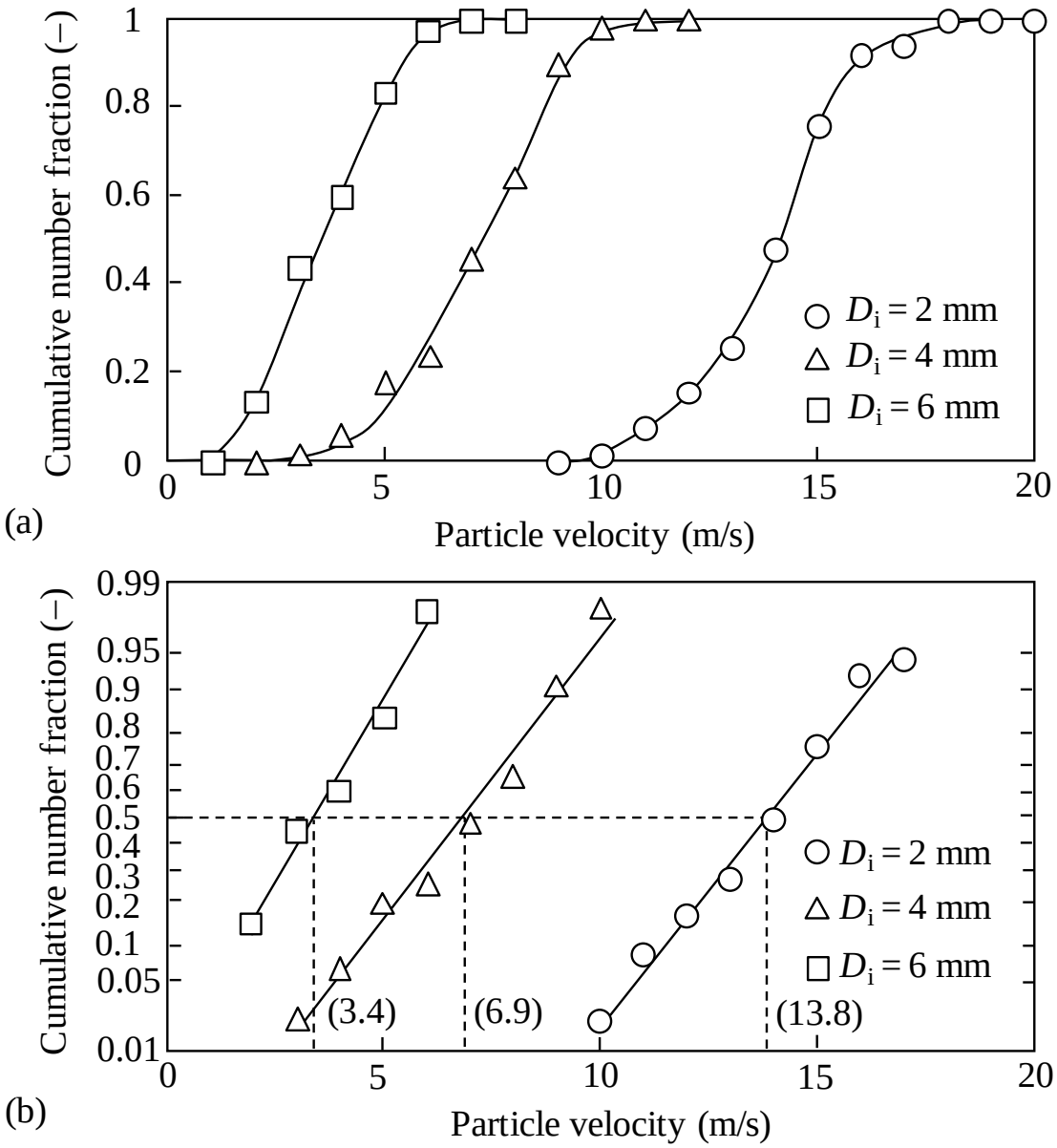

Figure 2.7 Particle velocity distribution: (a) plain graph; (b) normal graph.

(a) D_i = 2 mm

(b) D_i = 4 mm

(c) D_i = 6 mm

1 mm

Figure 2.8 Effect of tube diameter on agglomerate formation (view from behind, *L*: 50 mm, exposure time: 1/6000 s).

agglomerates seem to have a loosely packed structure.

Figure 2.9 shows the particle size distribution of the dry ice particles for different glass tube sizes. The data shows unsymmetrical distributions, which means a small amount of larger agglomerates were produced. The data are plotted on a lognormal graph, as shown in Fig. 2.9 b. Although they are not necessarily expressed as lognormal distributions, the geometric mean diameters, D_{ag50}, and apparent geometric standard deviations, σ_{ag} (= $(D_{ag84.1}/ D_{ag15.9})^{0.5}$), can be determined, i.e. for D_i = 2, 4, and 6 mm, D_{ag50} = 55, 85, and 183 μm, and σ_{ag} = 1.2, 1.5, and 1.5 μm, respectively.

2.3.3 Interparticle collisions on the agglomeration of dry ice particles in the glass tube

Dry ice particles can collide with each other in the flow, and produce agglomerated particles, which depends on the experimental conditions such as residence time of the dry ice particles in the glass tube. The residence time can be calculated by dividing the tube length by each average particle velocity (see Fig. 2.7). The residence time for D_i = 2, 4, and 6 mm are, respectively, 3.6, 7.2, and 14.7 ms. Since the average particle size ranges from 55 to 183 μm (see Fig. 2.9), a large number of collisions of primary particles are needed to produce such large agglomerates. However, the particle collisions can hardly be achieved in the limited residence time.

Figure 2.10 shows the typical images of the dry ice particles flowing out of the tube with a length of (a) 50 and (b) 150 mm. From the length and the direction of the trajectories of the dry ice particles, it is known that the particle velocity in Fig. 2.10 a was slower and the velocity vector was more random comparing with that in Fig. 2.10 b. When using a long tube, more dry ice particles will sublimate due to more heat exchange with atmosphere. As a result, the gas to solid ratio increases and the particle velocity increases. However, the particle size was almost the same irrespective of the tube length even though the residence time is increased in this experimental condition. Accordingly, there may be another important factor in the agglomeration process of dry ice particle. The glass tube has great influence on the particle agglomeration, and

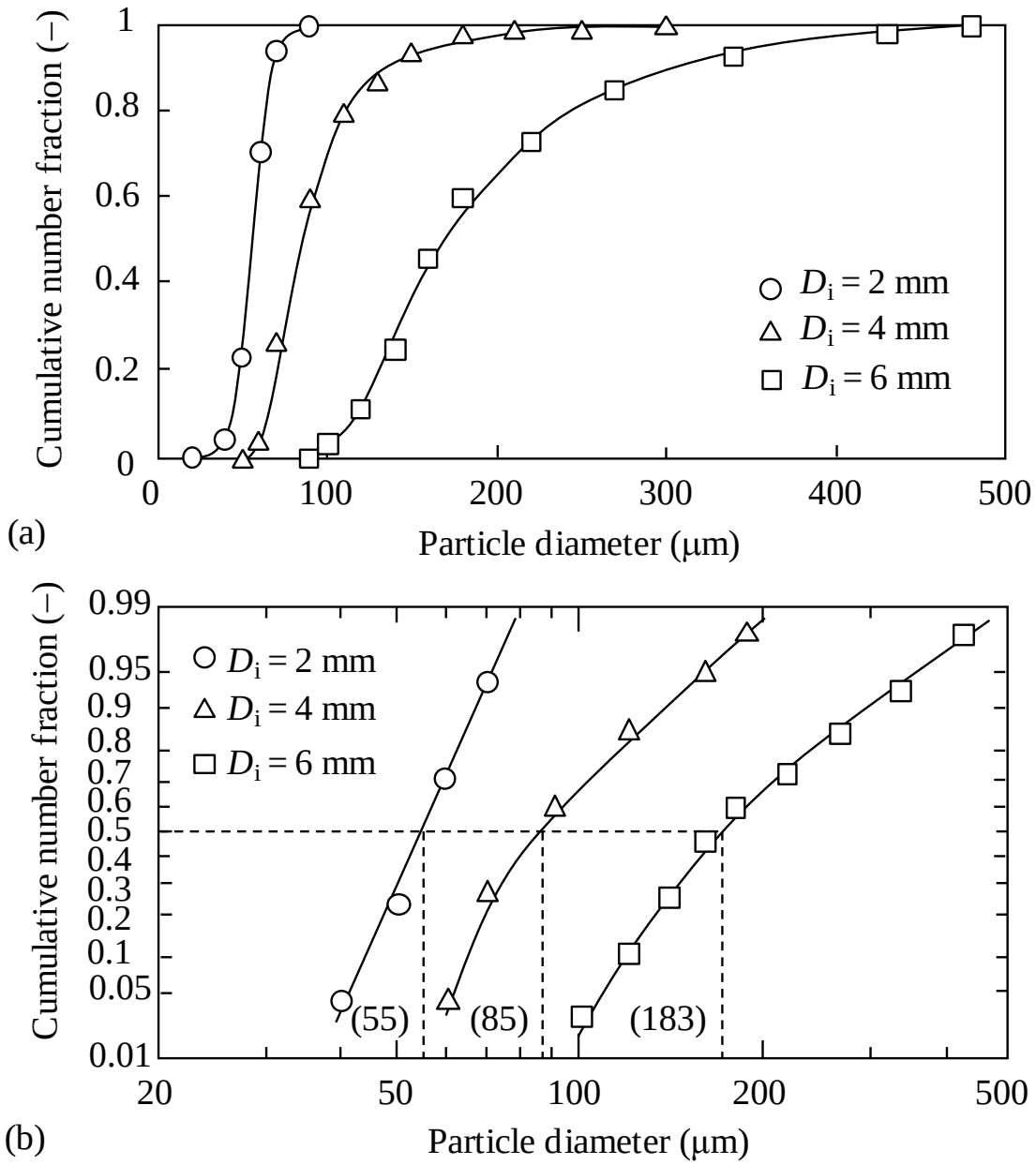

Figure 2.9 Cumulative particle size distribution:
(a) plain graph; (b) lognormal graph.

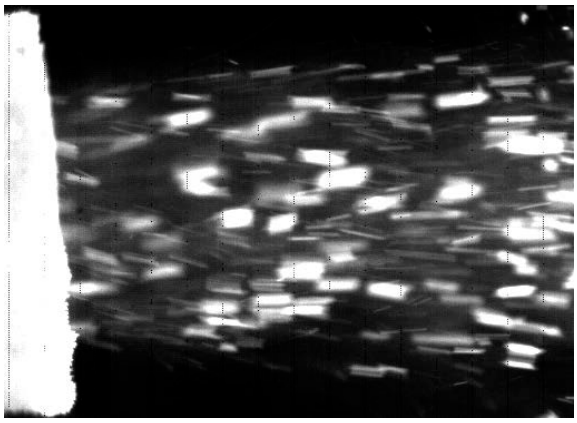

(a) L = 50 mm

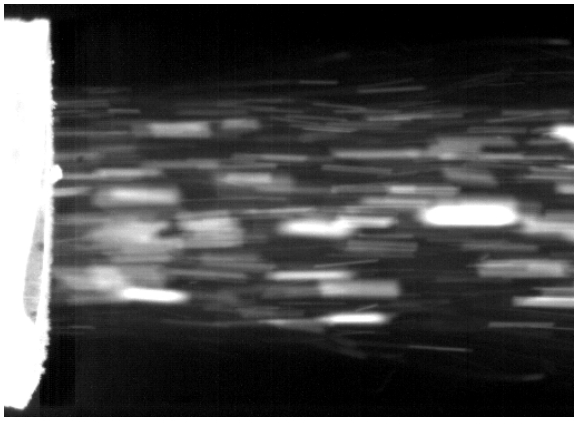

(b) L = 150 mm

1 mm

Figure 2.10 Effect of tube length on agglomerate formation (D_i: 4 mm, exposure time: 1/6000 s).

the tube wall may affect the agglomeration process. Further discussion is presented in the next section.

2.3.4 Effect of particle deposition and reentrainment on the agglomeration of dry ice particles in the glass tube

In general, fine particles in gas－solids pipe flow deposit on a wall surface and form a particle layer. The drag force acting on the layer increases with the mass of deposited particles and agglomerated particles are reentrained readily from the layer [Adhiwidjaja *et al.*, 2000]. Also, the collision of the flowing particles to the deposition layer enhances the reentrainment. Finally, the particle deposition and the reentrainment become in equilibrium [Theerachaisupakij *et al.*, 2003]. To investigate the formation of the deposition layer of dry ice particles, another experiment was carried out. A glass plate was placed in parallel to the axis of the expanded flow to observe the formation of the deposition layer from the side. The distance d from the plate surface and the expanded flow axis was varied to simulate the flow in the glass tube of different diameter. A high speed camera with a zoom lens was used to observe the formation of the deposition layer. The dry ice particles ejected from the nozzle began to deposit on the glass plate when the surface temperature was sufficiently low. The dry ice deposition layer gradually formed and the thickness increased as time elapsed.

Figure 2.11 shows the deposition layer of the dry ice particles formed on the glass plate placed at different distances. For d = 1 mm, the dry ice particle deposition layer was densely packed and the surface was smooth. The thickness of the layer increased with increasing horizontal distance from the nozzle outlet, as shown in Fig. 2.11 a. Thicker deposition layers were also observed for d = 2 and 3 mm (Fig. 2.11 b and c). Furthermore, it was found that the deposition layer in Fig. 2.11 c was formed away from the nozzle outlet (x = 25 mm) and had a loosely packed structure. Since the interaction between particles is small in the loosely packed structure, agglomerated particles can be easily reentrained from the deposition layer even though the flow velocity is relatively low. The size of the agglomerated particles increases as the packing density of the

deposition layer decreases. Therefore, the agglomerated dry ice particles shown in Figs. 2.6 and 2.8 are considered to be caused by the particle deposition and reentrainment.

Next, we explain the details of the temperature variation of the jet flow from the tube shown in Fig. 2.5 by the particle deposition and reentrainment. When the wall temperature is lowered by the expanded flow, the dry ice particles ejected from the nozzle begin to deposit on the tube wall. The dry ice deposition layer is gradually formed. During this phenomenon, the temperature of the jet flow from the glass tube decreases and approaches a stable value. When the agglomerated particles begin to reentrain from the deposition layer, the thermal equilibrium in this system is not maintained and the temperature of the flow decreases again. Once the particle deposition and reentrainment is in equilibrium, the temperature of the flow is stable again.

Since the deposition layer is composed of dry ice particles, it is of great interest to investigate the structure of the deposition layer. Figure 2.12 shows the optical microphotographs of the dry ice particle deposition layer formed on the glass plate placed at d = 1 and 3 mm. The deposition layer was formed in a stripe shape and orientated toward the flow direction. Many dry ice particles of several micrometers in diameter were observed in the deposition layer. It was found that the sizes of the dry ice particles observed in the deposition layer were almost the same, irrespective of the packing structure, as shown in Fig. 2.12. The fine particles are thought to be the primary particles of dry ice produced through nucleation and condensation in the expanding flow. Therefore, the agglomerated particles reentrained will also consist of the fine dry ice particles.

In the present work, the agglomeration process of dry ice particles was discussed on the basis of the experimental facts. Quantitative analysis can be taken up in the next step.

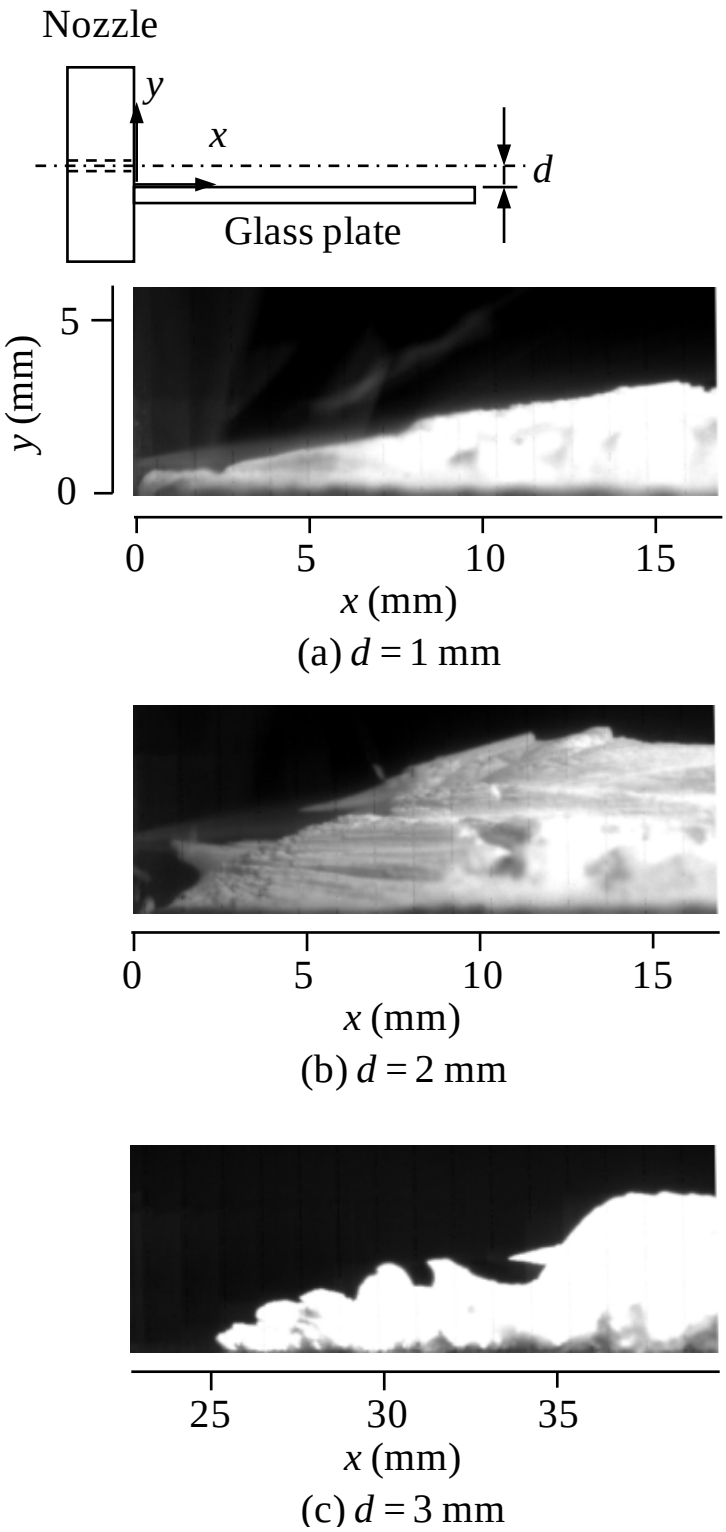

Figure 2.11 Deposition layer of dry ice particles formed on glass plate (exposure time: 1/6000 s).

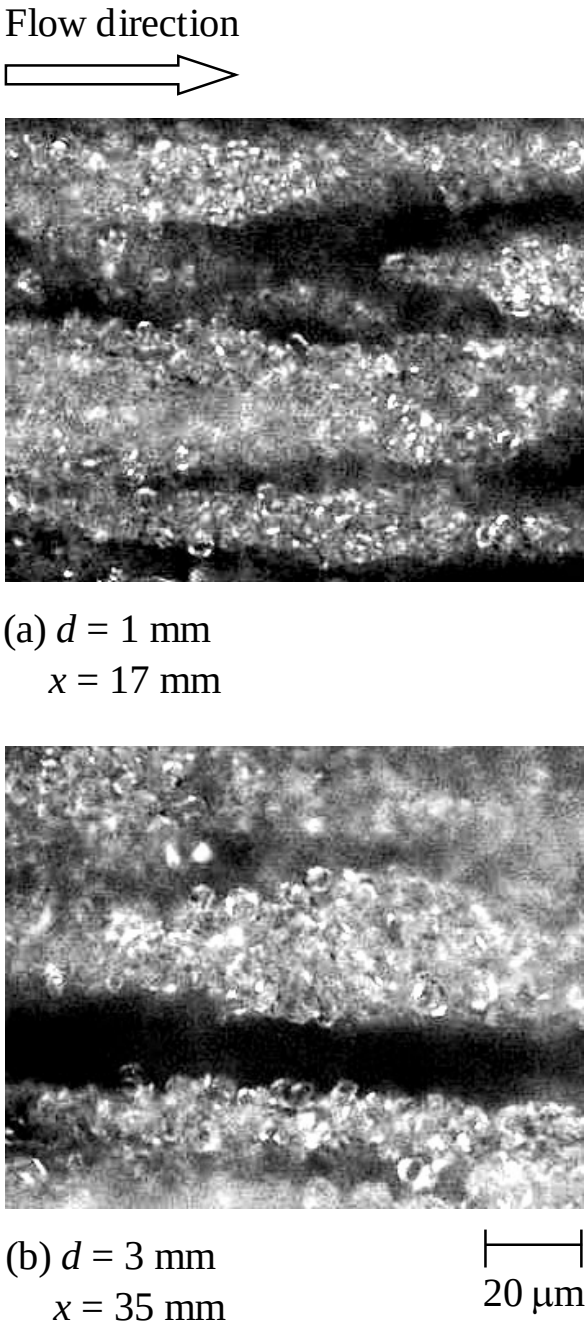

Figure 2.12 Deposition layer of dry ice particles observed through an optical microscope (d is described in Fig. 2.11).

2.4 Conclusions

The agglomeration process of dry ice particles was studied by measuring the temperature of the jet flow and the tube wall and observing the phenomena, and the mechanism for dry ice agglomeration was discussed. The following conclusions were drawn:

(1) The dry ice jet is able to be kept at a lower temperature by adding a glass tube to the outlet of the expansion nozzle. The temperature of dry ice jet decreases and approaches a stable temperature in the early stage; then moves to a second stable temperature. The dry ice particles agglomerated are observed visually after the second reduction of the temperature.

(2) The particle velocity and size were analyzed through the images taken by the high speed camera. Tube size has great influence on the particle size and shape as well as velocity. Since the residence time is limited, a large number of collisions of primary particles can hardly be achieved; thus the agglomerates observed cannot be produced by the interparticle collisions in the flow.

(3) After the dry ice particles produced deposit on the wall and form a particle layer, agglomerates are reentrained from the layer into the jet flow. As a result, dry ice particles can be observed visually in the jet flow.

(4) A microscopic observation shows that the deposition layer consists of fine dry ice particles of several micrometers. The agglomerated particles reentrained from the deposition layer will also consist of the fine dry ice particles.

Chapter 3
Size Measurement of Dry Ice Particles by Laser Diffraction

3.1 Introduction

From our observation in Chapter 2, dry ice primary particles can agglomerate up to hundred micrometers in size through the tube chamber. From the optical microphotographs taken, we determined that the agglomeration is formed under the particle deposition and reentrainment theory. A strong correlation was found between the jet flow velocity and the size of the agglomerates; higher jet flow velocity led to smaller dry ice agglomerates, and lower velocity led to larger ones. This means the particle size of dry ice can be determined by handling the particle deposition layer. In the previous study, the agglomerated dry ice particles were recognized by microscopic observation; however, the primary particles cannot be directly observed in the jet flow. To expand on this work it would be beneficial to investigate the size distribution of primary dry ice particles and their agglomerates through an in-situ size measurement.

The study in this chapter focuses on the in-situ measurement of dry ice particles produced by expanding liquid CO_2 and the agglomerates formed out of the tube chamber, through laser diffraction. The size distribution and the quantity of dry ice particles are quantitatively analyzed to investigate particle's growth, agglomeration, and sublimation, occurring in the jet flow. For explaining the details of the agglomeration process based on the particle deposition and reentrainment theory, the relationship between the size of agglomerates and the flow velocity is quantitatively discussed. In addition, the radial variation of particle size and the quantity of dry ice along the flow direction is investigated to ascertain the effective flowing distance where the dry ice can be effectively utilized.

3.2 Experimental apparatus and procedures

Figure 3.1 shows a schematic diagram of the experimental apparatus. High purity liquid carbon dioxide was used to produce dry ice particles. A flexible thermally

insulated hose, 2 m long and 15 mm in inner diameter was connected between a high pressure carbon dioxide cylinder and an expansion nozzle. A pressure gauge was installed to measure the pressure of the carbon dioxide. In this study, the pressure was kept at 5.5 MPa. Figure 3.2 shows the details of the nozzle. Three nozzle sizes were used for introducing the different flow rates of the dry ice jet. The mass flow rates for 0.1, 0.2 and 0.5 mm nozzles were 0.2, 0.5, 2.9 g/s, respectively. To produce agglomerated dry ice particles, an acrylonitrile-butadiene-styrene (ABS) tube of 2, 4, or 6 mm inner diameter and 50 mm in length was attached to the outlet of the expansion nozzle. The size distribution of the dry ice particles ejected from the nozzle or the tube was measured in-situ with a particle size analyzer (Spraytec, Malvern Instruments Inc.) based on the laser diffraction method. The laser beam, with a diameter of 20 mm, was oriented perpendicular to the dry ice jet.

In the measurements, beam steering was observed and affected the size distribution of dry ice particles. This occurs when a significant volume of jet gas or another gaseous phase apart from air is present in the measurement zone. Gases such as high pressure jets have a very different refractive index compared to air. This causes the laser beam to be defocused, leading to a high scattering signal on the first set of detector channels. Although this signal is not caused by particle scattering, it is interpreted as coarse particles. To overcome this problem, the detector range has to be limited. For the measurement of primary dry ice particles, the particle diameter range was limited to below 50 μm because it was confirmed that primary dry ice particles were less than several tens of micrometer from observations using a high-speed microscope camera. For the measurement of agglomerates of dry ice particles, the range was limited to less than 300 μm. This range is determined by considering the appropriate particle diameter of the agglomerates with minimizing the extent of the noise caused by the beam steering.

The attenuation, which is defined as the natural logarithm of the ratio of the intensity of the incident light to that of the light passing through the jet flow, was used for the analysis of the particle concentration in the dry ice jet. These calculations were

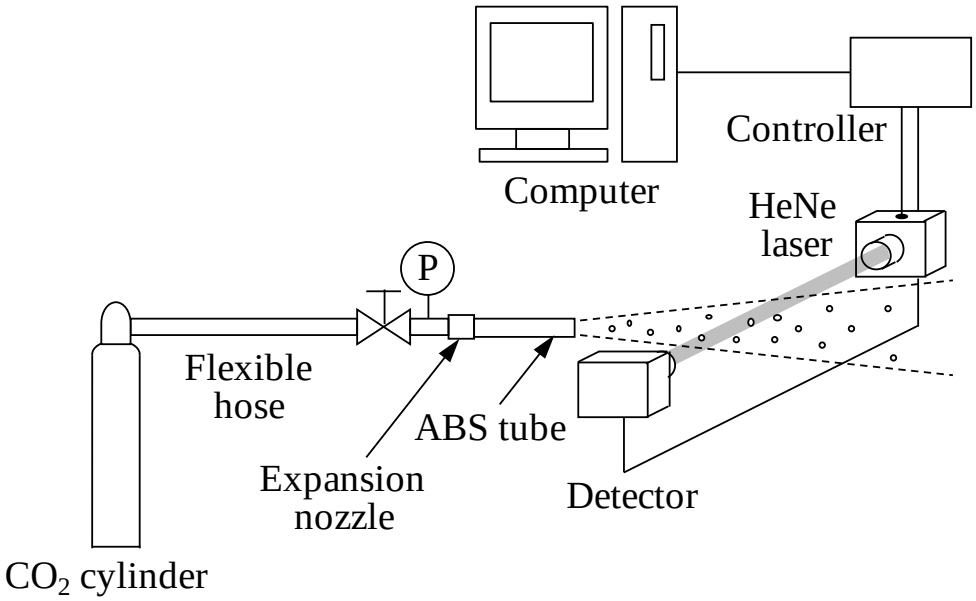

Figure 3.1 Schematic diagram of experimental apparatus.

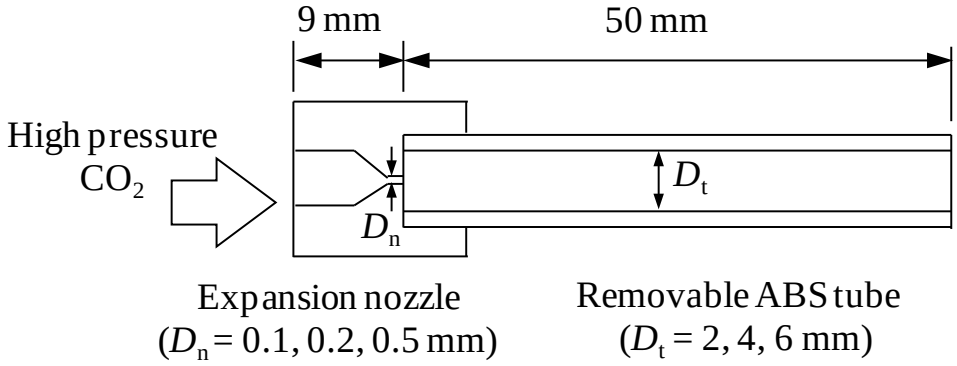

Figure 3.2 Cross section of an expansion nozzle and a tube.

carried out using a patented multiple scattering algorithm based on Mie theory [Harvill and Holve, 1998]. The accuracy of this measurement system was ensured up to 96% obscuration, in which our experiments were conducted. All the experiments were conducted under room conditions (20 ± 2 ºC; 1 atm).

3.3 Results and discussion

3.3.1 Effect of nozzle diameter on production of dry ice particles

The size distributions by mass of dry ice particles ejected from the expansion nozzles with different diameters were measured by the laser diffraction method. Figure 3.3 shows the cumulative size distributions of dry ice particles ejected from the 0.5 mm nozzle at different distances, d_n, from the nozzle outlet. The mass median diameter of the dry ice particles is about 1 μm at d_n = 10 mm and increases up to several micrometers as the measurement distance from the nozzle increases. This result indicates that the dry ice particles produced from the expansion nozzle grow in the jet flow. Furthermore, each size distribution appears to be a log-normal distribution.

Figure 3.4 shows the cumulative particle size distributions of dry ice particles ejected from the 0.2 mm nozzle. The mass median diameter increases with increasing distance for $d_n < 40$ mm. This feature is similar to that of the 0.5 mm nozzle, shown in Fig. 3.3. However, the particle size distribution obtained at $d_n \geq 40$ mm differs from the other distributions as it is skewed towards larger particles. In addition, the distribution is not unimodal but bimodal at d_n = 50 mm. These results are probably caused by the following two competing phenomena; one is the growth of dry ice particles in the gaseous carbon dioxide jet, and the other is the sublimation from particle surfaces. In general, the dry ice particles in the jet center will keep growing by condensation of high-concentration gaseous CO_2 or particle agglomeration. On the other hand, the dry ice particles in the exterior of the jet will sublimate readily due to a greater rate of heat transfer with atmosphere. For the smaller nozzle, the gas velocity is lower due to the lower mass flow rate, providing sufficient time for particles to grow larger than those of

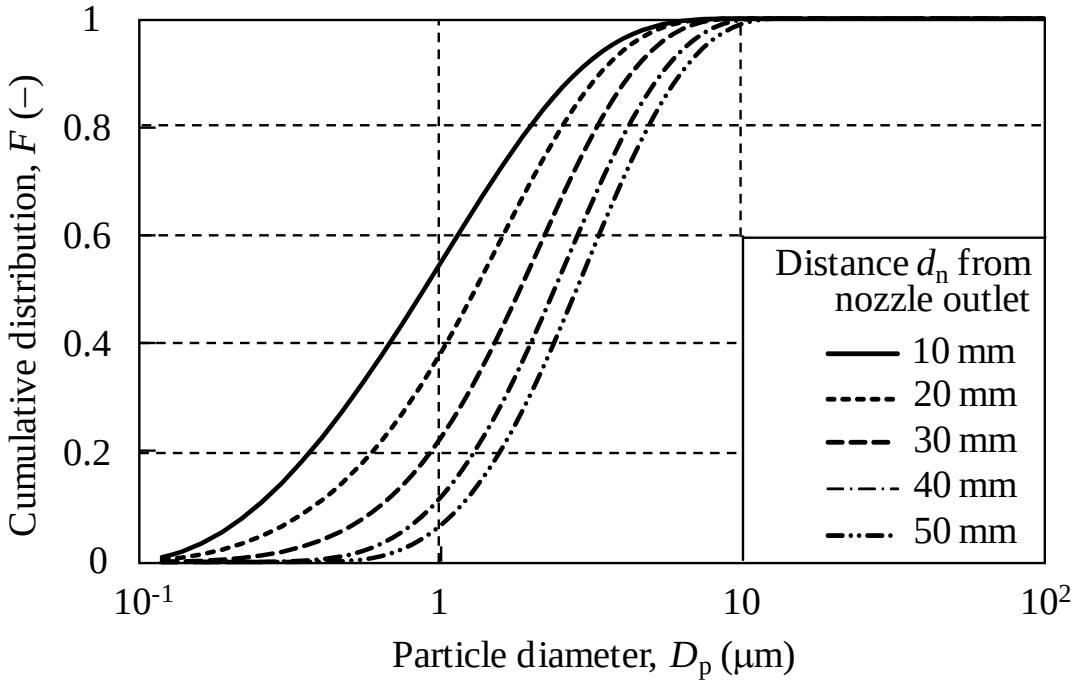

Figure 3.3 Cumulative size distributions of dry ice particles ejected from an expansion nozzle (nozzle diameter, D_n = 0.5 mm).

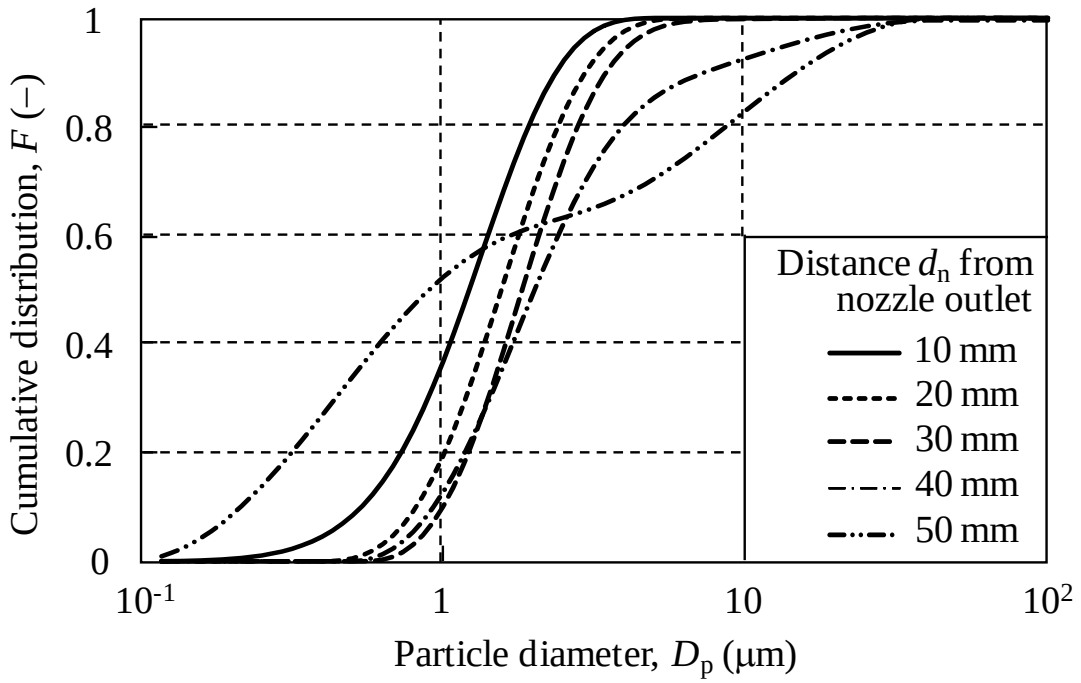

Figure 3.4 Cumulative size distributions of dry ice particles ejected from an expansion nozzle (nozzle diameter D_n = 0.2 mm).

0.5 mm nozzle. On the other hand, smaller particles will rapidly shrink due to sublimation. For the smaller nozzle diameter, the mass flow rate is reduced; hence it is difficult to maintain the temperature of the jet flow in the required range due to the heat exchange with the surrounding atmosphere. As a result, a smaller nozzle diameter will enhance the rate of sublimation.

Figure 3.5 shows the results for the 0.1 mm nozzle. The particle size distribution obtained at d_n = 5 mm looks like a log-normal distribution , but for $d_n \geq 10$, but for $d_n \geq$ 10 mm, the size distribution changes from unimodal to bimodal. The particle diameter increases with increasing distance for $10 \leq d_n \leq 20$ mm, but the trend reverses remarkably for d_n = 25 mm, where a notable reduction is observed. The flow rate for the 0.1mm nozzle is so small that sublimation occurs at a shorter distance from the nozzle outlet.

In order to observe more clearly the effect of the nozzle diameter and the distance from the nozzle outlet on the production of the dry ice particles, the mass median diameters of dry ice particles obtained under various conditions are plotted in Fig. 3.6. For the 0.5 mm nozzle diameter, the mass median diameter increases linearly with distance from 1 to 3 μm for distances of 10 and 50 mm, respectively. For the 0.2 mm nozzle diameter, the mass median diameter increases linearly with the distance in the range of $10 \leq d_n \leq 40$ mm, but decreases at $d_n \geq 40$ mm. For the 0.1 mm nozzle diameter, the increase in mass median diameter with distance is more erratic than for the other nozzle diameters, the mass median diameter decreases from d_n = 20 mm.

The amount of dry ice particles in the jet flow can be inferred from the attenuation determined by the laser diffraction method. Figure 3.7 shows the relationship between the attenuation and the distance from the nozzle outlet for three nozzle sizes. For the 0.5 mm nozzle, the attenuation is high; this is because the mass flow rate of carbon dioxide is high and a large number of particles are produced. Since the mass flow rate decreases with decreasing nozzle diameter, the attenuation is lower for smaller nozzle diameters. The dry ice jet spreads radially downstream; thus, the attenuation decreases with the distance from the nozzle outlet. In addition, sublimation will cause a decrease in

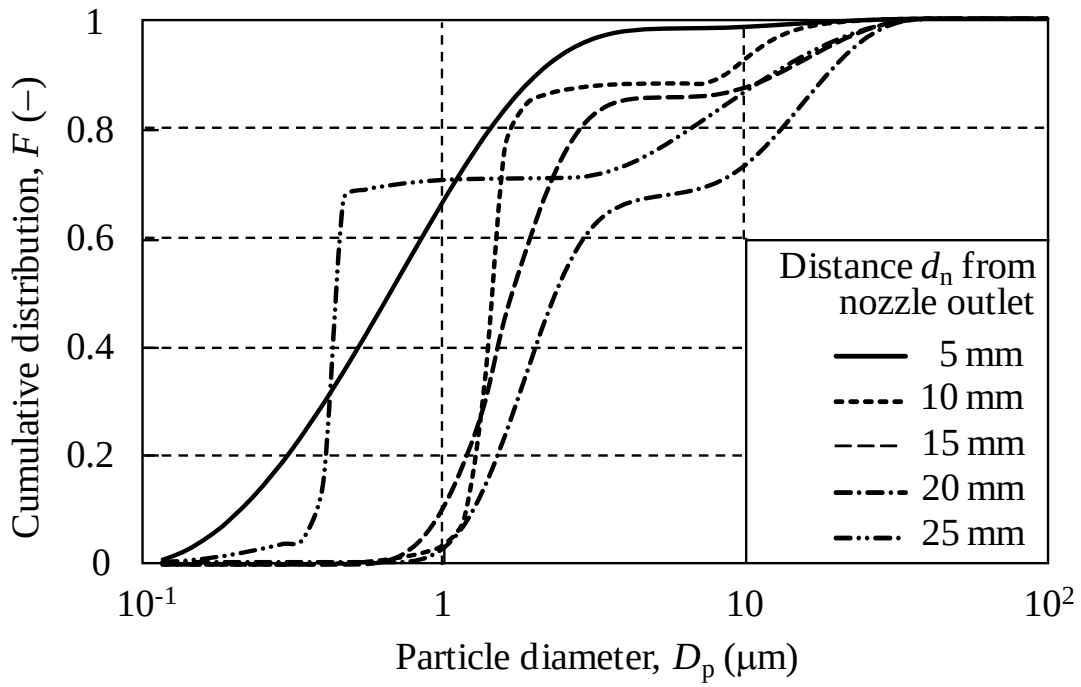

Figure 3.5 Cumulative size distributions of dry ice particles ejected from an expansion nozzle (nozzle diameter D_n = 0.1 mm).

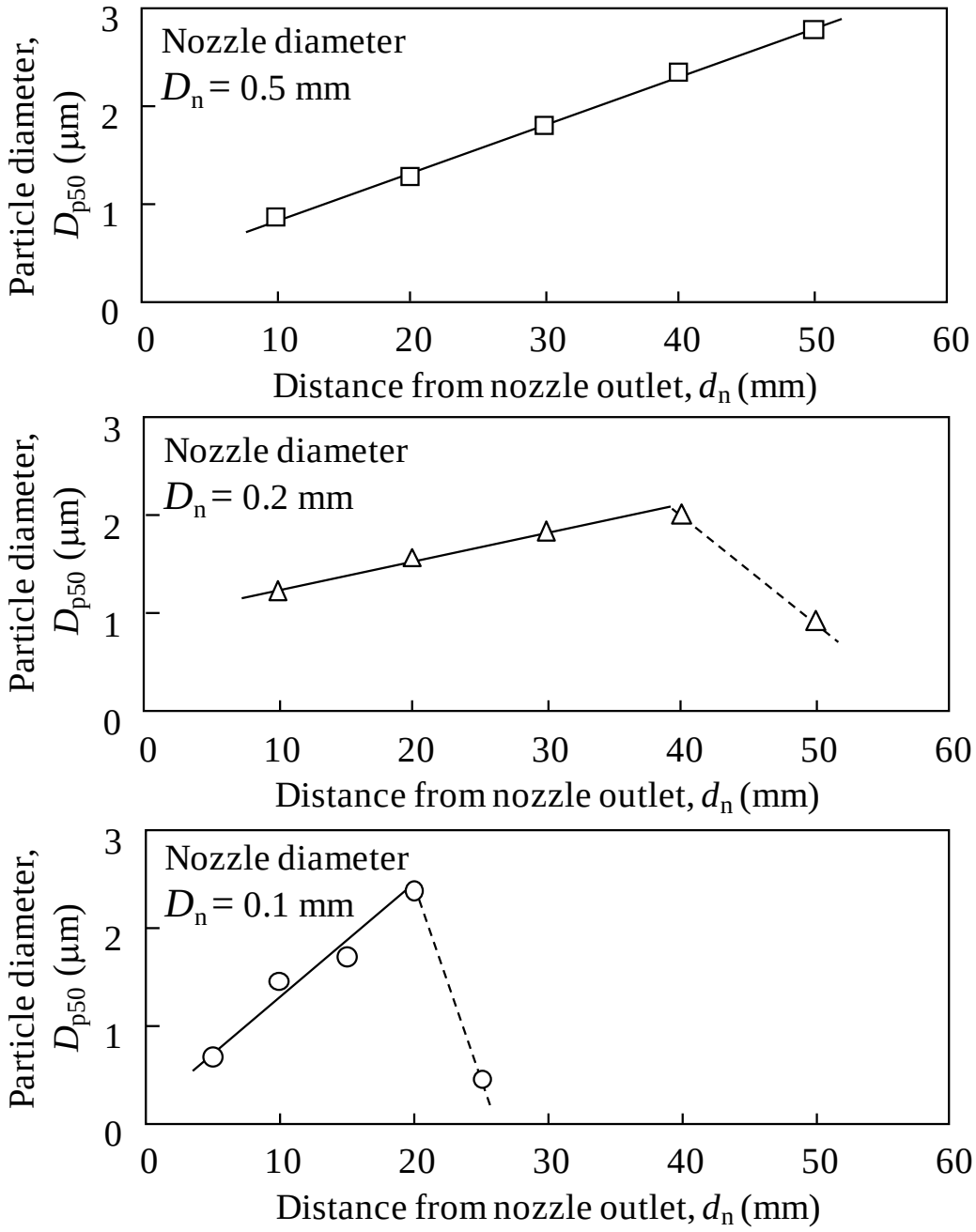

Figure 3.6 Effect of nozzle diameter on mass median diameter of dry ice particles.

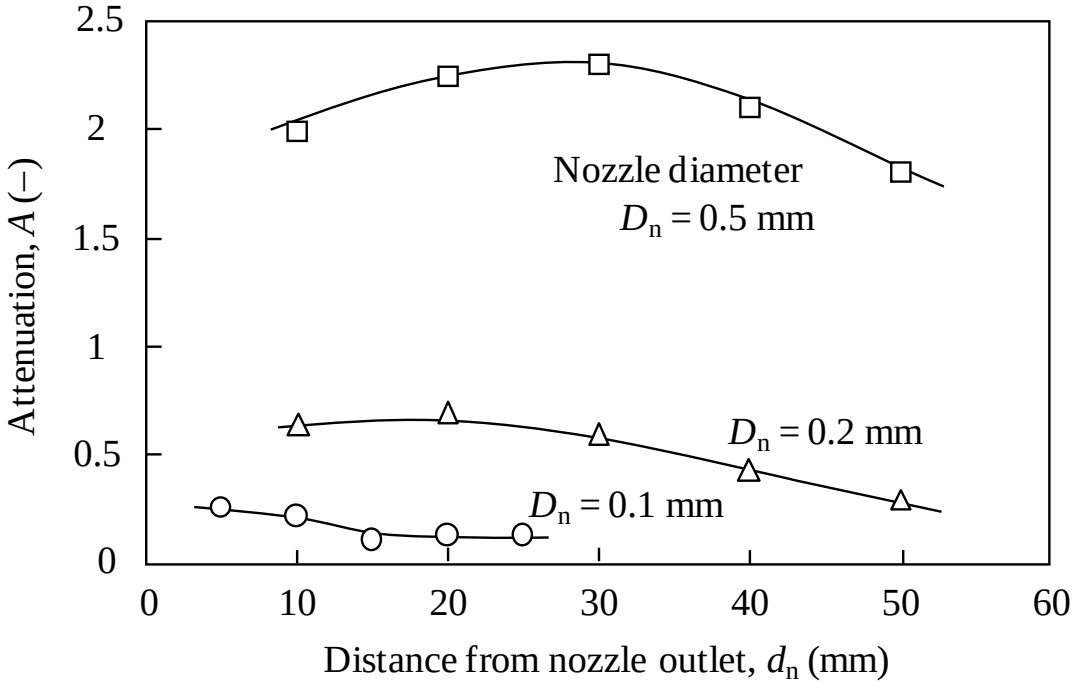

Figure 3.7 Attenuation of dry ice jet ejected from expansion nozzle.

attenuation at larger distances.

3.3.2 Agglomeration of dry ice particles in the ABS tubes

In Chapter 2, it is concluded that dry ice particles formed agglomerates by depositing on the inner walls of a tube attached to the expansion nozzle. However, no measurement of agglomerate size was carried out then. Here in this work agglomerates were produced using different size tubes and their size distribution was analyzed in-situ using the technique discussed in Section 3.2.

Figure 3.8 shows the cumulative size distribution of agglomerates of dry ice particles, obtained using the 0.5 mm nozzle and the 6 mm tube. The mass median diameter of the agglomerates is about 100 μm, which is much larger than that of the particles produced without the tube (~1 μm, see Fig. 3.3). Each distribution appears to be log-normal, and the dependence of the distance d_t from the tube outlet on the particle size distribution is found to be small. However, the mass fraction of smaller particles slightly decrease with the increase of distance d_t. The smaller particles might further agglomerate or sublimate in the jet flow. The influence of sublimation is not seen in larger agglomerated particles.

Figure 3.9 shows the results for the 0.1 mm nozzle and the 2 mm tube. The particle size distributions are similar to those in Fig. 3.8, and the influence of sublimation is not seen in this experiment. In addition, many particle size measurements were carried out under different conditions, i.e. with 0.1, 0.2, and 0.5 mm nozzles, and the 2, 4, and 6 mm tubes, showing that the results were generally similar to each other. However, slight differences can be seen by changing the nozzle diameter.

Figure 3.10 shows the results measured at d_t = 40 mm using the 6 mm tube for the three investigated nozzle diameters. When the nozzle diameter is changed from 0.1 to 0.5 mm, the mass median diameter varies from 100 μm to 80 μm. As a large amount of liquid carbon dioxide is expanded from the 0.5 mm nozzle, the flow velocity in the tube is high. The variation of the mass median diameter is thought to be caused by the difference in the flow conditions. The effect of the flow conditions, including the

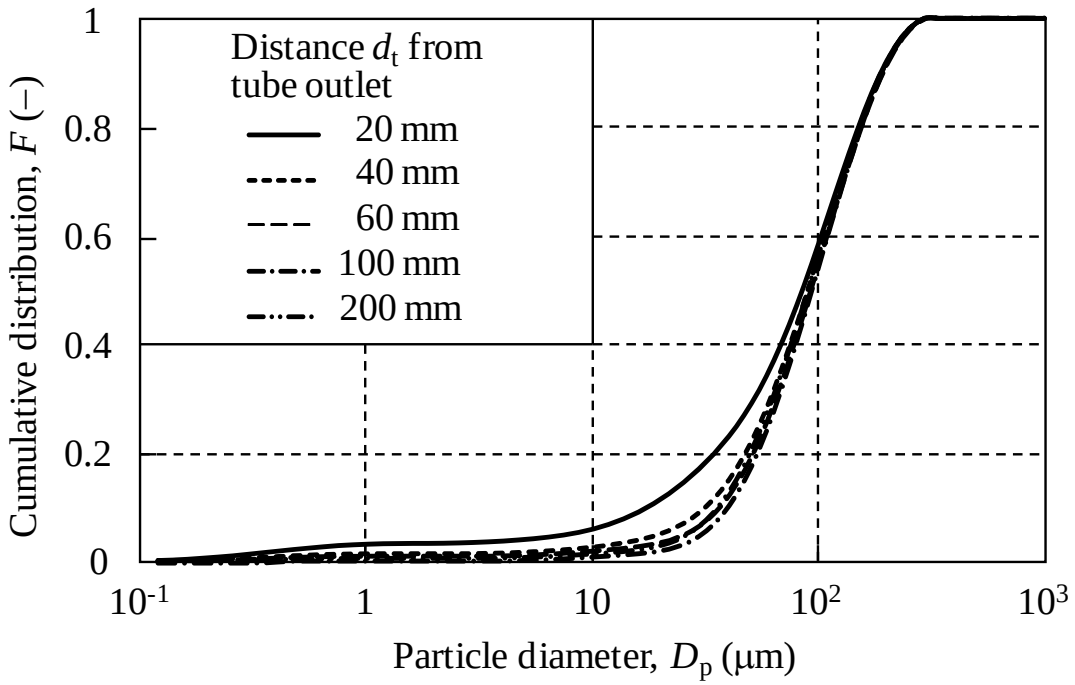

Figure 3.8 Cumulative size distribution of dry ice particles ejected from tube (nozzle diameter D_n = 0.5 mm, tube diameter D_t = 6 mm).

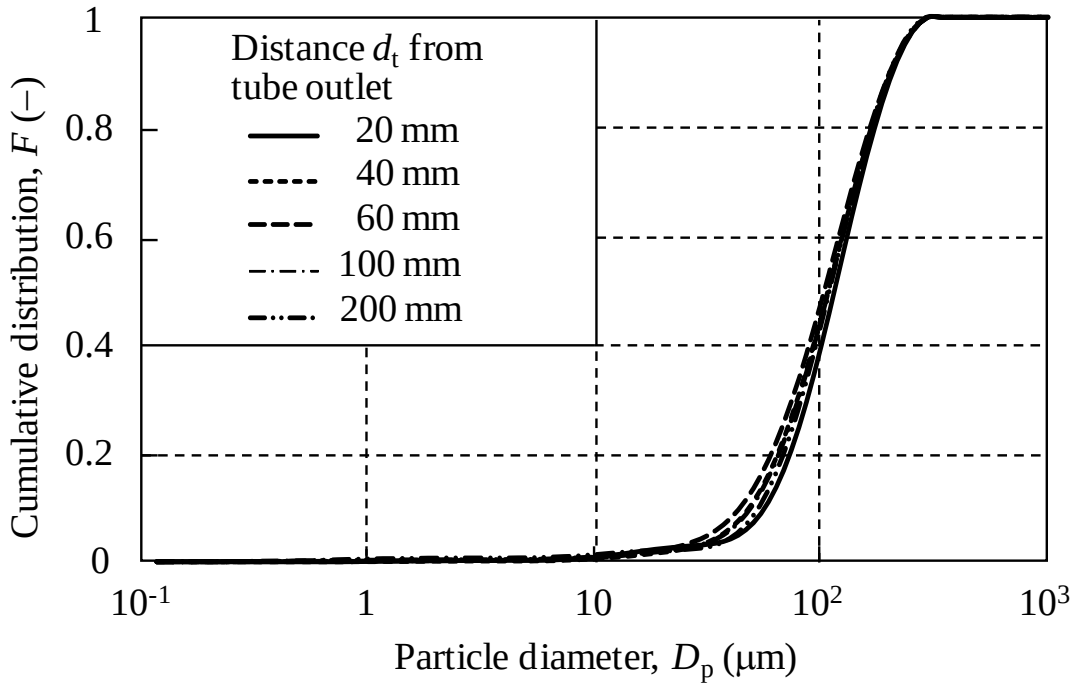

Figure 3.9 Cumulative size distribution of dry ice particles ejected from tube (nozzle diameter D_n = 0.1 mm, tube diameter D_t = 2 mm).

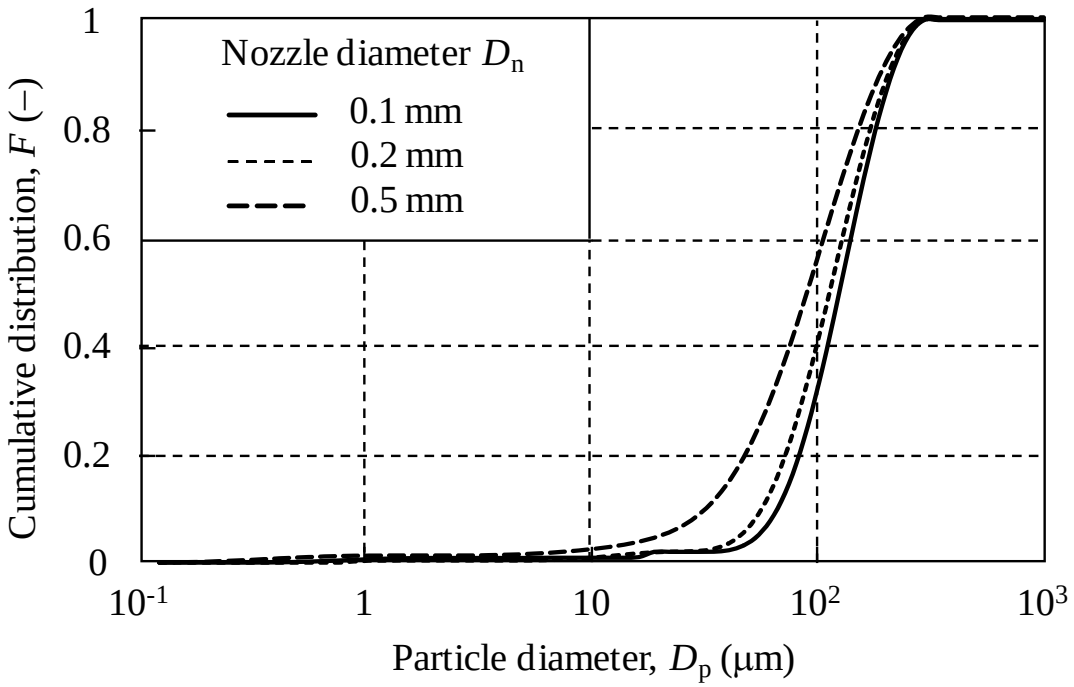

Figure 3.10 The effect of nozzle diameter on cumulative size distribution of dry ice particles ejected from tube (D_t = 6 mm, d_t = 40 mm).

residence time and the flow velocity in the tube, on the agglomeration is discussed in detail in Sections 3.3.3 and 3.3.4.

Next, the amount of agglomerated dry ice particles was evaluated from the attenuation data. Figure 3.11 shows the relationship between the attenuation and the distance from the tube outlet for different tube and nozzle diameters. The attenuation decreases with increasing distance from the tube outlet. This is because the dry ice jet expands radially downstream, therefore the particle concentration of dry ice particles decreases with the distance from the tube outlet. Furthermore, it is found that the attenuation increases with the increase of the nozzle and tube diameters. Since the mass flow rate of carbon dioxide increases with increasing nozzle diameter, the attenuation is high for a large nozzle diameter. As the tube diameter increases, the cross section area of the jet flow increases. As a result, the number of particles detected in the cross section area increases; thus, the attenuation increases.

3.3.3 Effect of interparticle collision on agglomeration

Dry ice particles can collide with each other in the flow and produce agglomerated particles by adhesion forces; therefore, the inter-particle collisions are generally taken into account in the agglomeration process. The concentration of primary particles and the residence time in the tube are the dominant factors in determining agglomerate size. To estimate the fraction of primary particles remaining after the agglomeration process, γ, the following equation is applied [Friedlander, 2000].

$$\gamma = \frac{n_{1,\mathrm{t}}}{n_{1,0}} = \frac{1}{(1 + t/\tau_{\mathrm{B}})^2}, \tag{3.1}$$

where $n_{1,\mathrm{t}}$ is the concentration of primary particles after the agglomeration process, $n_{1,0}$ is the initial concentration of primary particles, t is the residence time and τ_{B} is the characteristic time.

From the theoretical calculation based on the experimental conditions where the

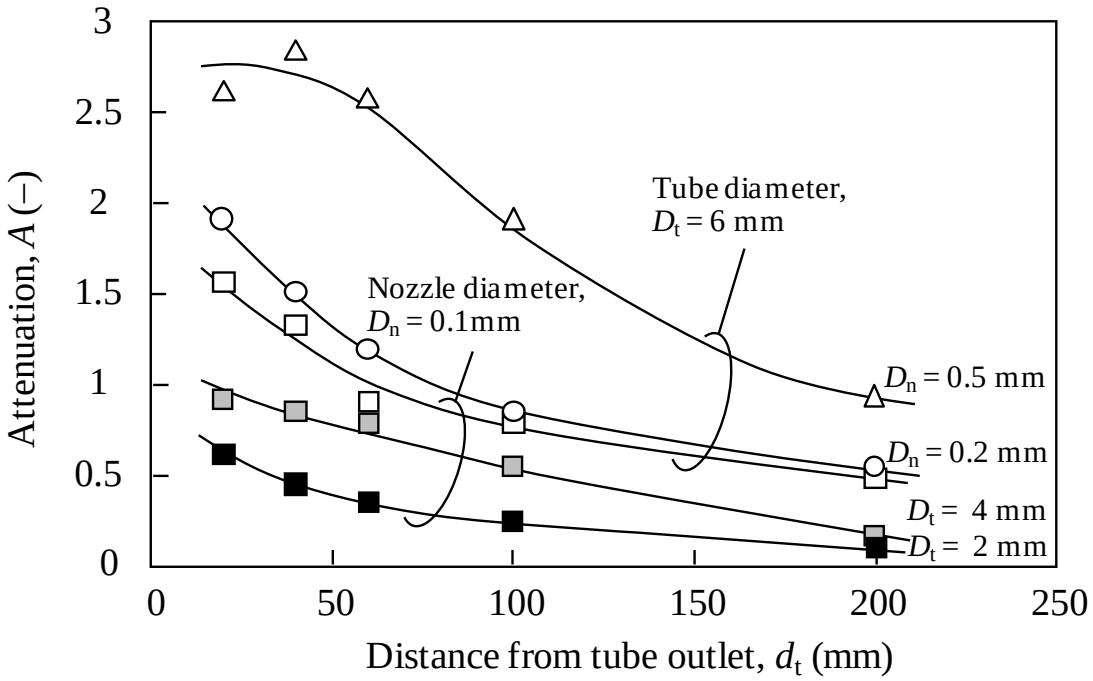

Figure 3.11 Attenuation of dry ice jet ejected from the tubes.

value of t/τ_B is estimated to be less than 0.02, the fraction of primary particles remaining is over 95%. This indicates that most of the primary particles cannot agglomerate by interparticle collisions alone when the residence time is less than 30 ms, which is calculated on the basis of the experimental results. In the experiment, a large number of agglomerates about 100 μm in mass median diameter are produced and ejected from the tube. Therefore, additional factors affecting the agglomeration in the tube should be taken into consideration.

3.3.4 Flow velocity in a tube

In this work, interparticle collisions are not considered to be the main mechanism for agglomeration in the tube, as mentioned previously in Section 3.3.3. Agglomeration is believed to be due to particle deposition and reentrainment on the tube wall [Matsusaka and Masuda, 1996; Adhiwidjaja *et al*., 2000; Theerachaisupakij *et al*., 2003]. Primary particles deposit on the tube wall and form a deposition layer; then, agglomerates are entrained from the deposition layer by aerodynamic drag. The collision of the flowing particles to the deposition layer also enhances reentrainment. Under steady state operation particle deposition and reentrainment are in equilibrium. Since these phenomena depend on the gas flow velocity, this may be a key parameter for agglomeration.

The average gas flow velocities for nozzle diameters of 0.1, 0.2 and 0.5 mm, tube diameters of 2, 4 and 6 mm and distances from the tube of 20, 40 and 60 mm have been obtained experimentally. Figure 3.12 shows the effect of the flow velocity on the mass median diameter of the agglomerates. The mass median diameter tends to decrease with an increase in the flow velocity. As the separation force acting on the deposition layer increases with the flow velocity, smaller agglomerates can be reentrained by this mechanism. Therefore, the experimental relationship is reasonably good, and the gas flow velocity will be an important parameter to predict the agglomeration of dry ice particles in the tube.

3.3.5 Distribution of particles in the jet flow

Particle size measurements were carried out at different radial positions in the jet flow ejected from the tube. The nozzle diameter was 0.1 mm and the tube diameter was 4 mm. Figure 3.13 shows the mass median diameter and the attenuation of the dry ice jet as a function of radial position, r. The mass median diameter in the central axis of the jet flow is about 110 μm, and slightly decreases with the increase of the radial position, r, at d_t = 20 and 60 mm (see Fig. 3.13 a). For d_t = 60 mm and r = 18 mm, the mass median diameter decreases to about 80 μm. As the jet flow expands downstream, larger agglomerates go straight along the jet axis because of their inertia, while smaller agglomerates spread in the radial direction. In addition, since the exterior of the jet is exposed to a greater rate of heat transfer with atmosphere, the agglomerates would sublimate at a faster rate with increased radial distance. As a result, the profile as a function of the radius of the jet flow will deviate from a flat distribution with increasing flow distance. The attenuation of the dry ice jet shows that the profile expands radially along the flow direction (see Fig. 3.13 b). The agglomerates are shown to be well dispersed in the jet flow. However, if the distance from the tube end is large, the effect of sublimation will be noticeable.

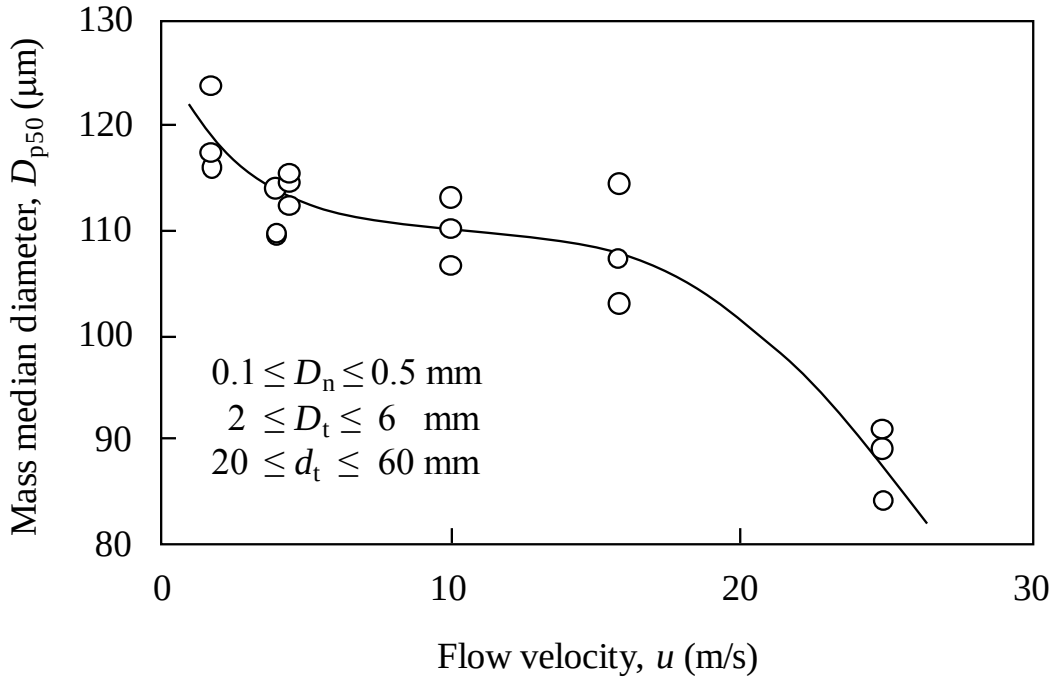

Figure 3.12 Effect of flow velocity on mass median diameter of agglomerated dry ice particles.

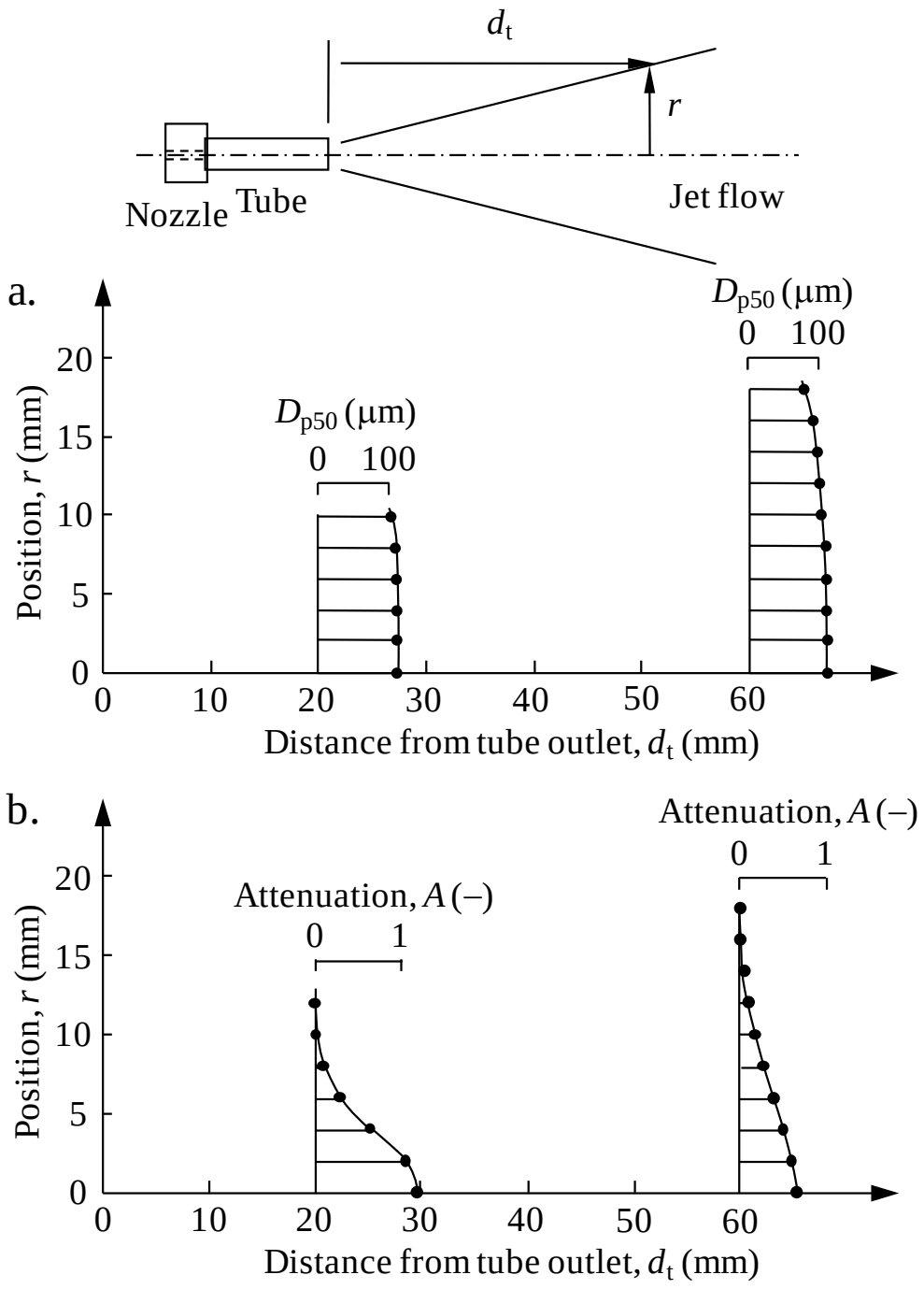

Figure 3.13 Distribution of dry ice particles in jet flow:
a) mass median diameter, b) attenuation (D_n = 0.1 mm, D_t = 4 mm).

3.4 Conclusions

The size distribution and attenuation of the dry ice particles produced by rapid expansion of liquid carbon dioxide were analyzed online, downstream of the nozzle or the tube by a laser diffraction method. The conclusions were drawn as follows:

(1) With the experimental setup used in this work, the mass median diameter of the dry ice particles ejected from the expansion nozzle is about 1 μm. The particle size distribution is roughly log-normal. The particles grow in the jet flow and in the tubes. However, the sublimation of dry ice also occurs, and becomes noticeable at a distance from the nozzle outlet, where the particle size starts to reduce. As a result of the simultaneous phenomena of particle growth in the jet center and sublimation in the exterior, a bimodal size distribution exists at greater distances, arising from the size distributions of the primary particles and the agglomerated ones. For smaller expansion nozzles sublimation occurs at a shorter distance from the nozzle outlet, because the reduced flow rate results in a more rapid increase in temperature of the jet flow due to heat exchange with the atmosphere.

(2) Under the prevailing aerodynamic conditions, the primary particles agglomerate to about 100 μm in mass median diameter by passing through the tube attached to the outlet of the nozzle. The mass median diameter of the agglomerates is not very sensitive to the nozzle diameter and varies from 100 μm to 80 μm when the latter is changed from 0.1 to 0.5 mm.

(3) A simple account of interparticle collisions in the tubes showed that most of the primary particles cannot agglomerate due to a collision mechanism in the short residence time within the tube.

(4) The agglomeration process is considered to be by particle deposition on the tube wall and reentrainment. Primary particles deposit on the tube wall and form a deposition layer; then, agglomerates are entrained from the deposition layer by aerodynamic drag and the collision of the flowing particles. The particle deposition and reentrainment reach an equilibrium rate if the process is operated sufficiently long to reach a steady state. The mass median diameter tends to decrease with the

increase of the flow velocity. This is because the separation force acting on the deposition layer increases with the flow velocity, smaller agglomerates can therefore be reentrained.

(5) As the jet flow extends radially downstream, larger agglomerates travel along the jet axis, while smaller agglomerates spread out in the radial direction, following more easily the gas streamlines. As a result, the profile as a function of the radius of the jet flow deviates from a flat distribution with increasing flow distance.

Chapter 4

Effect of Particle Impact on Surface Cleaning Using Dry Ice Jet

4.1 Introduction

4.1.1 Dry ice blasting for removing fine particles

As mentioned in Chapter 1 and 2, dry ice particles can be utilized as a blasting media for cleaning. The contaminants adhering to the surface can be removed by the dry ice particles without secondary contamination. Therefore, this dry cleaning method is particularly well adopted for industrial manufacturing process where high cleanliness is required. In many industrial fields, fine particles are the main contaminants in the manufacturing process; failure to remove the contaminants will result in degradation in product quality. For example, a conductive particle less than 1 μm in size adhering to a substrate in an integrated circuit package can cause an electrical short circuit.

The combination of the dry ice impact and aerodynamic drag in dry ice blasting is considered to be effective on the removal of fine particles. To direct the expanding dry ice jet flow to the cleaning target, a tube is usually equipped in the cleaning system. According to the previous studies, the primary dry ice particles will agglomerate as the jet flow pass through the tube. The impact of the agglomerated dry ice particles is therefore considered important, even though the removal mechanism is not yet clear.

4.1.2 Theoretical particle removal model

There are several possible removal mechanisms for dry ice cleaning: (1) kinetic separation based on the momentum transfer from the dry ice particles to contaminants, (2) aerodynamic drag separation, (3) chemical separation caused by the dissolution of residues into liquid carbon dioxide, and (4) electrostatic separation caused by the sweep of the contaminants combined with the charged dry ice particles [Sherman *et al.*, 1991; Hills, 1995; Jackson and Carver, 1999]. The kinetic separation and the aerodynamic drag separation have been investigated by taking into account the forces acting on a

particle adhering to a surface [Kousaka *et al.*, 1980; Wang, 1990; Tsai *et al.*, 1991; Matsusaka and Masuda, 1996; Adhiwidjaja *et al.*, 2000; Theerachaisupakij *et al.*, 2003]; particle removal was explained by the moments of the forces. Figure 4.1 shows the basic concept of a moment balance model for a particle adhering to a substrate. There are three main forces: impact force caused by an airborne particle (F_c), drag force (F_d), and adhesion force (F_a). Gravitational force can be neglected since the contaminants are generally small. In this figure, D_{p1} and D_{p2} are the diameters of the airborne particle and the particle adhering to the substrate, respectively, ϕ is the impact angle, θ is the contact angle based on elastic deformation, and M_t is the moment of force at the center of mass of the particle, which is caused by the shear flow. The balance of the moments of forces is represented by

$$\{F_c \cos\phi\,(\sin\phi+\cos\theta)+F_d\cos\theta\}\frac{D_{p2}}{2}+M_t=\{F_c\sin\phi(\cos\phi+\sin\theta)+F_a\sin\theta\}\frac{D_{p2}}{2}. \quad (4.1)$$

The moment balance model was also used for dry ice cleaning and showed that rolling removal of particulate contaminants is more significant than sliding removal based on the force balance [Toscano and Ahmadi, 2003]. However, if the particulate contaminants are not spherical, the sliding model may be significant [Banerjee and Campbell, 2005]. To fully elucidate the mechanism of particle removal, fundamental research is needed, and the phenomenon needs to be observed microscopically. In addition, the measurement of the temperature of the dry ice jet is important to analyze the removal efficiency since the state of the dry ice particles in a jet flow depends on the temperature as described in Chapter 2.

In this chapter, the removal of monosized fine particles adhering to a surface by dry ice blasting is experimentally investigated. The purpose of the study is to make clear the impact effect of dry ice particles in the removal process. Particle removal is observed by a high-speed microscope camera and the time course of the removal efficiency is obtained. Also, the jet temperature, related to the state of dry ice particles, is continuously measured and correlated to the variation of the removal efficiency.

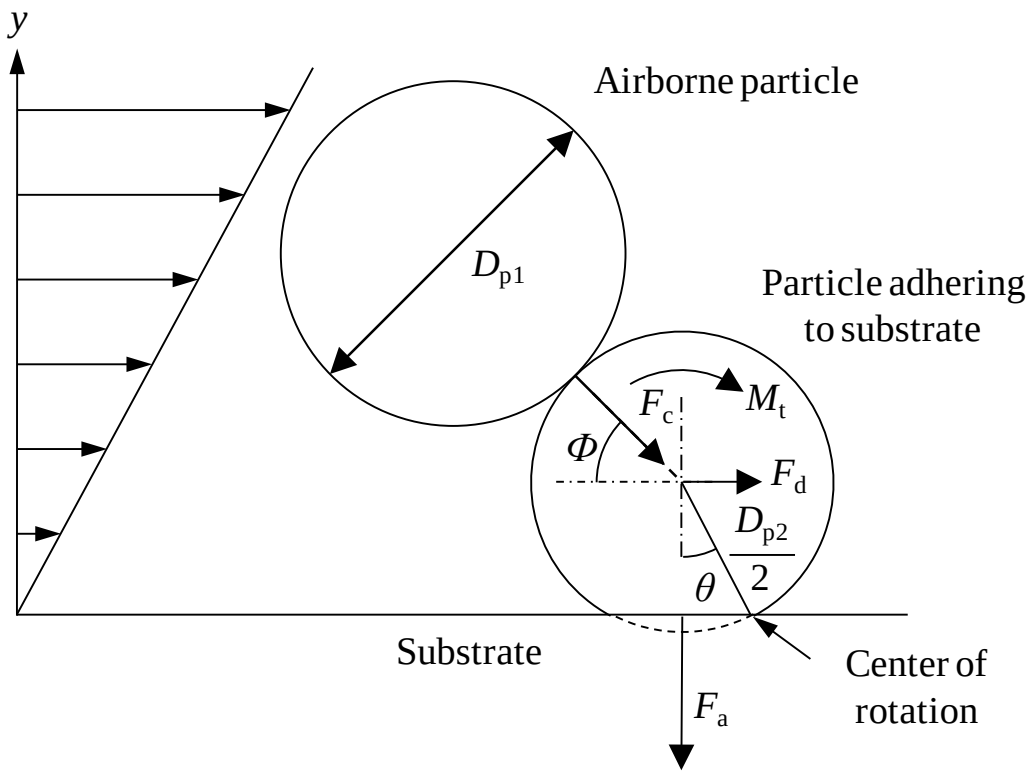

Figure 4.1 Simple model of particle impact in shear flow field.

In addition, theoretical calculations based on the moment balance model are carried out to discuss the impact effect of dry ice particles by comparing with the aerodynamic drag effect.

4.2 Experimental apparatus and procedure

Figure 4.2 shows the experimental apparatus for surface cleaning by dry ice blasting. The dry ice jet was produced by expanding high-purity liquid CO_2. To do this, a flexible hose made of stainless steel was connected to a high-pressure CO_2 cylinder. At the end of the hose, a needle valve was installed to control the flow rate of the dry ice jet. A pressure gauge was set at the inlet of the needle valve to measure the inner pressure of the CO_2; the pressure measured in the experiments was over 6 MPa. The flexible hose and the needle valve were thermally insulated to reduce heat transfer between the environment and the equipment. A 50 mm long acrylonitrile-butadiene-styrene (ABS) tube was installed at the end of the needle valve to serve as an agglomeration chamber. The agglomerated dry ice particles were exhausted from the tube with the carbon dioxide gas.

A test plate (76 × 26 mm) made of 1 mm thick transparent glass was fixed in the surface cleaning experiment. The plate was previously contaminated by monosized spherical latex particles with diameters of 2.92 μm and 0.75 μm (Duke Scientific Corp.). The preparation procedure is as follows: (1) colloidal particles were aerosolized by a nebulizer; (2) particles carried by the airflow were dried by passing though an annular cylinder containing silica gel; (3) the airborne particles deposited onto the surface of the plate. The initial number of particles per unit area of the surface was about 100 mm^{-2} for the 2.92-μm particles and about 600 mm^{-2} for the 0.75-μm particles.

Figure 4.3 shows the configuration of the ABS tube and test plate. The inner diameter of the ABS tube used for the experiment was 6 mm. The angle of incidence was $\pi/4$ radian and the distance from the tip of the tube to the center of the test plate was 20 mm in the axial direction. To evaluate the strength of the jet flow on the surface,

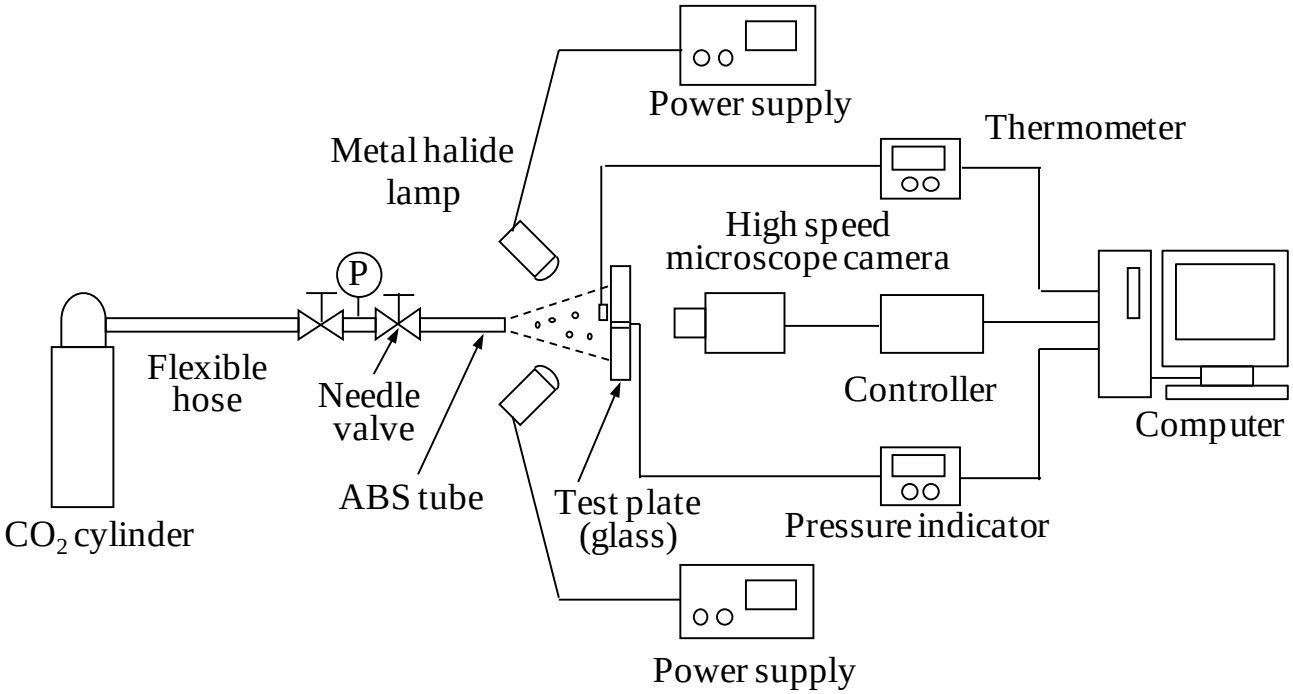

Figure 4.2 Schematic diagram of experimental apparatus.

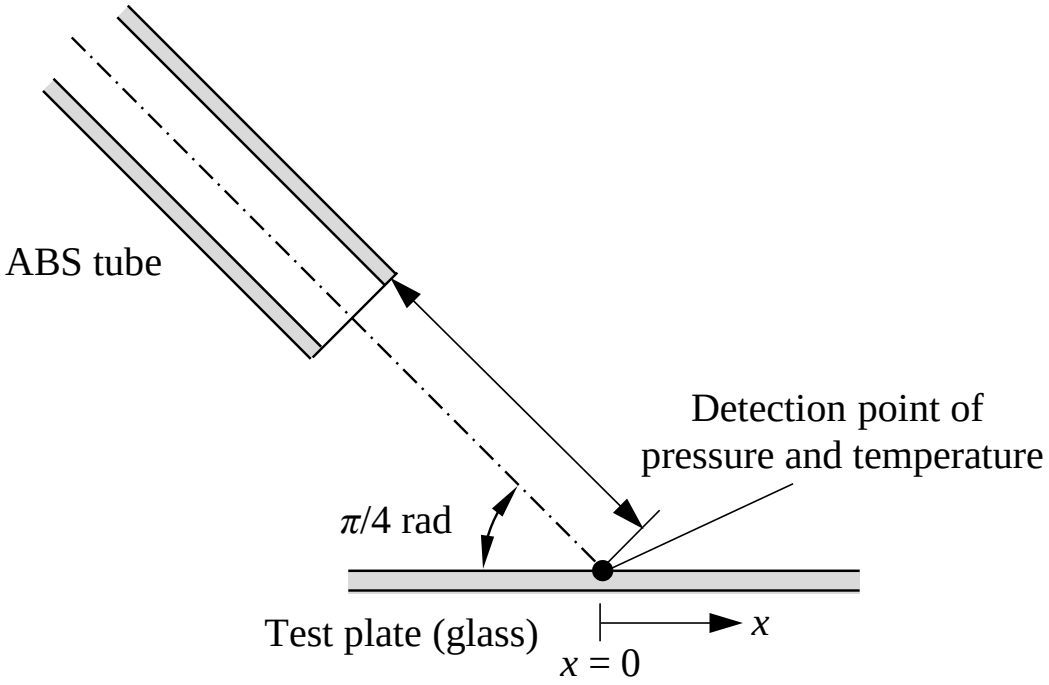

Figure 4.3 Details of ABS tube and test plate.

the local pressure at the center of the surface, i.e., at the impingement point of the jet axis, was measured by a pressure sensor (AP-43, Keyence Corp.). A pressure tap of about 1 mm in diameter was installed at the test plate, and the pressure sensor was connected from behind. The temperature of the dry ice jet was also measured at the same position using a thermometer. Particle removal was observed from behind the test plate using a high-speed microscope camera (Fastcam-Max, Photron Ltd.). The efficiency of the removal of particulate contaminants was obtained by digital image analysis.

All the experiments were conducted at room conditions (temperature: 25 ± 2 °C; RH: 40–60%).

4.3 Results and discussion

4.3.1 Local pressure on surface

Figure 4.4 shows the local pressure at the impingement point of the jet axis as a function of the mass flow rate of the dry ice jet and air jet. To observe the variation of the particle removal efficiency in detail, low mass rates were used. The pressures were measured under steady state conditions with flow temperatures of 25 °C and about −70 °C for the air jet and dry ice jet, respectively. The local pressure increased with the mass flow rate, and the results for both the air and dry ice jets are similar. Since the local pressure correlates with the mass flow rate of the jet flow, the local pressure can be used to evaluate the strength of the jet flow.

4.3.2 Effective cleaning area

To investigate the particle removal efficiency, test plates contaminated with monosized latex particles were cleaned by the dry ice jet. The removal efficiency, η, is defined by

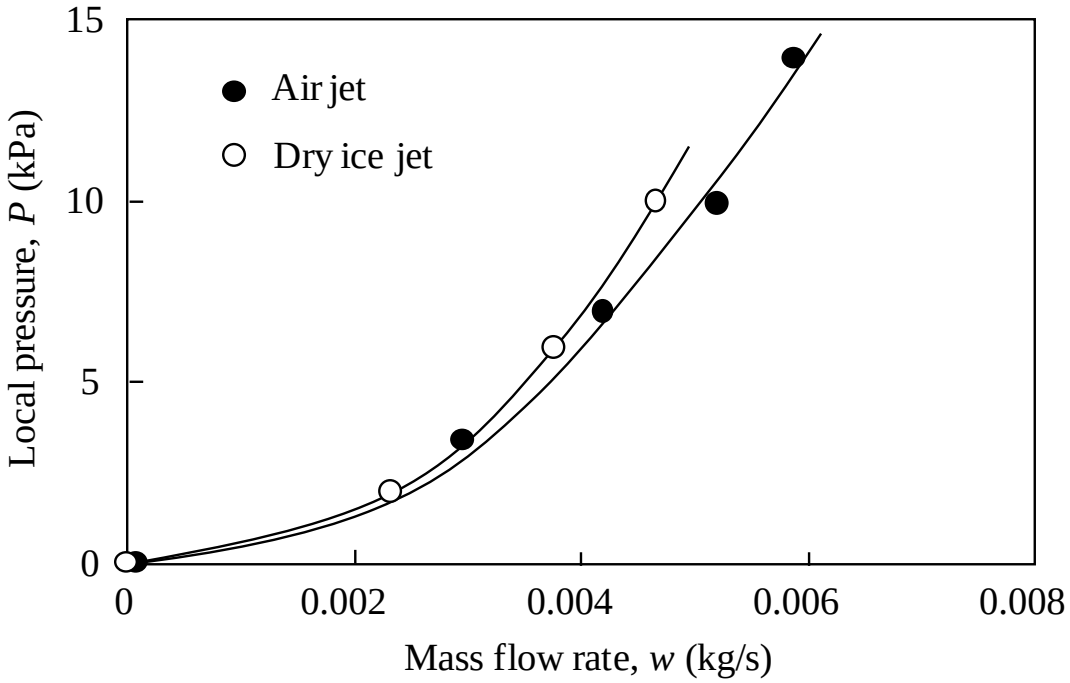

Figure 4.4 Local pressures of jet flows at the center of the test plate.

$$\eta = \frac{N_0 - N_r}{N_0}, \tag{4.2}$$

where N_0 is the initial number of particulate contaminants adhering to the test plate and N_r is the number of the residual particulate contaminants.

Figure 4.5 shows the efficiency of the removal of 2.92-μm particulate contaminants as a parameter of the local pressure. In this experiment, the duration of dry ice blasting was set at 10 s. The particulate contaminants were completely removed at the center of the plate and downstream; however, the removal efficiency decreased at a point 15 mm from the center toward the opposite side, and reached zero at $x = -25$ mm. The effective removal area increased with an increase in the local pressure. Although the experiments were conducted under different RHs in a range of 40–60%, there was no effect of the RH on removal efficiency.

An experiment to remove 0.75-μm particulate contaminants was also carried out. The results are shown in Fig. 4.6. Although the removal efficiency was lower than that for the 2.92-μm particulate contaminants, common characteristic features were evident, i.e., the removal efficiency was high downstream but low on the opposite side. Since submicron-sized contaminants are more difficult to remove from the surface, a higher local pressure was required to increase the removal efficiency.

4.3.3 Time-dependent particle removal efficiency

Figure 4.7 shows the time course of the efficiency of the removal of 2.92-μm particulate contaminants adhering to the center of the surface. The onset time ($t = 0$) is the time at which the valve is opened. When using dry ice blasting, particle removal begins after a delay of a few seconds after starting the experiment, and the removal efficiency increases as time elapses. In addition, the particle removal efficiency quickly increases with increased in the local pressure. The median values of the time to remove the contaminants at local pressures of 2, 6, and 10 kPa were 2.2, 1.6, and 0.9 s, respectively. As the local pressure increases, the aerodynamic drag force acting on the

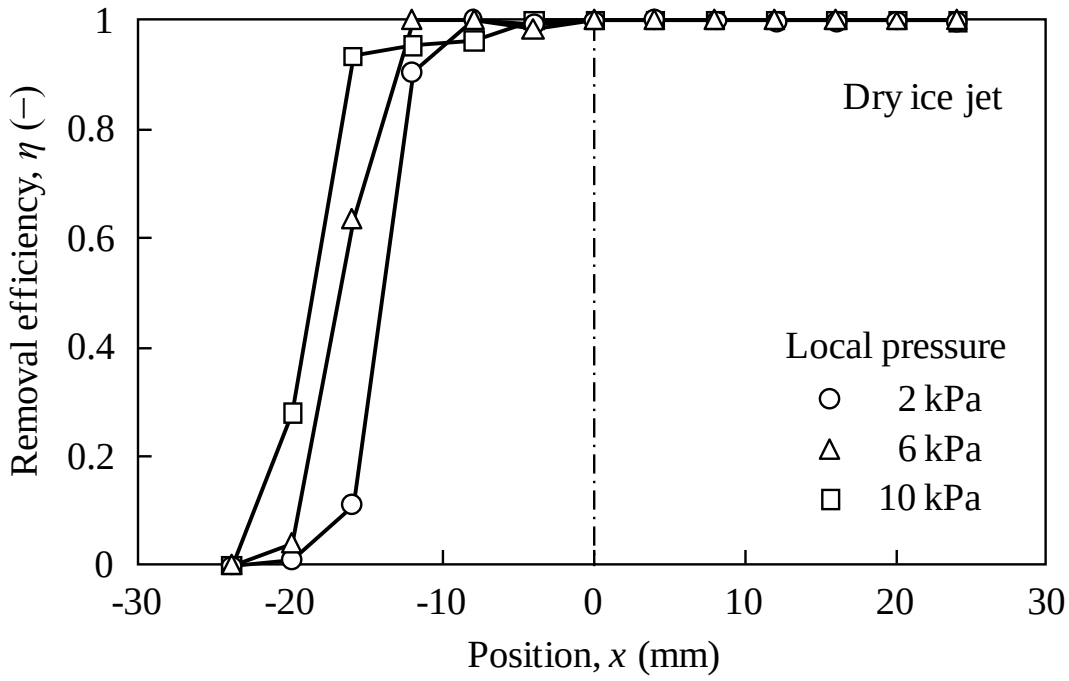

Figure 4.5 Removal efficiency profile for D_{p2} = 2.92 μm (the origin is the impinging point).

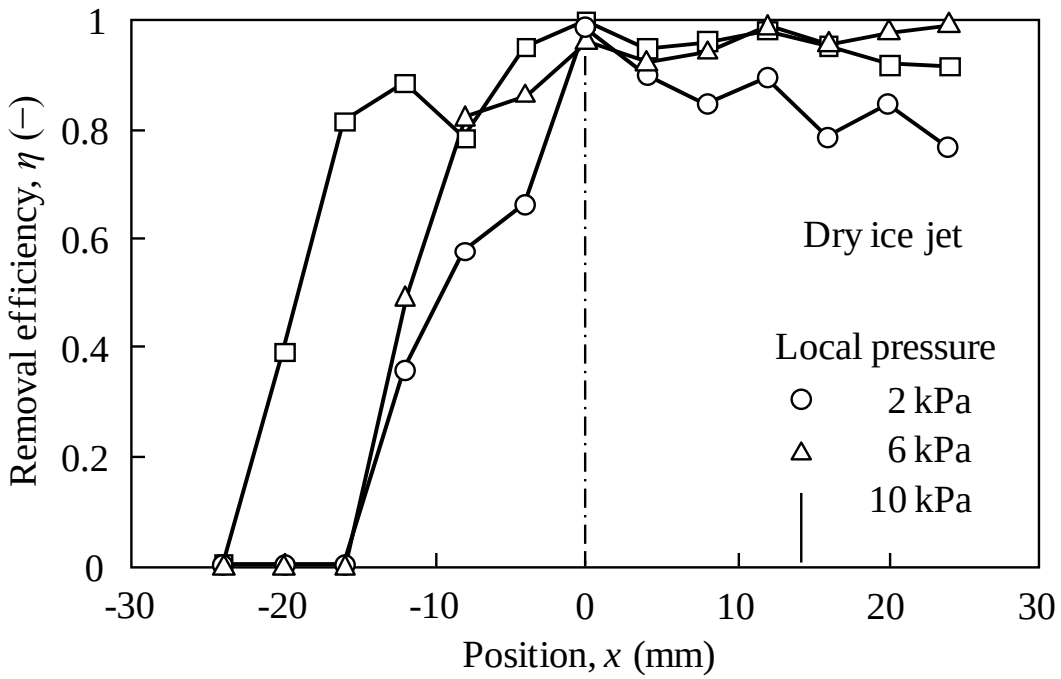

Figure 4.6 Removal efficiency profile for D_{p2} = 0.75 μm (the origin is the impinging point).

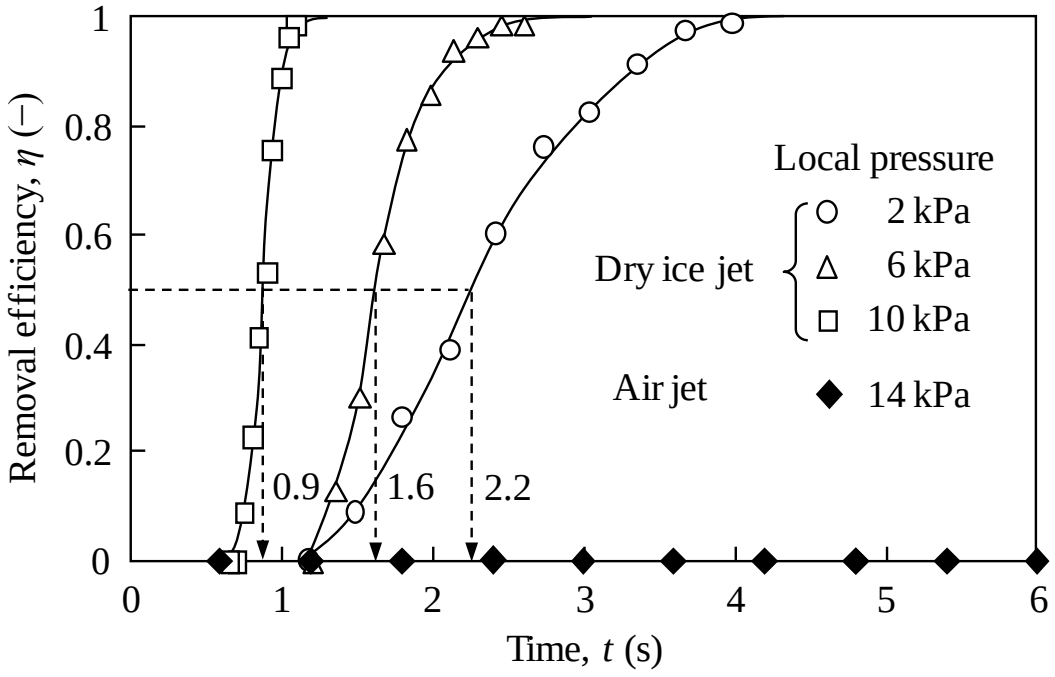

Figure 4.7 Time course of particle removal efficiency for D_{p2} = 2.92 μm.

contaminants also increases; however, the drag force is not a main factor in the removal of the particles. This is evident in that the air jet is not effective for particle removal even though the local pressure is higher for the air jet than that for the dry ice jet, as shown in Fig. 4.7. The dry ice jet has a gas-solid two-phase flow; thus, the impact force between the dry ice particles and the contaminants is important for particle removal. In addition, the low temperature of the dry ice jet will cause the decrease of relative humidity, reducing the effect of liquid bridge force. If the temperature is sufficiently low, the liquid bridge force will further be changed into the interaction force between solids with the ice; therefore, the adhesion force will also be affected.

Figure 4.8 shows the experimental results for the 0.75-μm particulate contaminants. The dry ice jet can remove even submicron-sized particles; however, the time to remove them is longer than that for the 2.92-μm particulate contaminants. The median values of the time required to remove the 0.75-μm particles at the local pressures of 2, 6, and 10 kPa were 9.2, 7.5, and 6.1 s, respectively. The median time for removal is an important factor in evaluating dry ice cleaning. To elucidate the time dependence, the state of the dry ice jet flow as well as the conditions of the contaminants must be discussed. Since the state of the dry ice jet varies according to the temperature, the time-dependency of the temperature must be determined.

4.3.4 Temperature of the dry ice jet

The CO_2 exists as a gas at room conditions; however, as liquid CO_2 expands to atmospheric pressure, the temperature of the jet flow decreases and dry ice particles are produced. Therefore, the state of the dry ice particles in the jet flow is strongly related to the temperature and pressure. Figure 4.9 shows the time course of the temperature of the dry ice jet over which the temperature decreases from room temperature to about −70 °C. In this experiment, there were two stages of temperature reduction. A similar tendency was reported in the experimental results of Chapter 2. After the second temperature decrease, many agglomerated dry ice particles were produced in the jet flow. Since these experiments were conducted at rather low mass flow rates, the temperature decrease can be clearly observed. At a higher local pressure, the

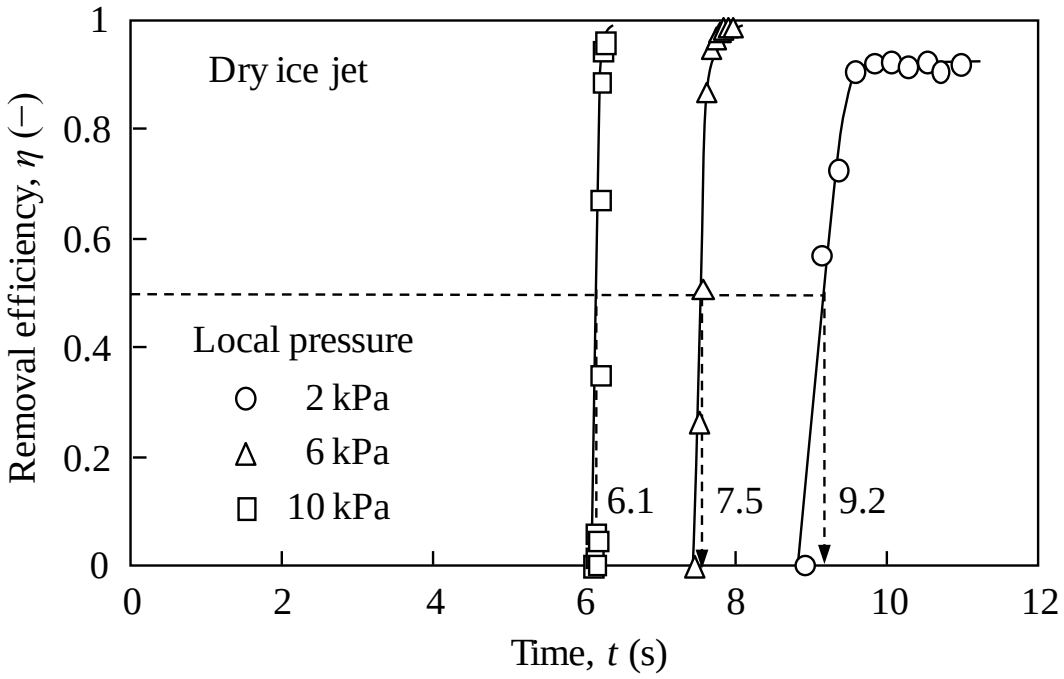

Figure 4.8 Time course of particle removal efficiency for D_{p2} = 0.75 μm.

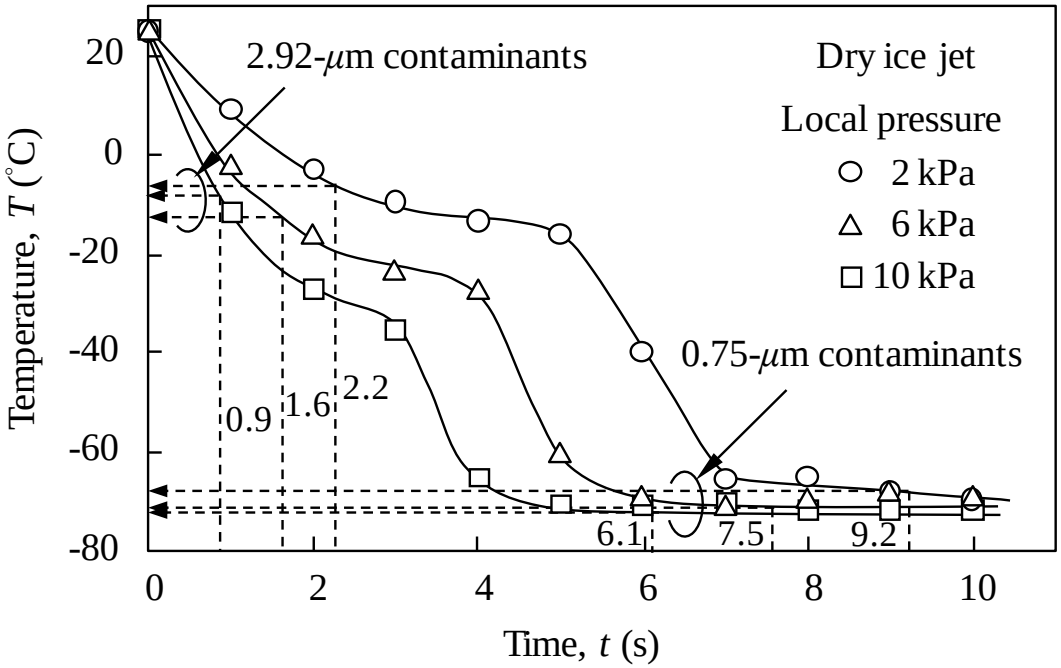

Figure 4.9 Temperature of dry ice jet.

temperature quickly decreases because large amounts of liquid carbon dioxide expand resulting in efficient cooling of the jet flow. Therefore, dry ice particles are more quickly produced at higher local pressures; the collisions of the dry ice particles with the contaminants will enhance the removal efficiency. In addition, the adhesion force between the contaminants and the surface can be affected by the temperature. If water molecules accumulate at the contact point at room temperature and a liquid bridge is formed, the contaminants experience a liquid bridge force in addition to the van der Waals force. When the temperature is sufficiently decreased by the dry ice jet, the water will freeze, and the liquid bridge force will be changed into the interaction force between solids with the ice. This phenomenon will also affect the removal efficiency.

To correlate the temperature with the particle removal efficiency, the median values of the time to remove the contaminants (Figs. 4.7 and 4.8) are added into Figure 4.9. The temperatures for the removal of the 2.92-μm and 0.75-μm contaminants were about −10 °C and −70 °C, respectively. Therefore, the time dependency of the removal can be well explained by the temperature variation of the dry ice jet.

4.3.5 Particle removal rate

A normalized particle removal rate is obtained by differentiating the particle removal efficiency with respect to time. The rates for the removal of 2.92- and 0.75-μm particulate contaminants at half removal efficiency are shown in Fig. 4.10.

The removal rate increases with increases in the local pressure. This is a natural consequence of the increase in the strength of the jet flow. In addition, this figure shows that the removal rate for 0.75-μm particles is much higher than that for 2.92-μm particles. The difference caused by the contaminant size can be explained as follows. Submicron-sized contaminants are more difficult to remove than micron-sized contaminants; thus, removal of the submicron-sized contaminants occurs at lower temperatures at which a larger number of agglomerated dry ice particles are formed to collide with the contaminants. The impact force will be enhanced with an increase in the inertia of the agglomerated dry ice particles. In addition, they do not sublimate as

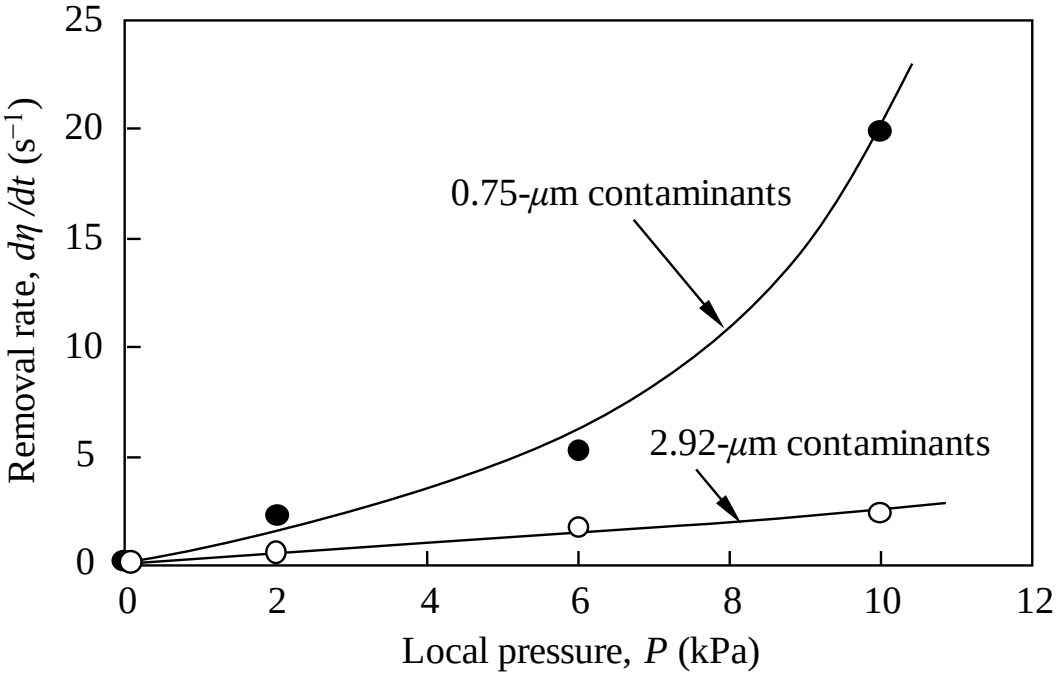

Figure 4.10 Particle removal rate by dry ice blasting.

quickly as smaller dry ice particles and are therefore more effective for particle removal. On the other hand, micron-sized contaminants can be removed at a higher temperature than submicron-sized contaminants. Under these conditions, the lack of agglomerated dry ice particles would result in a lower removal rate.

4.3.6 Effect of the impact of dry ice particles on particulate contaminant removal

When applying gas-solid two-phase flow to surface cleaning, particulate contaminants on the surface experience both an aerodynamic drag force and an impact force of the airborne particles. To elucidate the mechanism of particle removal, a moment balance model can be applied (see Fig. 4.1). Three moments of force, M_a caused by adhesion force (F_a), M_c caused by the impact of the dry ice particle (F_c) and M_d caused by the aerodynamic drag (F_d), are generally taken into account in the model. The three moments are presented as

$$M_a = F_a \sin\theta \frac{D_{p2}}{2}, \tag{4.3}$$

$$M_c = F_c \left(\cos\phi \cos\theta - \sin\phi \sin\theta\right) \frac{D_{p2}}{2}, \tag{4.4}$$

and

$$M_d = F_d \cos\theta \frac{D_{p2}}{2} + M_t, \tag{4.5}$$

where D_{p2} is the particle diameter of the contaminant adhering to the surface, M_t is the moment about the center of mass of the particle caused by the shear flow, θ is the contact angle of the contaminant, and ϕ is the impact angle. The contact angle (θ) can be calculated using the JKR theory (see Appendix (A)).

The adhesion force, F_a, is then given according to the JKR theory.

$$F_a = \frac{3}{4}\pi W_{23} D_{p2}, \tag{4.6}$$

where W_{23} is the surface energy per unit area of two materials.

The impact force, F_c, is given by

$$F_c = 1.12 k_{12}^{-2/5} m^{3/5} D^{1/5} v^{6/5}, \tag{4.7}$$

where k_{12} is the elastic characteristic of two materials, m is the reduced mass ($= m_1 m_2 /(m_1 + m_2)$), D is the reduced particle diameter ($= D_{p1} D_{p2} /(D_{p1} + D_{p2})$), and v is the impact velocity [Timosenko and Goodier, 1970].

The drag force (F_d) is given by

$$F_d = \frac{3\pi f \mu u D_{p2}}{C_c}\left(1 + 0.15\,\mathrm{Re}_{p2}^{\,0.687}\right), \tag{4.8}$$

where f is the dimensionless coefficient, which is introduced to account for the wall effect, with a value of 1.7009 [O'Neill, 1968], μ is the fluid viscosity, u is the fluid velocity at the center of the contaminant (see Appendix (B)), Re_{p2} is the particle Reynolds number, and C_c is the Cunningham slip correction factor, which is given by

$$C_c = 1 + \frac{2\lambda}{D_{p2}}\left\{1.257 + 0.4\exp\left(\frac{-1.1 D_{p2}}{2\lambda}\right)\right\}, \tag{4.9}$$

where λ is the mean free path of CO_2.

The moment about the center of mass of the contaminant in the shear flow (M_t) (see Fig. 4.1) can be expressed as

$$M_t = \frac{2\pi g \mu u {D_{p2}}^2}{C_c}, \tag{4.10}$$

where g is the dimensionless coefficient, which is introduced to account for the wall effect, with a value of 0.944 [O'Neill, 1968]. The impact angle (ϕ) is fixed at $\pi/4$ radian taking into account the experimental conditions. To make a collision between two spherical particles at this impact angle, the diameters are geometrically restricted, i.e.,

$$D_{p1} \le \left(3 + 2\sqrt{2}\right) D_{p2}. \tag{4.11}$$

All the constants used in the calculation, which are based on the conditions of the experiments carried out under a local pressure of 10 kPa, are listed in Table 4.1.

Figure 4.11 shows the calculated results for the moments acting on the particulate contaminants as a function of the particle diameter of the dry ice, D_{p1}. For 2.92-μm particulate contaminant, as shown in Fig. 4.11 a, M_d is less than M_a in this calculated condition, showing that only the aerodynamic drag is not sufficient to remove the contaminant. However, M_c+M_d, which is shown in a dashed line, can exceed M_a. The result indicates that M_c is the dominant moment responsible for the particle removal. For the 0.75-μm particulate contaminant (see Fig. 4.11 b), the difference between M_a and M_d is larger, but the intersection of M_c+M_d and M_a is at smaller D_{p1}. This indicates M_c is more important for the removal of small particles.

Next, to evaluate the impact of a dry ice particle on the removal of a particulate contaminant, the moment ratio, r^*, is introduced:

$$r^* = \frac{M_c}{M_d}. \tag{4.12}$$

Figure 4.12 shows the relationship between the calculated moment ratio (r^*) and the particle diameter of the dry ice, D_{p1}, as a parameter of the particle diameter of the contaminants, D_{p2}. The calculated results for the 2.92-μm and 0.75-μm particulate contaminants are indicated by a dotted line and broken line, respectively. The moment ratio (r^*) increases with increasing particle diameter (D_{p1}) with decreasing particle diameter (D_{p2}). Here, it is worth noting that the collision of the dry ice particles with the contaminant particles is much more effective for their removal than the aerodynamic drag. The particle diameter of the agglomerated dry ice measured in-situ by a laser diffraction method was several tens of micrometers. Therefore, the impact force is particularly significant for removing small particles.

Table 4.1 Constants used in theoretical calculation.

ϕ	(impact angle)	= π/4 radian
v	(impact velocity of dry ice particle)	= 41 m s^{-1}
ρ_1	(density of dry ice)	= 1.6×10^{3} kg m^{-3}
ρ_2	(density of polystyrene)	= 1.1×10^{3} kg m^{-3}
k_{12}	(elastic characteristic)	= 3.3×10^{-10} Pa^{-1}
k_{23}	(elastic characteristic)	= 2.5×10^{-10} Pa^{-1}
W_{23}	(surface energy per unit area)	= 2.4×10^{-2} J m^{-2}
μ	(viscosity of fluid at -78 ^{o}C)	= 7×10^{-5} Pa s
u_0	(core velocity of dry ice jet)	= 41 m s^{-1}
ρ	(density of fluid at -78 ^{o}C)	= 2.8 kg m^{-3}
λ	(mean free path at -78 ^{o}C)	= 2.8×10^{-8} m
γ	(solid-to-gas mass flow ratio)	= 0.43

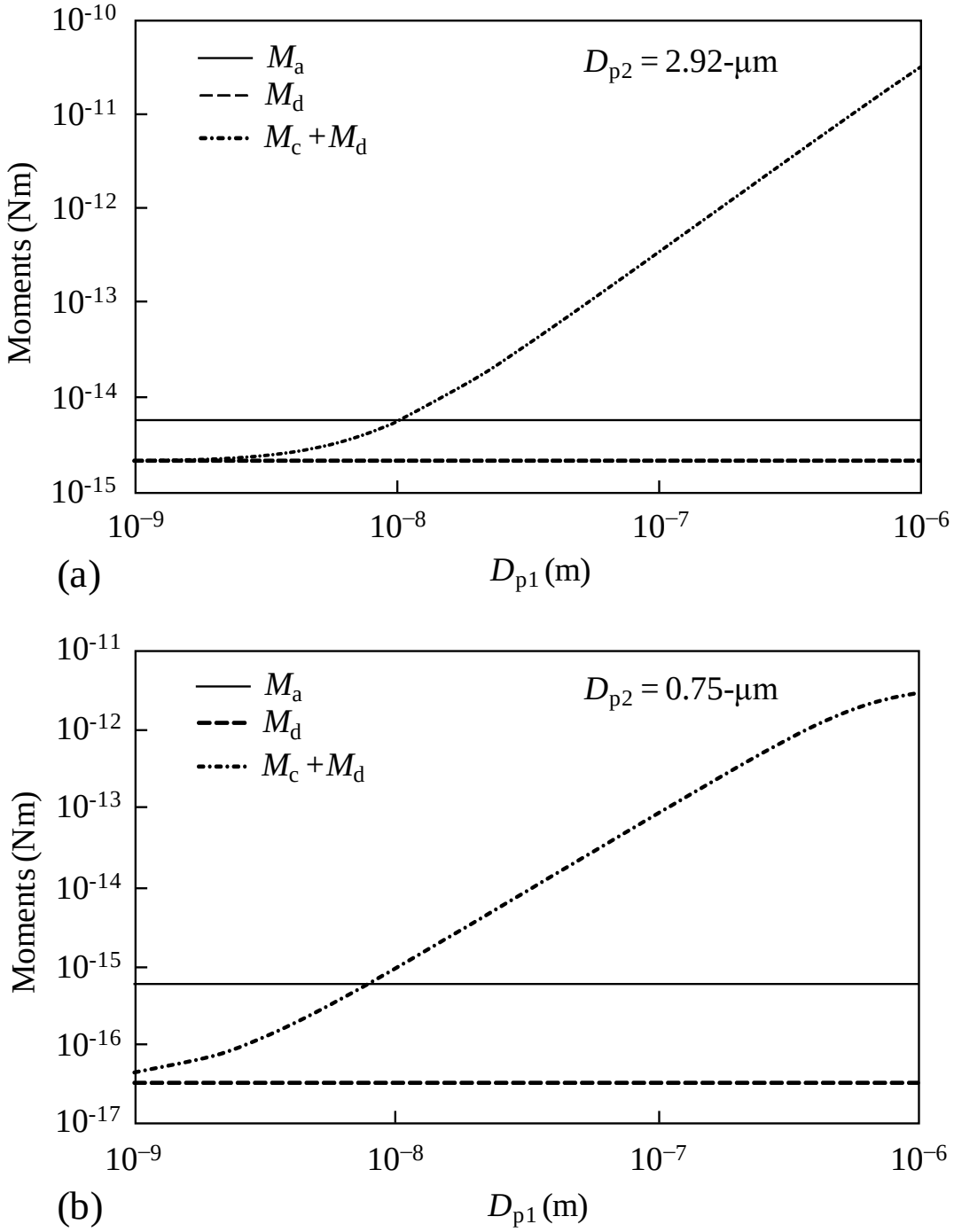

Figure 4.11 Moments acting on the particles adhering to the surface.

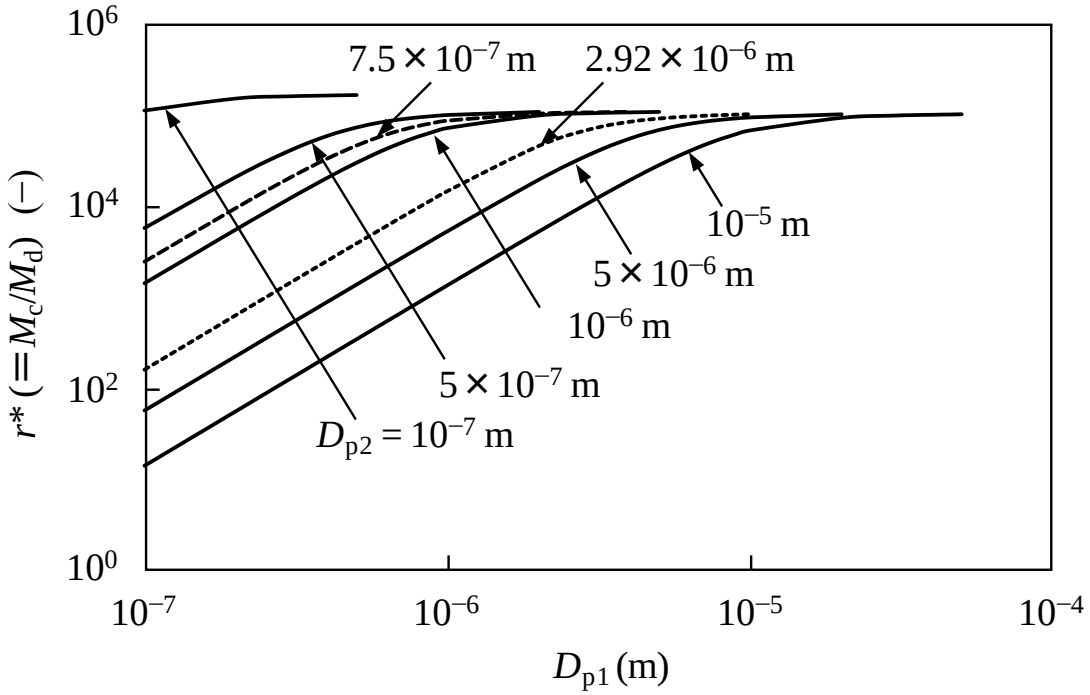

Figure 4.12 Effect of particle impact on particle removal.

4.4 Conclusions

The removal of particulate contaminants by dry ice blasting has been investigated. In this experiment, in-situ observation of the removal process was carried out and the time course of the particle removal efficiency was obtained. To explain the removal process, the temperature of the dry ice jet was measured and the mechanism for the removal of the contaminants was discussed based on calculated and experimental results. The conclusions were drawn as follows:

(1) The effective surface cleaning area and particle removal efficiency depend on the strength of the dry ice jet, which was evaluated by the local pressure on the surface. To remove submicron-sized contaminants, high local pressure is required. With the air jet, small contaminants are difficult to remove even at higher local pressures. This means that the effectiveness of particle removal by dry ice blasting is attributed to the collision of the dry ice particles with the contaminants.

(2) The particle removal efficiency of dry ice blasting increases with elapsed time, while the temperature of the jet flow decreases with elapsed time. By linking these results, the micron-sized particles are removed at about −10 °C and the submicron-sized particles are removed at about −70 °C irrespective of the local pressure. Therefore, the particle removal efficiency is closely related to the temperature of the jet flow. Since a large amount of agglomerated dry-ice particles formed at −70 °C, the submicron-sized particles were removed by the collision of the agglomerated dry ice particles.

(3) The particle removal rate obtained by differentiating the particle removal efficiency with respect to time can also be explained by the collision of dry ice particles with the contaminants. The high removal rate for submicron particles in the low jet temperature condition demonstrates the effect impact of the dry ice agglomerates.

(4) A particle removal model based on the moment balance theory was applied to the dry ice blasting system and the theoretical calculation result verifies the dominance of the impact effect of dry ice particles.

Chapter 5
Particle Removal Process during Impinging Dry Ice Jet Application

5.1 Introduction

As discussed in Chapter 4, dry ice blasting has shown good performance for the removal of monosized fine particles. The effect of dry ice impact is relatively larger than the aerodynamic drag during the removal. According to the experimental results, larger particles can be removed at the earlier stage of dry ice blasting, where the jet temperature is still around −10 °C. This indicates that fine particles with small adhesive force will be removed mainly by the aerodynamic force or impact force caused by the dry ice particles of small inertia. In other words, the impact force caused by the dry ice particles of large inertia is necessary for the removal of fine particles whose adhesive force is large. These two kinds of particle removal phenomena will occur in a real cleaning system because the fine particles generally differ in their adhesive forces, i.e. there is a distribution of the adhesive forces for the particles. To approach the real application of dry ice blasting, the removal process of fine particles having a size distribution is worth investigating.

The purpose of the study in this chapter is to clarify the particle removal process of polydisperse powder particles by applying the impinging dry ice jet. Substrates covered with powder particles are used for the investigation, and the time course of particle removal efficiency is taken into consideration. The experimental results are analyzed with a theoretical model. In addition, according to the results of the jet temperature effect on the state of dry ice particles, mentioned in Chapter 4, a relationship between the particle removal efficiency and the jet temperature should be discussed. Furthermore, the particle removal area caused by a dry ice impact and the removal frequency are evaluated through the in-situ observation of the removal process. Based on the experimental results, a system parameter is proposed to determine the optimum jet flow rate for efficient particle removal.

5.2 Material and methods

As a preliminary experiment for visualizing the surface cleaning, black resin (synthetic acrylic resin) dissolved in organic liquid was sprayed vertically on a test plate (76 × 26 mm; 1-mm thick transparent glass). Before the experiment of dry ice blasting onto the test plate was carried out, the resin was dried at room conditions for 1500 s until it formed a solid film. The average thickness of the film was 45 μm.

For particle removal, powder particles were dispersed and deposited on the test plate; subsequently, experiments were conducted to remove the particles from the surface by dry ice blasting. To observe the removal process, the test plate was covered with a large number of powder particles.

5.2.1 Deposition of particulate contaminants

Figure 5.1 shows a schematic diagram of the experimental apparatus to deposit the powder particles. The test plate was placed on a metal mesh in a cylindrical vessel. Spherical alumina particles with a mass median diameter of 3 μm and geometric standard deviation of 1.4 were dispersed using an ejector for 1 s. To control the air flow in the vessel, secondary air was introduced. The amount of particles deposited on the test plate was controlled by the air flow condition.

5.2.2 Removal of particulate contaminants

Figure 5.2 shows a schematic diagram of the experimental apparatus to remove the powder particles from the test plate surface by dry ice blasting. The dry ice jet was produced by expanding high purity liquid carbon dioxide. A flexible hose made of stainless steel—2 m in length and 15 mm in inner diameter—was connected to a high-pressure carbon dioxide cylinder. At the end of the hose, a needle valve was installed in order to adjust the flow rate of the dry ice jet. A pressure gauge was also installed at the inlet of the needle valve in order to measure the inner pressure of the liquid carbon dioxide. The pressure measured in the experiments was approximately 5.5 MPa. To reduce heat transfers between the environment and equipment, the flexible hose and needle valve were thermally insulated. Further, to produce agglomerated dry

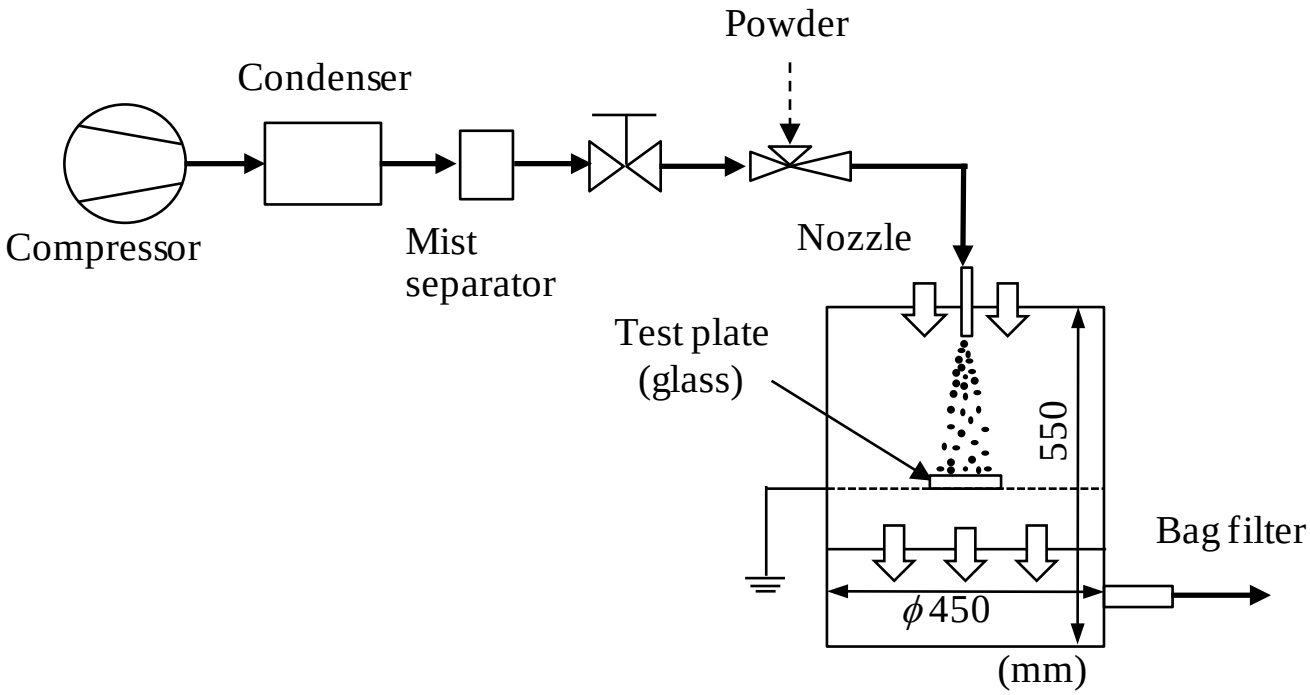

Figure 5.1 Preparation of test plate.

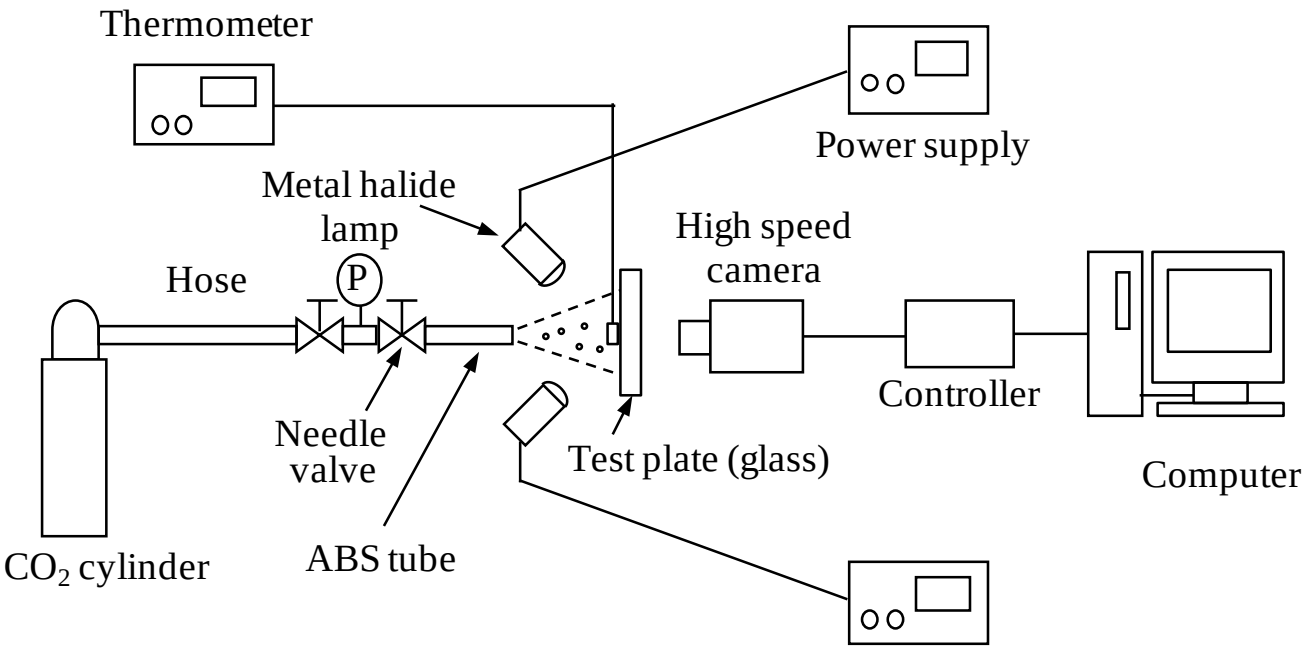

Figure 5.2 Experimental apparatus.

ice particles, a 50-mm long acrylonitrile-butadiene-styrene (ABS) tube with 6-mm inner diameter was installed at the end of the needle valve. Agglomerated dry ice particles ejected from the tube with the carbon dioxide gas were directed toward the test plate. The angle of incidence of the dry ice jet against the surface was $\pi/4$ radian, and the distance from the tip of the tube to the test plate was 20 mm in the axial direction.

To measure the temperature of the impinging dry ice jet, a temperature sensor was installed around the stagnant point. The particle removal process was observed from behind the test plate using a high-speed microscope camera (Fastcam–Max, Photron Ltd.). The frame rate in the experiments was 250 or 500 fps. All the experiments were conducted at 20 ± 2 ºC, and the relative humidity was controlled at 20–40% to avoid disturbances caused by liquid bridge forces.

5.2.3 Analysis method

To quantitatively analyze the particle removal process, particle removal efficiency, removal area, and removal frequency were obtained from the images captured by the high-speed microscope camera. The particle removal efficiency was determined by two methods—digital counting of the number of particles remaining on the surface and measuring the image brightness. The latter method was used in cases where the digital counting was difficult, for example, when the surface was completely covered with the powder particles. The removal area caused by a dry ice impact was determined from the equivalent circle diameter. The removal frequency was determined from the variations in the removal efficiency at intervals of 2 ms.

5.3 Results and discussion

5.3.1 Visualization of the particle impact caused by the dry ice jet

As mentioned in Chapter 4, the impact effect of the dry ice particles dominates the removal efficiency. Thus, it is of interest to directly observe the particle impact on surface cleaning. To visualize surface cleaning, a black resin film was coated on a test plate by spraying and drying the solution; then, the surface cleaning experiment was

carried out. The angle of incidence was $\pi/4$ radian and the distance from the tip of the tube to the plate was 20 mm in the axial direction. To remove the black resin film, a higher flow velocity is needed; thus, narrow ABS tube with a 4 mm inner diameter was used. Although an air jet was not able to remove the resin film, a dry ice jet accomplished the removal. Figure 5.3 shows a series of microscopic images taken at intervals of 40 milliseconds. The observation point was about 1 mm from the impingement point along the flow direction. Due to the cooling of the resin film by the dry ice jet, a brittle fracture occurred in the film. The resin film was broken into small fragments by the impact of the dry ice particles and each fragment was removed from the plate. This phenomenon of particle impact will also occur for particle removal, even though the removal mechanism is different from the filmy contaminants.

5.3.2 Particle removal efficiency

Figure 5.4 shows micrographs of the particles on the test plate during dry ice blasting. When the jet flow rate was 1.4 g/s, most of the particles remained on the surface for approximately 8 s after the experiment began and were then almost completely removed within 0.2 s (Fig. 5.4 a). When the flow rate was 4.92 g/s, 20% of the particles were removed in the first 3 s, and the remaining particles were removed within 0.05 s (Fig. 5.4 b). These microscopic observations indicate that rapid particle removal begins with a time delay that decreases as the flow rate increases. The dry ice particles ejected from the tube can be visually observed after approximately 8 s and 3 s for jet flow rates of 1.4 g/s and 4.92 g/s, respectively. The rapid particle removal is probably caused by the visible dry ice particles.

Figure 5.5 shows the time courses of particle removal efficiency as a parameter of the jet flow rate. These results were obtained after digitally counting the number of particles remaining on the surface. When the jet flow rate was more than 2.2 g/s, the removal efficiency gradually increased with elapsed time and rapidly increased after a certain time is exceeded. Further, the maximum removal efficiency increased while the time needed to reach the maximum removal efficiency decreased as the jet flow rate

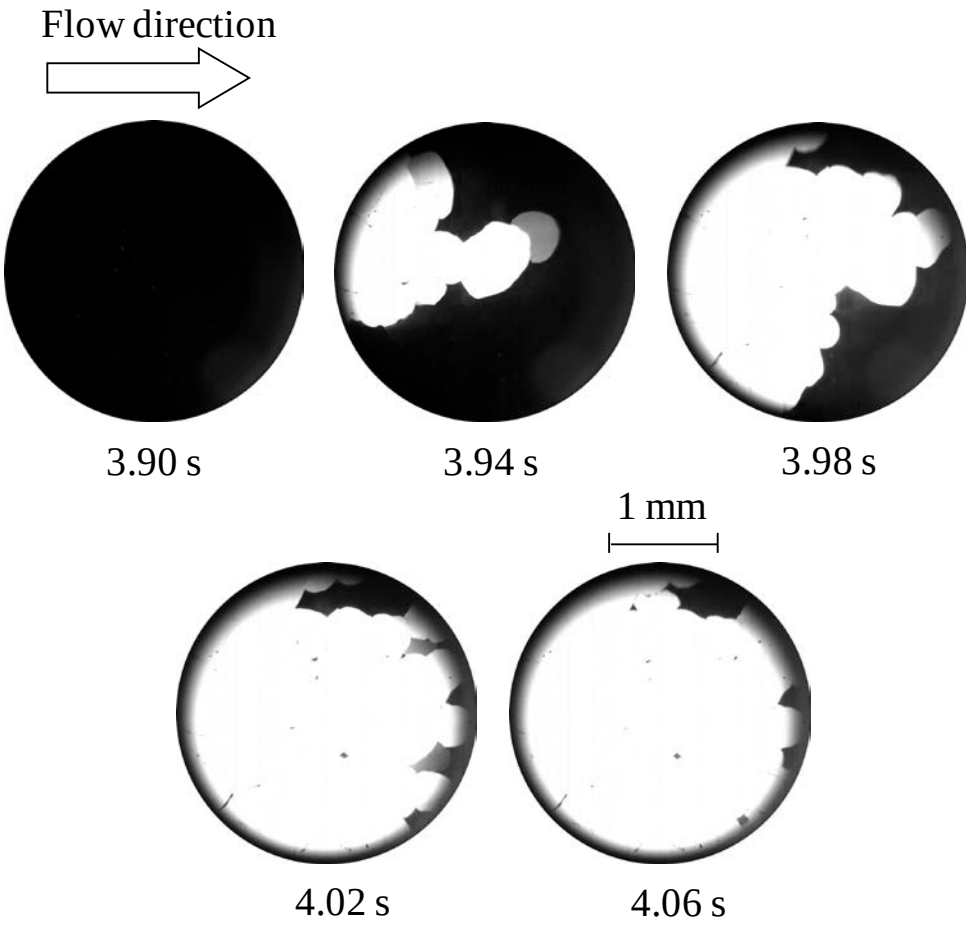

Figure 5.3 Visualization of impact effect of dry ice jet.

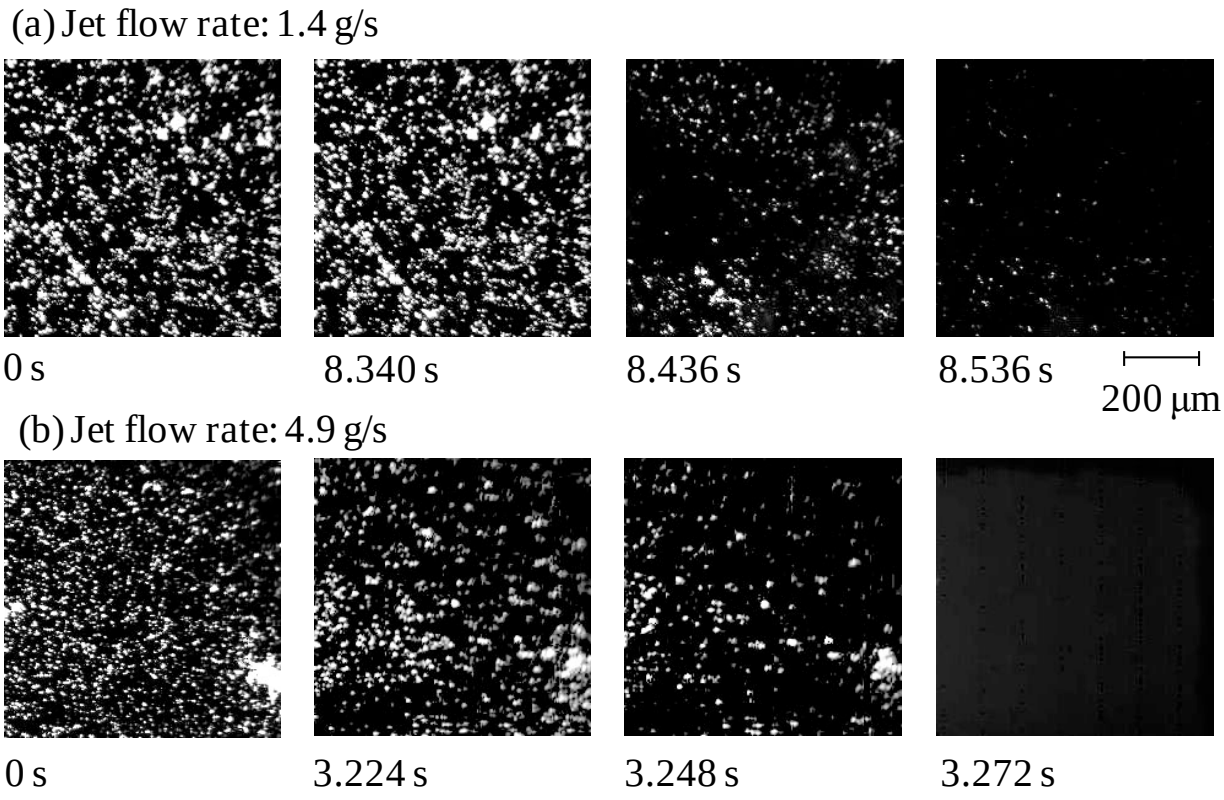

Figure 5.4 Micrographs of particle removal by dry ice blasting (frame rate: 250 fps).

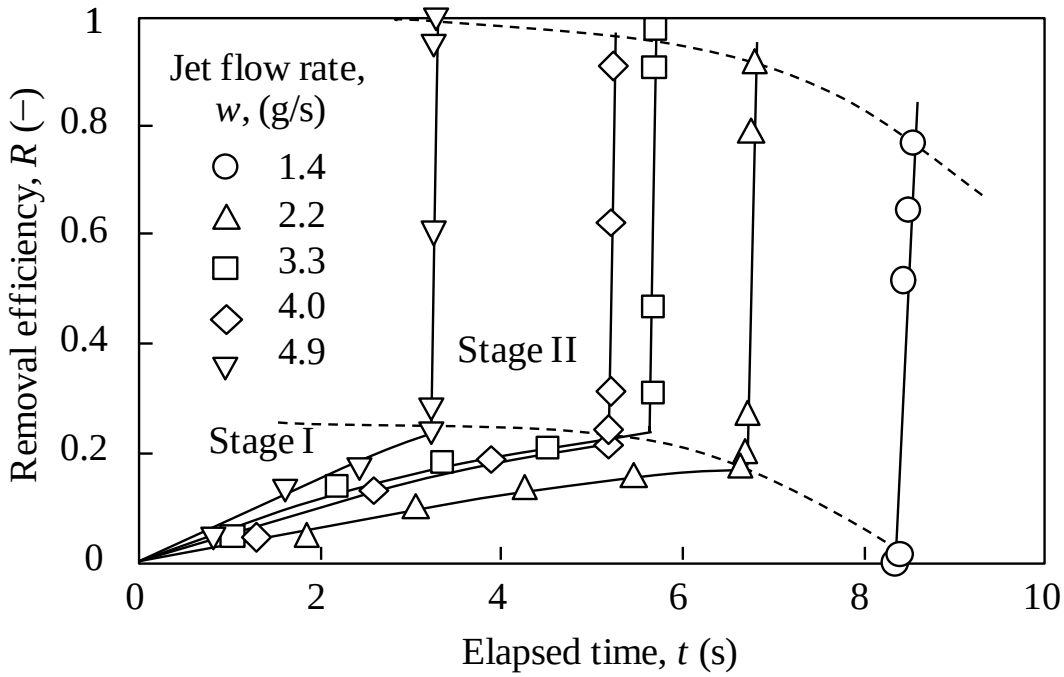

Figure 5.5 Time courses of particle removal efficiency.

increased; this was because the separation force acting on the particles adhering to the test plate increases with the mass flow rate. Figure 5.5 also shows that the removal process comprises two stages—stage I for slow particle removal and stage II for rapid particle removal.

5.3.3 Theoretical analysis for slow removal stage

When the separation force overcomes the adhesion force between the particles and surface, the particles will be removed from the surface. In fact, the adhesion force of each particle is not constant, and hence, the particle removal efficiency depends on the adhesive force distribution. It is noteworthy that the separation force caused by the dry ice blasting has temporal and special variations. Furthermore, the particle removal flux is proportional to the number density of the removable particles; therefore, the particle removal flux can be expressed as follows (Eq. 5.1):

$$\frac{-dN}{dt} = \frac{N - N_{\mathrm{u}}}{\tau} \ , \tag{5.1}$$

where N is the total number density of particles adhering to the surface; N_{u}, the number density of unremovable particles whose adhesion force is larger than the separation force; t, the elapsed time; and τ, a time constant. The analytical solution of Eq. (5.1) under the initial condition $N = N_0$ at $t = 0$ is given by

$$N - N_{\mathrm{u}} = (N_0 - N_{\mathrm{u}}) \exp(-\frac{t}{\tau}). \tag{5.2}$$

The particle removal efficiency $R = (N_0 - N)/N_0$ is expressed as

$$R = R_{\max(\mathrm{I})} \left[1 - \exp\left(-\frac{t}{\tau} \right) \right], \tag{5.3}$$

where $R_{max(I)} = (N_0 - N_u)/N_0$, i.e., the maximum removal efficiency at the slow removal stage.

Figure 5.6 shows the experimental and theoretical results calculated using Eq. (5.3) for the removal efficiency at the slow removal stage corresponding to the condition of $N_0 > N_u$. Since the experimental results are in agreement with the theoretical ones, the removal efficiency can be characterized by two parameters—maximum removal efficiency $R_{max(I)}$ and time constant τ—that vary with the jet flow rate.

Figure 5.7 shows the two parameters as a function of the jet flow rate. The estimated $R_{max(I)}$ increases with the jet flow rate, while τ decreases. These variations can be explained by the fact that the separation strength increases with the jet flow rate.

5.3.4 Temperature dependence of dry ice jet

Figure 5.8 shows the time courses of the temperature of dry ice jet as a parameter of the jet flow rate. There are two distinct temperature reduction stages—a slow temperature reduction stage from room temperature to –10 °C and a rapid temperature reduction stage from –10 to –70 °C. The dry ice jet became white after the second temperature reduction stage; this indicates that many agglomerated dry ice particles are produced and ejected. A similar phenomenon has been mentioned in Chapter 4. Further, at higher flow rates, the temperature decreases quickly because a large amount of liquid carbon dioxide is expanded, and the jet flow is cooled efficiently in the ABS tube. Therefore, the dry ice particles are produced more quickly at higher flow rates, and the subsequent agglomeration of the particles is enhanced. The effects of the temperature of the dry ice jet on the particle removal efficiency are shown in Fig. 5.9. When the jet temperature is in the range from room temperature to –70 °C, the particle removal efficiency is approximately 20% or less. Further, when the temperature reaches approximately –70 °C, the particle removal efficiency increases rapidly. Even if the temperature does not reach approximately –70 ^{o}C, small primary dry ice particles can be produced. However, the contaminant particles strongly adhering to the surface cannot be removed by the impacts of the small primary dry ice particles. When the jet temperature

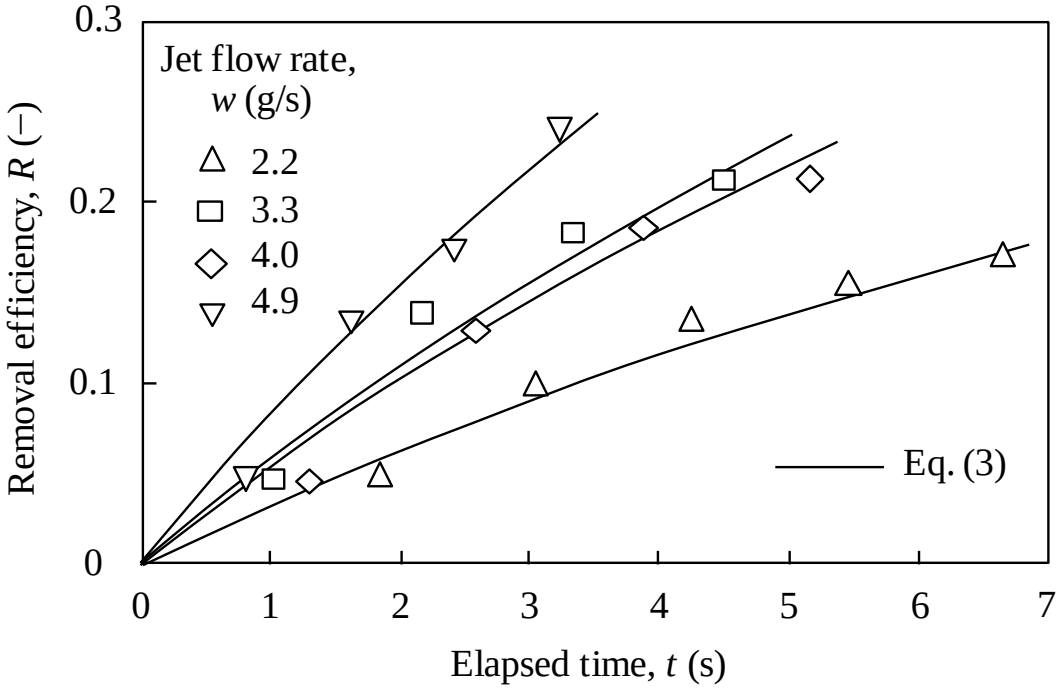

Figure 5.6 Theoretical estimation of particle removal efficiency.

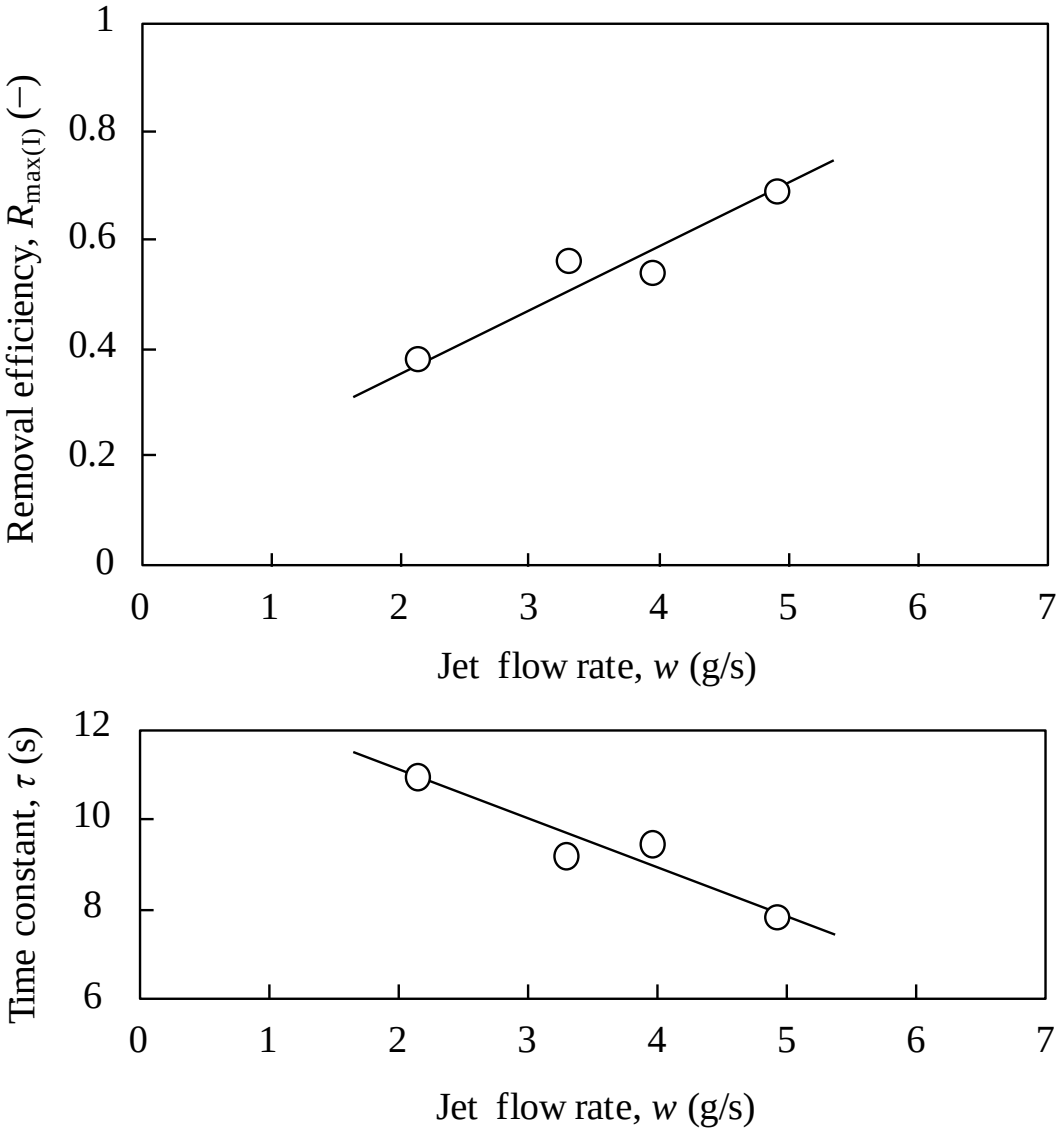

Figure 5.7 Values of fitting parameters $R_{max(I)}$ and τ in Eq. (5.3).

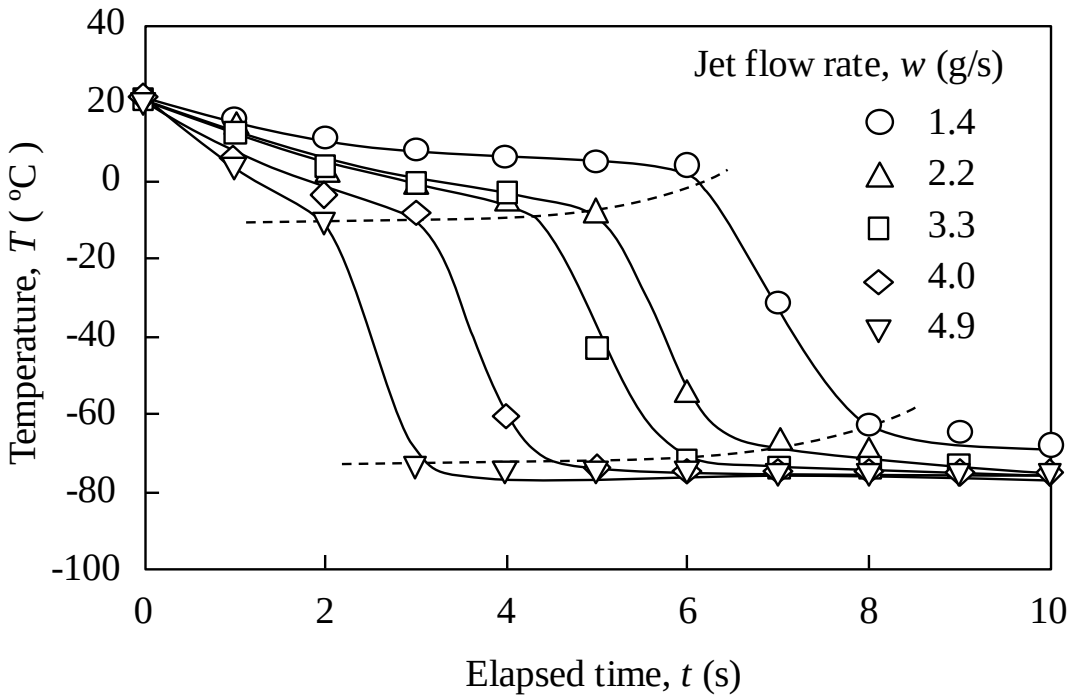

Figure 5.8 Time courses of temperature of dry ice jet.

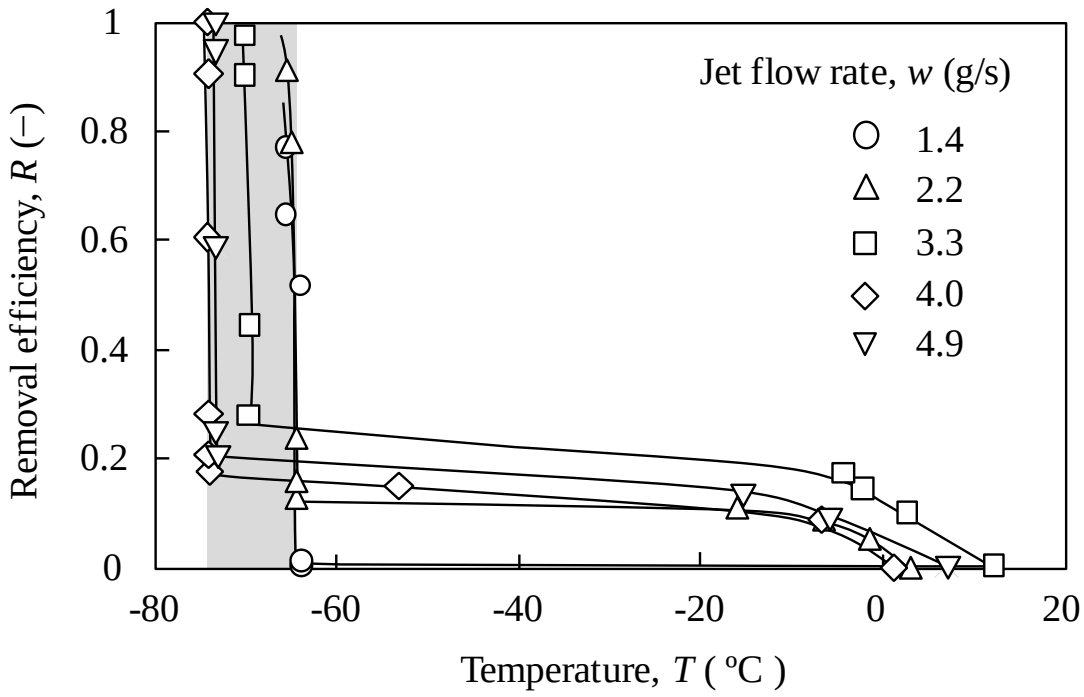

Figure 5.9 Relationship between particle removal efficiency and jet temperature.

reaches approximately –70 °C, many agglomerates of dry ice particles are produced and they can collide with the contaminant particles; consequently, most of the particles adhering to the surface are removed by the impact of the agglomerates of the dry ice particles. In this manner, the two stages of the particle removal process—slow and rapid particle removal stages—can be explained well by the variations in the jet temperature.

5.3.5 Removal area and frequency at rapid removal stage

Most of the contaminant particles are removed at the rapid removal stage, and hence, the impact of agglomerates is very important for the particle removal. In this sub-section, the removal area caused by the impact of an agglomerate of dry ice particles and the removal frequency are discussed in detail.

Figure 5.10 shows a series of microscopic images of the test plate covered with powder particles during the rapid removal stage. The three typical images were taken at intervals of 2 ms using the high-speed microscope camera. In these images, the dry ice jet flows from left to right with an angle of $\pi/4$ radian against the surface. The powder particles on the test plate appear white whereas the test plate surface has a black appearance. Further, black spots appeared after the particles are removed from the surface by the impact of an agglomerate of dry ice particles. The images show that the number of black spots increased with elapsed time. Since the agglomerates of dry ice particles collided with the surface at a certain angle, the shape of the black spots tended to be elliptical. At the rapid removal stage, the equivalent circle diameter of most of the black spots was less than several hundred micrometers. Further, the mass median diameter of the contaminant particles was 3 μm; thus, many particles could be removed at the impact.

Figure 5.11 shows the distributions of the equivalent circle diameter of the removal area. These results were obtained from the experiments conducted at low jet flow rates, such as 1.4 and 2.2 g/s, where each removal area could be distinguished. The median values of the distribution were 40 and 25 μm at the jet flow rates of 1.4 and 2.2 g/s, respectively, or, in other words, the removal area decreases as the jet flow rate increases.

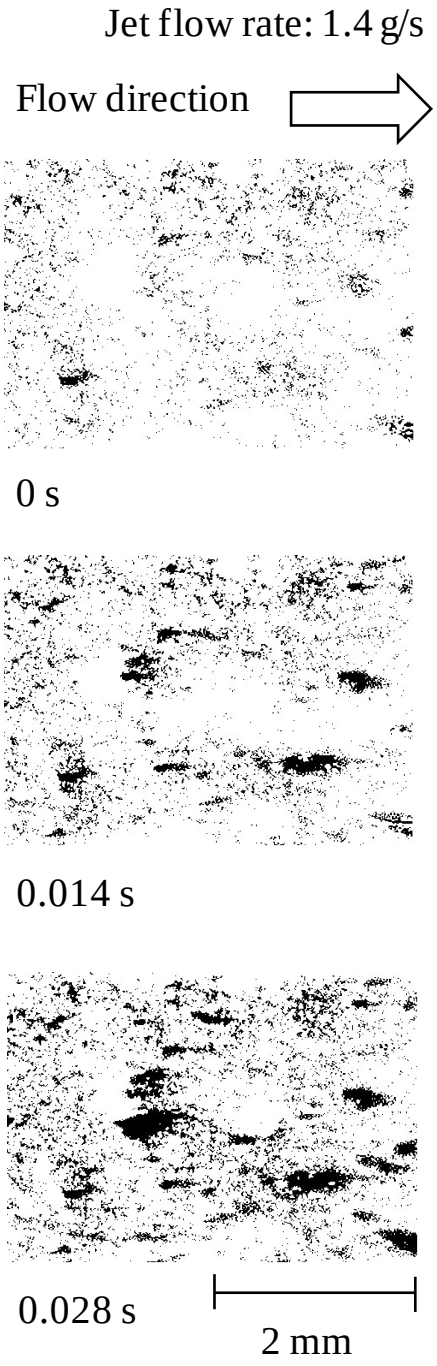

Figure 5.10 Micrographs of particle removal by dry ice impact at rapid removal stage (frame rate: 500 fps).

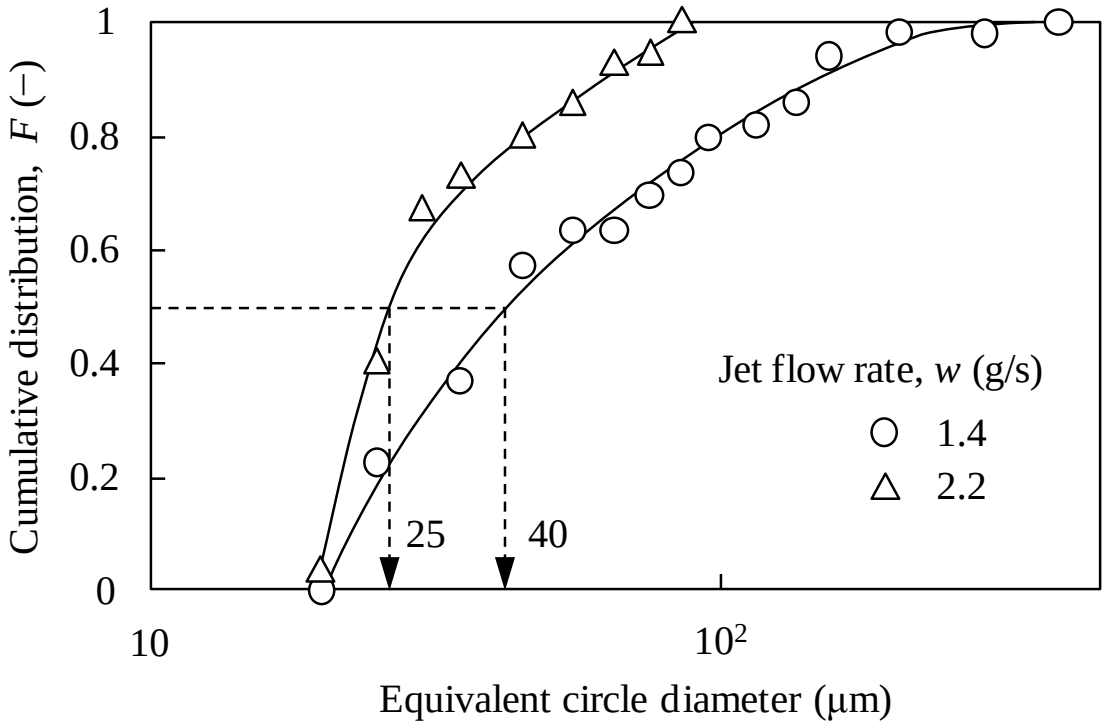

Figure 5.11 Cumulative distribution of removal area at rapid removal stage.

These results are in agreement with the fact that smaller agglomerates collide with the surface at higher flow rates. To quantitatively analyze the particle diameter of dry ice particles at the low jet flow rate, observation of the dry ice jet at 1.4 g/s was carried out by the high-speed microscope camera as well. The particle diameter of the agglomerated dry ice was found to be about 15 μm in equivalent circle diameter, with a solid-to-gas mass flow ratio of 0.43, which was obtained from the pressure-enthalpy diagram of CO_2 under the adiabatic expansion process of liquid CO_2. According to the results, the particle diameter of the agglomerated dry ice is smaller than equivalent circle diameter of the removal area observed, indicating that the agglomerates deformed and moved during their impact on the surface at the impinging angle.

The microscopic observations with the high-speed camera also give the removal frequency. When the jet flow rates were 1.4 and 2.2 g/s, the removal frequencies were 940 and 6780 Hz/mm^2, respectively. The removal frequency can be increased by increasing the concentration and velocity of the agglomerates of dry ice particles; the removal frequency thus increases with the jet flow rate.

Since the particle removal efficiency depends on both the removal area and frequency, the product of these factors should be considered for the evaluation of the particle removal. The removal area ratio was 0.39 (= $(25/40)^2$) at the jet flow rate of 2.2 to 1.4 g/s, while the frequency ratio was 7.2 (= 6780/940) under the same condition. Therefore, the effects of the jet flow rate on the removal area were opposite to those on the removal frequency. In this manner, the experimental results show that since the effects of removal frequency on particle removal are more significant, higher jet flow rates are more effective for the particle removal.

5.3.6 Evaluation of particle removal by dry ice jets

The particle removal frequency at the rapid removal stage under the conditions of higher jet flow rates is too high to analyze each particle removal even by using a high-speed micro camera. Hence, we measured the brightness of the images and analyzed the normalized particle removal efficiency R_{II} from 0 to 1 at each rapid

removal stage.

Figure 5.12 shows the time courses of the normalized particle removal efficiency R_{II} at the rapid removal stage as a parameter of the jet flow rate. R_{II} increases with the elapsed time, whereas the removal time needed to reach $R_{II} = 1$ decreases as the jet flow rate increases. When the jet flow rates are higher than 3.3 g/s, the removal time is less than 0.02 s.

To quantitatively evaluate the particle removal system using dry ice jets, we propose a system parameter η that is defined as follows:

$$\eta = \left(\frac{R'_{II50}}{w} \right), \tag{5.4}$$

where R'_{II50} is the derivative of R_{II} with respect to time at the median value and w is the jet flow rate. This parameter indicates the effect of the removal rate with consideration of the CO_2 consumption. Therefore a high value is preferred because a large amount of particles adhering to the surface can be removed with less CO_2 consumption.

Figure 5.13 shows the relationship between this system parameter η and the jet flow rate. η varies with the jet flow rate, and its value increases sharply after a certain jet flow rate is exceeded; however, the increase is limited at higher jet flow rates. Therefore, it is ineffective to excessively increase the jet flow rate. Further, this relationship can be used to determine the optimum jet flow rate for dry ice blasting.

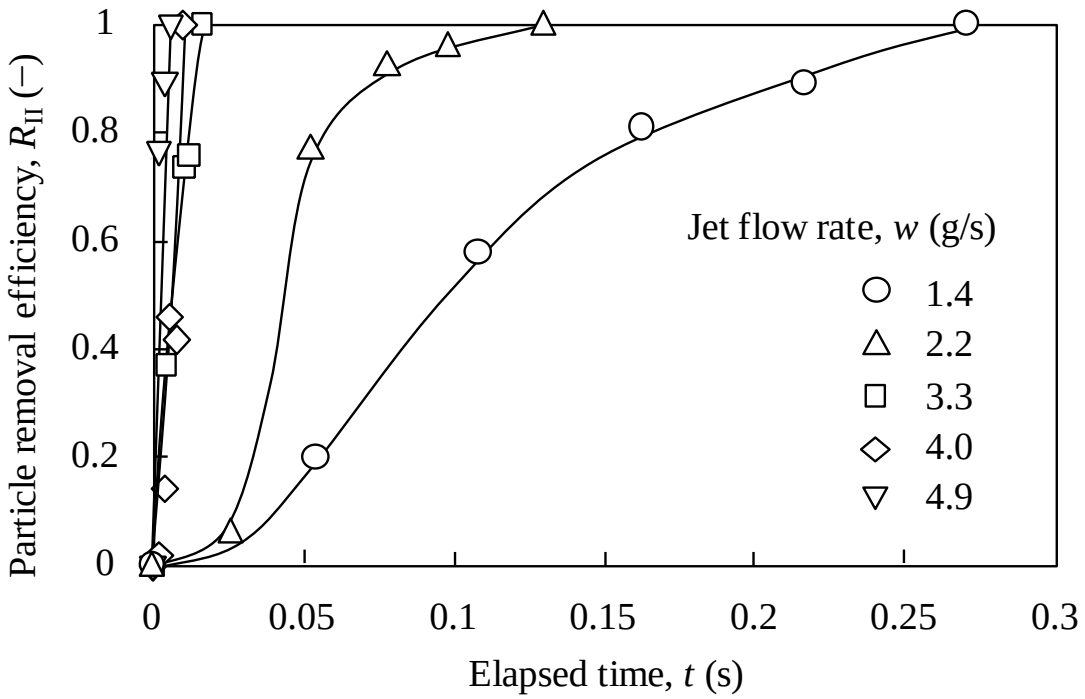

Figure 5.12 Normalized particle removal efficiency at rapid removal stage.

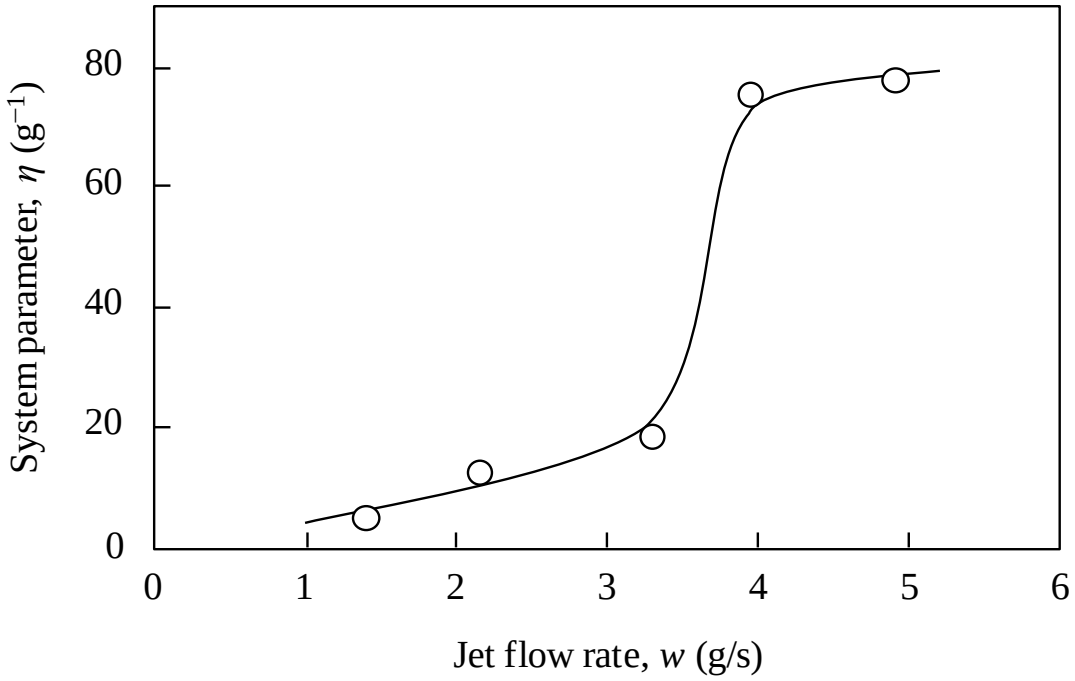

Figure 5.13 Impact efficiency of removal process.

5.4 Conclusions

In this study, we have investigated the removal process of fine particles adhering to the test plate using impinging dry ice jets. Further, by conducting quantitative analyses of the particle removal efficiency as a function of time elapsed and the variations in the temperature of the dry ice jet, the key factors for the particle removal processes were analyzed. The conclusions of the study can be summarized as follows:

(1) The impact effect of the dry ice jet can be visually observed by the removal of a resin film covering a surface. The resin film broke into small fragments and was then removed. This phenomenon will also occur in the particle removal process, even though the particle removal mechanism is different from the filmy contaminants.

(2) The particle removal process consists of two stages—slow removal stage and rapid removal stage—that are related to variations in the temperature of the dry ice jet.

(3) The slow removal stage occurs from room temperature to –70 °C, whereas the rapid removal stage occurs at approximately –70 °C; at this temperature, many agglomerates of dry ice particles are produced and collide with the contaminant particles.

(4) The particle removal efficiency at the slow removal stage can be explained by a theoretical equation with two parameters.

(5) Most of the contaminant particles on the surface are removed in the rapid removal stage; here, the key factors are the removal area due to the impact of an agglomerate of dry ice particles and the removal frequency. Moreover, as the jet flow rate increases, the removal area decreases, but the removal frequency increases. For the particle removal, the removal frequency is more significant than the removal area. Therefore, high jet flow rates are more effective for particle removal.

(6) A system parameter defined as the ratio of the particle removal rate to the jet flow rate can be used to quantitatively evaluate the particle removal and to determine the optimum jet flow rates for dry ice blasting.

Chapter 6
General Conclusions

In this dissertation, dry ice jet produced by expanding liquid CO_2 was extensively investigated through an in-situ observation and measurement. The dry ice particles in the jet flow were particularly focused and the research topics were mainly divided into i) fundamental investigation of the phenomena of particle production, growth, agglomeration, and sublimation in the dry ice jet flow, which were discussed in Chapter 2 and 3; and ii) the application for particle removal where the particle impact effect, removal mechanism and optimum flowing conditions were studied in detail and summarized in Chapter 4 and 5. Unlike other particles, the state of dry ice particles, such as particle size and concentration, is fairly sensitive to the ambient temperature; hence, the effect of the jet temperature was taken into consideration in terms of the state change of dry ice jet and its corresponding particle removal efficiency of fine particles adhering to the surface.

In Chapter 2, the agglomeration process of dry ice particles flowing through a tube chamber was analyzed through an in-situ microscopic observation. Compared with the dry ice jet ejected from the expansion nozzle outlet, where dry ice particles cannot be visually observed, agglomerated dry ice particles can be clearly observed after the primary particles pass though the additional tube chamber. Two stages of temperature reduction occurred in the jet flow was found to correspond to the agglomeration process. The tube size has great influence on the particle size and shape as well as velocity of the dry ice particles. For explaining the agglomeration process, a large number of collisions of primary particles can hardly be achieved due to the limited residence time. On the other hand, primary particles of about several micrometers were observed in a dry ice deposition layer on the surface of a plate, indicating the agglomerates observed from the tube outlet were those reentrained from the deposition layer inside the tube chamber. According to the observation results, particle deposition and reentrainment, will dominate the agglomeration process of the dry ice particles.

In Chapter 3, an in-situ size measurement based on the laser diffraction method was performed to analyze the size distribution and the quantity of dry ice particles in the jet. The measurement results show that the primary dry ice particles generated by expanding liquid CO_2 is about 1 μm, and the distribution is approximately log-normal. The profiles of particle size distribution varies with the flowing distance, meaning that the primary dry ice particles still keep growing or agglomerating in the jet flow, while some of them begin to shrink due to the effect of sublimation at a far flowing distance, where a bimodal distribution can be obtained. The particle size increases to about 100 μm after a tube chamber was installed to the expansion nozzle, showing the primary particles effectively agglomerated in the tube chamber. A simple evaluation of interparticle collisions in the tubes shows that most of the primary particles cannot agglomerate due to a collision mechanism in the short residence time within the tube. The mass median diameter tends to decrease with the increase of the flow velocity, showing the separation force acting on the deposition layer increases with the flow velocity and smaller agglomerates can therefore be reentrained. This result agrees well with the dominance of the theory of particle deposition and reentrainment in the agglomeration process. In addition, the profile of particle size and quantity as a function of radial direction was obtained along with the flowing distance, providing the information for the effective work distance.

In Chapter 4, dry ice blasting, as a dry cleaning method with highly increasing interest, was applied on the removal of monosized fine particles adhering to the surface. The effect of particle impact was investigated through an in-situ microscopic observation and theoretical discussion. Micron or sub-micron fine particles, which cannot be removed by the air jet, were almost removed by the dry ice jet, indicating the effectiveness of particle removal by dry ice blasting is attributed to the collision of the dry ice particles with the contaminants. The profiles of the time course of particle removal efficiency differ in the diameter of the fine particles, and can be mainly divided into a high (−10 °C) and low (−70 °C) temperature regions by linking these results to the jet temperature profiles. The high removal rate for submicron particles in the low jet

temperature condition demonstrates the effect impact of agglomerated dry ice particles. Furthermore, a particle removal model based on the moment balance theory was applied to the dry ice blasting system and the theoretical calculation result verifies the dominance of the impact effect of dry ice particles.

Chapter 5 extended the work of dry ice blasting on the removal of monosized particles. The removal process of fine particles differing in size was studied in terms of the particle removal efficiency, jet temperature effect, particle removal area, and removal frequency. According to the two stages—slow removal stage and rapid removal stage—increase in the profiles of particle removal efficiency, two removal mechanisms can be ensured in the particle removal process and were found to relate to the variation of jet temperature. The phenomena of the slow removal stage can be explained by a theoretical equation considering the removal of fine particles whose adhesive forces are in a distribution, while the rapid removal stage deviates from the theory. The rapid removal stage, occurring as the jet temperature was about −70 °C, was caused by the effect impact of agglomerated dry ice particles. In this removal stage, the particle removal frequency of the fine particles was found to be more significant than the removal area caused by the particle impact. In addition, a system parameter considering the particle removal area, frequency, and the jet flow rate can be applied to optimize the particle removal.

The research work provides useful insights into the dynamic analysis of the production process of dry ice particles in the jet flow and the particle removal process by the impinging dry ice jet. The particle size and amount of dry ice varies with jet temperature, flow velocity and flowing distance; thus, an equipment design for generating dry ice jet, such as the expansion nozzle and the tube chamber, should be focused on the above parameters. For particle removal from surfaces, the impact caused by the flowing dry ice particle is dominant compared with aerodynamic drag. Therefore, the condition of the dry ice jet should be properly controlled. Furthermore, the dynamic analysis of the surface cleaning in dry ice blasting should be used to determine the optimum operation conditions.

When applying dry ice particles in industrial cleaning processes, the removal efficiency is influenced by the environmental conditions, such as temperature and relative humidity. Also, the wall material used in the equipment is worth investigating; the interaction between dry ice particles and the wall surface will vary with the wall material.

The reduction and recycle of CO_2 in industrial processes are becoming an imperative issue to prevent the greenhouse problems. Since dry ice jet is capable of many industrial applications where high cleanliness is required, the efficient use of dry ice jet is considered to meet the increasing needs of green house gas reduction. In particular, the development of effective CO_2 recycle system to stably provide dry ice jet is necessary.

Appendix

(A) Calculation of the Contact Angle, θ in Eq. (4.3), (4.4) and (4.5)

The contact angle of the spherical particle adhering to the surface (θ) is given by

$$\theta = \sin^{-1}\left(\frac{2a_s}{D_{p2}}\right), \tag{A1}$$

where a_s is the contact radius at separation, which is evaluated on the basis of the JKR theory as follows:

$$a_s = \left(\frac{9\pi k_{23} D_{p2}{}^2 W_{23}}{32}\right)^{1/3}, \tag{A2}$$

where W_{23} is the surface energy per unit area and k_{23} represents the elastic characteristics of two materials and is defined as

$$k_{23} = \frac{1-\nu_2^2}{E_2} + \frac{1-\nu_3^2}{E_3}, \tag{A3}$$

where ν is Poisson's ratio and E is Young's modulus. The subscripts 2 and 3 represent the adhesive particulate contaminant and the wall, respectively.

(B) Calculation of the Fluid Velocity, *u* in Eq. (4.8) and (4.10)

The friction velocity (u^*) of the impinging jet flow is approximated by

$$u^* = \frac{u_0}{20}, \tag{B1}$$

where u_0 is the core velocity of the dry ice jet [Toscano and Ahmadi, 2003].

On the basis of the law of wall, the fluid velocity at the center of the adhesive particle (u) is represented by

$$u = \frac{D_{p2}\rho u^{*2}}{2\mu}, \tag{B2}$$

where ρ is the density of fluid.

References

Adhiwidjaja, I., Matsusaka, S., Tanaka, H. and Masuda, H. Simultaneous phenomenon of particle deposition and reentrainment: effects of surface roughness on deposition layer of striped pattern, *Aerosol Sci. Technol.*, **33**, 323 (2000)

Ahmadi, G., Guo, S. G. and Zhang, X. Y. Particle adhesion and detachment in turbulent flows including capillary forces, *Particul. Sci. and Technol.*, **25**, 59 (2007)

Allen, S. D. Method and appts. for removing minute particles from surface - by interposing energy transfer medium between surface and particles and irradiating such that particles are removed by explosive evapn., U.S. Patent, 4987286-A (1991)

Arieda, Y., Iwasaki, T., Watano, S., Iwamoto, D. and Hamada, K. Particulate design of dry powder inhalation by a novel supercritical freeze granulation, *J. Soc. Powder Technol., Japan*, **43**, 434 (2006)

Asia Industrial Gases Association, *Carbon Dioxide*, AIGA 068/10, Globally Harmonised Document Based on CGA G-6, 7th edn (2009)

Banerjee, S. and Campbell, A. Principles and mechanisms of sub-micrometer particle removal by CO_2 cryogenic technique, *J. Adhesion Sci. Technol.*, **19**, 739 (2005)

Broecker R. Nozzle device for ejection of carbon dioxide particles or pellets to clean e.g. ink grease from substrate, has diverging portion with media size changer for changing particles from one size to another smaller size for ejection from nozzle, U.S. Patent, 2010170965-A1 (2010)

Busnaina, A. A. and Dai, F. Megasonic cleaning, *Semicond. Int.*, **20**, 85 (1997)

Cleavelin, C. R. Silicon dioxide removal in anhydrous HF gas, *Semicond. Int.*, **10**, 94 (1987)

Cleaver J. W. and Yates, B. Mechanism of detachment of colloidal particles from a flat substrate in a turbulent flow, *J. Coll. Interface Sci.*, **44**, 464 (1973)

Dangwal, A. and Müller, G. Effective removal of field-emitting sites from metallic surfaces by dry ice cleaning, *J. Appl. Phys.*, **102**, 044903 (2007)

Donahue, T. J. and Reif R. Silicon epitaxy at 650-800°C using low-pressure chemical

vapor deposition both with and without plasma enhancement, *J. Appl. Phys.*, **57**, 2757 (1985)

Dong, S. J., Song, B., Hansz, B., Liao, H. L. and Coddet, C. Improvement in the properties of plasma-sprayed metallic, alloy and ceramic coatings using dry-ice blasting, *App. Surf. Sci.*, **257**, 10828 (2011)

Friedlander, S. K. *Smoke, Dust, and Haze*, 2nd edn, Oxford University Press, New York, pp. 188-221 (2000)

Ghidini, G. and Smith, F. W. Interaction of H_2O with Si(111) and (100) critical condition for growth of SiO_2, *J. Electrochem. Soc.*, **131**, 2924 (1984)

Gotoh, K., Karube, K., Masuda, H. and Banba, Y. High-efficiency removal of fine particles deposited on a solid surface, *Advanced Powder Technol.*, **7**, 219 (1996)

Gotoh, K., Kida, M. and Masuda, H. Effect of particle diameter on removal of surface particles using high speed air jet, *Kagaku Kogaku Ronbunshu*, **20**, 693 (1994a)

Gotoh, K., Takebe, S. and Masuda, H. Effect of surface material on particle removal using high speed air jet, *Kagaku Kogaku Ronbunshu*, **20**, 685 (1994b)

Gotoh, K., Takebe, S., Masuda, H. and Banba, Y. The effect of humidity on the removal of fine particles on a solid surface using high-speed air-jet, *KONA Powder and Particle*, **13**, 191 (1995)

Harvill, T. L. and Holve, D. J. Particle size measurement method for ELD instrument-measuring scattering signature, assigning initial value as current value, using current value for single scattering signature and performing iterative steps until convergence criterion is met, E.P. patent, 781986-B1 (1998)

Heloux, J. B., Boughaba, S., Ressejac, I., Sacher, E. and Meunier, M. CO_2 laser-assisted particle removal of submicron particles from solid surfaces, *J. Appl. Phys.*, **79**, 2857 (1996)

Hills, M. M. Carbon dioxide jet spray cleaning of molecular contaminants, *J. Vac. Sci. Technol. A*, **13**, 30 (1995)

Hoenig, S. A. Cleaning surfaces with dry ice, *Compressed Air Magazine*, **91**, 22 (1986)

Hymes, D. J. and Malik, I. J. Using double-sided scrubbing systems for multiple general

fab applications, *MICRO*, **14**, 55 (1996)

Imen, K., Lee, S. J. and Allen, S. D. Laser-assisted micron scale particle removal, *App. Phys. Lett.*, **58**, 203 (1991)

Ishikawa, Y., Takagi, Y. and Nakamichi, I. Low-temperature thermal oxidation of silicon in N_2O by UV-irradiation, *Jpn. J. Appl. Phys.*, **28**, L1453 (1989)

Itano, M., Jr., Kern, F. W., Miyashita, M. and Ohmi, T. Particle removal from silicon wafer surface in wet cleaning process, *IEEE Trans. Semicond. Manufact.*, **6**, 258 (1993)

Itano, M., Kezuka, T., Ishii, M., Unemoto, T., Kubo, M. and Ohmi, T. Minimization of particle contamination during wet processing of Si wafers, *J. Electrochem. Soc.*, **142**, 971 (1995)

Jackson, D. and Carver, B. Today's Forecast: It Looks Like Snow, *Precision Cleaning*, **8**, 16 (1999)

Jung, J. and Perrut, M. Particle design using supercritical fluids: Literature and patent survey, *J. Supercrit. Fluids*, **20**, 179 (2001)

Kally, N. and Matijevic, E. Particle adhesion in model systema XII. The effect of the surface potential and magnetic, *Colloids Surfaces*, **39**, 161 (1989)

Kasi, S. R. and Liehr, M. Vapor phase hydrocarbon removal for Si processing, *App. Phys. Lett.*, **57**, 2095 (1990)

Kelly, J. D. and Hovis, F. E. A thermal detachment mechanism for particle removal from surfaces by pulsed laser irradiation, *Microelectron. Eng.*, **20**, 159 (1993)

Kern, W. The evolution of silicon wafer cleaning technology, *J. electrochem. Soc.*, **137**, 1887 (1990)

Kim, M. H., Pettersen, J. and Bullard, C. W. Fundamental process and system design issues in CO_2 vapor compression systems, *Prog. Energy Combust. Sci.*, **30**, 119 (2004)

Kousaka, Y., Okuyama, K. and Endo, Y. Re-entrainment of small aggregate particles from a plane surface by air stream, *J. Chem. Eng. Jpn.*, **13**, 143 (1980)

Kuo, R. J. and Matijevic, E. Particle adhesion and removal in model system, *J. Colloid*

Interface Sci., **78**, 407 (1980)

Lao, K., Wu, W., Donohue, J., Prezyna, L. and Rembetsti, J. Microwave downstream plasma removes metal etch residue, *Semicond. Int.*, **20**, 231 (1997)

Layden, L. and Wadlow, D. High velocity carbon dioxide snow for cleaning vacuum system surfaces, *J. Vac. Sci. Technol. A*, **8**, 3881 (1990)

Lee, S. J., Imen, K. and Allen, S. D. CO_2 laser-assisted particle removal threshold measurement, *App. Phys. Lett.*, **61**, 2314 (1992)

Lee, S. J., Imen, K. and Allen, S. D. Laser-assisted particle removal from silicon surfaces, *Microelectron. Eng.*, **20**, 145 (1993)

Liao, S. M. and Zhao, T. S. An experimental investigation of convection heat transfer to supercritical carbon dioxide in miniature tubes, *Int. J. Heat Mass Transfer*, **45**, 5025 (2002)

Lippert, G., Thieme, H. J. and Osten, H. J. Soft cleaning by in vacuo ultraviolet radiation combined with molecular hydrogen gas before molecular beam epitaxial layer growth, *J. Electochem. Soc.*, **142**, 191 (1995)

Lorentzen, G. and Petterson, J. A new, efficient and environmentally benign system for car air-conditioning, *Int. J. Refrigeration*, **16**, 4 (1993)

Magee, T. J. and Leung, C. S. Scanning UV laser removal of contaminants from semiconductor and optical surfaces, *in: Particles on Surfaces 3: Detection, Adhesion and Removal*, Mittal K. L. (Editor), Plenum Press, New York, pp. 307-316 (1991)

Masuda, H., Gotoh, K., Fukada, H. and Banba, Y. The removal of particles from flat surface using a high-speed air jet, *Advanced Powder Technol.*, **5**, 205 (1994)

Matson, D. W. and Smith, R. D. Supercritical fluid technologies for ceramic-processing applications, *J. Am. Ceram. Soc*., **72**, 871 (1989)

Matsusaka, S. and Masuda, H. Particle reentrainment from a fine powder layer in a turbulent air flow, *Aerosol Sci. Technol.*, **24**, 69 (1996)

Mcintosh, R., Kuan, T. S. and Defresart, E. Hydrogen fluoride vapor etching for pre-epi silicon surface preparation, *J. Electron. Mater.*, **21**, 57 (1992)

Menon, V. B., Michaels, L. D., Donovan, R. P. and Ensor, D. S. Effects of particulate

size, composition, and medium on silicon-wafer cleaning, *Sol. State Technol.*, **32**, S7 (1989)

Merritello, R. J. Target item e.g. food processing equipment, surface treating method for use in e.g. food industry, involves producing flow of solid carbon dioxide entrained in ozone from carbon dioxide source and carrier gas, W.O. patent, 2008087544-A1 (2008)

Meyerson, B. S., Ganin, E., Smith, D. A. and Nguyen, T. N. Low temperature silicon epitaxy by hot wall ultrahigh vacuum/low pressure chemical vapor deposition techniques: surface optimization, *J. Electochem. Soc.*, **133**, 1232 (1986)

Momotsuka, Y., Maekawa, M. and Tokushima, T. Cleaning organic attachment e.g. resist from electronic component, involves irradiating solid-carbon-dioxide gas microparticles and solid-carbon-dioxide gas coarse grains to electronic component at preset time interval, J.P. patent, 2005238059-A (2005)

Moslehi, M. M. and Davis, C. J. Advanced epitaxial Si and Ge_xSi_{1-x} multiprocessing for semiconductor device technologies, *J. Mater. Res.*, **5**, 1159 (1990)

Narayanswami, N. A theoretical analysis of water cleaning using a cryogenic aerosol, *J. Electrochem. Soc.*, **146**, 767 (1999)

Niida, T., Kousaka, Y. and Furukawa, T. Removal of adhering particles of polystyrene latex and iron oxide on a wall by shear flow in water, *Part. Part. Syst. Charact.*, **6**, 69 (1989)

Niu, X. D., Yamaguchi, H., Iwamoto Y. and Neksa P. Experimental study on a CO2 solid–gas-flowbased ultra-low temperature cascade refrigeration system, *Int. J. Low Carbon Technol.*, **6**, 93 (2011)

Norström, M. O., Buchta, R. and Petersson, C. S. Dry cleaning of contact holes ultraviolet(UV) generated ozone, *J. Electochem. Soc.*, **132**, 2285 (1985)

Ohmi, T. Total room temperature wet cleaning of silicon surface, *Semicond. Int.*, **19**, 323 (1996)

Okazawa, M., Iwama, H., Sato, B., Kowase, H. and Hirasawa, N. Cleaning method for electric home appliance, involves supplying air that is charged with opposite polarity

of charged dry ice pellets to cleaning portion of target to be blasted by blast nozzle, U.S. Patent, 2002082179-A1 (2002)

O'Neill, M. E. A sphere in contact with a plane wall in a slow linear shear flow, *Chem. Eng. Sci.*, **23**, 1293 (1968)

Otani, Y., Emi, H., Morizane, T. and Mori, J. Removal of fine particles from wafer surface by pulse air jets, *Kagaku Kogaku Ronbunshu*, **19**, 114 (1993)

Otani, Y., Namiki, N. and Emi, H. Removal of fine particles from smooth flat surfaces by consective pulse air jets, *Aerosol Sci. Technol.*, **23**, 665 (1995)

Phares, D. J., Smedley, G. T. and Flagan, R. C. Effect of particle size and material properties on aerodynamic resuspension from surfaces, *J. Aerosol Sci.*, **31**, 1335 (2000)

Qin, K. and Li, Y. Mechanisms of particle removal from silicon wafer surface in wet chemical cleaning process, *J. Colloid Interface Sci.*, **261**, 569 (2003)

Reeks, M. W. and Hall, D. Kinetic models for particle resuspension in turbulent flows: theory and measurement, *J. Aerosol Sci.*, **32**, 1 (2001)

Reeks, M. W., Reed, J. and Hall, D. On the resuspension of small particles by a turbulent flow, *J. Phys. D*, **21**, 574 (1988)

Rudder, R. A., Fountain, G. G. and Markunas, R. J. Remote plasma-enhanced chemical-vapor deposition of epitaxial Ge films, *J. Appl. Phys.*, **60**, 3519 (1986)

Ruzyllo, J., Duranko, G. T. and Hoff, A. M. Preoxidation UV treatment of silicon wafers, *J. Electochem. Soc.*, **134**, 2052 (1987)

Sanganeria, M. K., Violette, K. E., Ozturk, M. C. and Harris, G. Low thermal budget in situ cleaning and passivation for silicon epitaxy in a multichamber rapid thermal processing cluster tool, *Mater. Lett.*, **21**, 137 (1994)

Sherman, R. Carbon dioxide snow cleaning, *Particulate Sci. Technol.*, **25**, 37 (2007)

Sherman, R., Grob, J. and Whitlock, W. Dry surface cleaning using CO_2 snow, *J. Vac. Sci. Technol. B*, **9**, 1970 (1991)

Sherman, R., Hirt, D. and Vane, R. Surface cleaning with the carbon dioxide snow jet, *J. Vac. Sci. Technol. A*, **12**, 1876 (1994)

Sherman, R. and Whitlock, W. The removal of hydrocarbons and silicon grease stains from silicon wafers, *J. Vac. Sci. Technol. B*, **8**, 563 (1990)

Shwartzman, S., Mayer, A. and Kern, W. Megasonic particle removal from solid state wafers, *RCA Rev.*, **46**, 81 (1985)

Silvestri, V. J., Nummy, K., Bendernagel, R., Kerr, D. and Phan, V. T. ULSI quality silicon epitaxial growth at 850 °C, *J. Electochem. Soc.*, **137**, 2323 (1990)

Smedley, G. T., Phares, D. J. and Flagan, R. C. Entrainment of fine particles from surfaces by gas jets impinging at normal incidence, *Exp. Fluids*, **26**, 324 (1999a)

Smedley, G. T., Phares, D. J. and Flagan, R. C. Entrainment of fine particles from surfaces by impinging shock waves, *Exp. Fluids*, **26**, 116 (1999b)

Smedley, G. T., Phares, D. J. and Flagan, R. C. Entrainment of fine particles from surfaces by gas jets impinging at oblique incidence, *Exp. Fluids*, **30**, 135 (2001)

Sonoda, R., Hara, Y., Iwasaki, T. and Watano, S. Improvement of dissolution property of poorly water-soluble drug by supercritical freeze granulation, *Chem. Pharm. Bull.*, **57**, 1040 (2009)

Spur, G., Uhlmann, E. and Elbing, F. Dry-ice blasting for cleaning: process, optimization and application, *Wear*, **233-235**, 402 (1999)

Stratford, S. M. and Anderson, R. S. Blasting stream producing system for cleaning mold cavities, has circular orifice designed to receive and pass stream without plugging, only when ice particle diameter and flow rate of regulator are of specific values, U.S. Patent, 2003073392 A1 (2003)

Swain E. A., Carter S. R. and Hoenig S. A. Agglomerating and accelerating carbon dioxide snow against surface to be cleaned - eliminating particle contamination on surface, eliminating complex solvent recovery systems by simple process, U.S. Patent, 5125979-A (1992)

Tabe, M. UV ozone cleaning of silicon substrates in silicon molecular beam epitaxy, *Appl. Phys. Lett.*, **45**, 1073 (1984)

Tam, A. C., Leung, W. P., Zapka,W. and Ziemlich, W. Laser cleaning techniques for removal of surface particulates, *J. Appl. Phys.*, **71**, 3515 (1992)

Taniguchi, S. Washing apparatus has control cover having opening at its tip, which controls pressure, velocity and direction of liquid carbon dioxide sprayed from outlet of nozzle, J.P. patent, 2001340816-A (2001)

Theerachaisupakij, W., Matsusaka, S., Akashi, Y. and Masuda, H. Reentrainment of deposited particles by drag and aerosol collision, *J. Aerosol Sci*., **34**, 261 (2003)

Theerachaisupakij, W., Matsusaka, S., Kataoka, M. and Masuda, H. Effects of wall vibration on particle deposition and reentrainment in aerosol flow, *Advanced Powder Technol.*, **13**, 287 (2002)

Timoshenko, S. P., and Goodier, J. N. *Theory of Elasticity*, 3rd edn, McGraw-Hill, New York, pp. 409-422 (1970)

Toscano, C. and Ahmadi, G. Particle removal mechanisms in cryogenic surface cleaning, *J. Adhesion*, **79**, 175 (2003)

Tsai, C. J., Pui, D. Y. H. and Liu, B. Y. H. Particle detachment from disk surfaces of computer disk drives, *J. Aerosol Sci.*, **22**, 737 (1991)

Wang, H-C. Effects of inceptive motion on particle detachment from surfaces, *Aerosol Sci. Technol.*, **13**, 386 (1990)

Watano, S. Design of nano drug for dry powder inhalation via supercritical carbon dioxide, *Drug Delivery Syst.*, **24**, 492 (2009)

Wen, H. Y. and Kasper, G. On the kinetics of particle reentrainment from surfaces, *J. Aerosol Sci.*, **20**, 483 (1989)

Whitlock, W. H., Weltmer, W. R. and Clark, J. D. Device for removing minute particles from substrate - involves expanding and coalescing carbon dioxide across orifices and chambers to produce stream of mixed gaseous and solid particles, U.S. Patent, 4806171-A (1989)

Wong, M., Moslehi, M. M. and Reed, D. W. Characterization of wafer cleaning and oxide etching using vapor-phase hydrogen fluoride, *J. Electrochem Soc.*, **138**, 1799 (1991)

Yamaguchi, H., Niu, X. D., Sekimoto, K. and Neksa P. Investigation of dry ice blockage in an ultra-low temperature cascade refrigeration system using CO2 as a working

fluid, *Int. J. Refrigeration*, **34**, 466 (2011)

Yamaguchi, H., Zhang, X. R. and Fujima, K. Basic study on new cryogenic refrigeration using CO_2 solid–gas two phase flow, *Int. J. Refrigeration*, **31**, 404 (2008)

Yamaguchi, H. and Zhang, X. R. A novel CO_2 refrigeration system achieved by CO_2 solid–gas two-phase fluid and its basic study on system performance, *Int. J. Refrigeration*, **32**, 1683 (2009)

Yamamoto, T., Periasamy R., Donovan, R. P. and Ensor, D. S. Flow cell for real time observation of single particle adhesion and detachment, *J. Adhesion Sci. Technol.*, **8**, 543 (1994)

Yang, S. C., Huang, K. S. and Lin, Y. C. Optimization of a pulsed carbon dioxide snow jet for cleaning CMOS image sensors by using the Taguchi method, *Sens. and Actua. A*, **139**, 265 (2007)

Yoon, C. N., Kim, H., Kim, S. G. and Min, B. H. Removal of surface contaminants by cryogenic aerosol jets, *Korean J. Chem. Eng.*, **16**, 96 (1999)

Zhang, X. R. and Yamaguchi, H. Forced convection heat transfer of supercritical CO_2 in a horizontal circular tube, *J. Supercrit. Fluids*, **41**, 412 (2007)

Zhang, X. R. and Yamaguchi, H. An experimental study on heat transfer of CO_2 solid–gas two phase flow with dry ice sublimation, *Int. J. Thermal Sci.*, **50**, 2228 (2011)

Zhou, Z. H., Aydil, E. S., Gottscho, R. A., Chabal, Y. J. and Reif, R. Real-time, in situ monitor of room-temperature silicon surface cleaning using hydrogen and ammonia plasma, *J. Electrochem. Soc.*, **140**, 3316 (1993)

Acknowledgements

This thesis is a summary of my work conducted at the Laboratory of Particle Technology, Department of Chemical Engineering, Kyoto University, from 2008 to 2012.

I am greatly indebted to Dr. Shuji Matsusaka, Professor of the Department of Chemical Engineering, Kyoto University, for his excellent and persistent supervision together with constant support throughout this work. Undoubtedly, the work could not be completed smoothly without his constructive suggestion and valuable comments. Under his instruction, I have learned the knowledge and skills of being a researcher from conducting a research project, implementing experiments and writing scientific papers. Therefore, again, I would like to express my sincere appreciation to Prof. Matsusaka.

It is my great pleasure and honor to have two supervisors of this thesis, Dr. Minoru Miyahara and Dr. Masahiro Ohshima, Professors of the Department of Chemical Engineering, Kyoto University. I would like to express my deep gratitude for their critical and careful proofreading of my original manuscript. The valuable remarks and important corrections given by the professors guided me to substantially improve this thesis.

I would like to express my sincere appreciation to Mr. Hiroyuki Maruyama, Assistant Professor at the Department of Chemical Engineering, Kyoto University, for helping to create new idea of research topics and to solve the problems in experiments. Through the friendly discussion with him, I have obtained much significant advice of this work. I would also like to show my great gratitude to Mr. Masatoshi Yasuda, Technical Expert at the Department of Chemical Engineering, Kyoto University, for his constant technical support and kindly instructions on the operation of the experimental devices.

It is a great honor for me to have research collaboration with the research group of Dr. Mojtaba Ghadiri, Professor at Institute of Particle Science and Engineering,

University of Leeds, UK. I am heartily thankful to Prof. Ghadiri for his great support on providing the experimental apparatus and giving the critical suggestions of the research work in Chapter 3. I would also like to show my honest appreciation to the collaborating members, Dr. Colin Hare and Dr. Graham Calvert, for the great help on the experimental setup and the fruitful discussion.

I wish to give many thanks to Mr. Susumu Hayakari for providing the technical support on data analysis in Chapter 2 and the co-working student, Mr. Daisuke Hirama, for his productive efforts and contributions in Chapter 5. I always appreciate the kindness and help given by all the members of the Prof. Matsusaka's laboratory. Because of their mental and physical support, the life in Japan becomes more colorful and brilliant since my first year as a research student. I am very thankful to Ms. Harumi Yoshimoto, Secretary of the laboratory, for her kindly help on the secretarial work.

It is my great fortune to have several nice friends who always give me happiness and encouragement. I will always treasure and memorize the time being with them.

I would like to thank the Interchange Association, Japan, for providing me the financial support during my education in Kyoto University. Obviously, I cannot certainly concentrate on the research without the warm fellowship.

Finally, I would like to express my deepest appreciation to my respective and beloved grant father, grant mother, father, mother, brothers, sisters and, of course, my wife, for their understanding and affectionate support. I will never forget the love they give me.

List of Publications

Original research papers in journal:

Chapter 2

Liu, Y.-H., H. Maruyama and S. Matsusaka; Agglomeration process of dry ice particles produced by expanding liquid carbon dioxide, Advanced Powder Technology, 21, 652-657 (2010)

Chapter 3

Liu, Y.-H., G. Calvert, C. Hare, M. Ghadiri and S. Matsusaka; Size measurement of dry ice particles produced from liquid carbon dioxide, Journal of Aerosol Science, 48, 1-9 (2012)

Chapter 4

Liu, Y.-H., H. Maruyama and S. Matsusaka; Effect of particle impact on surface cleaning using dry ice jet, Aerosol Science and Technology, 45, 1519-1527 (2011)

Chapter 5

Liu, Y.-H., D. Hirama and S. Matsusaka; Particle removal process during application of impinging dry ice jet, Powder Technology, 217, 607-613 (2012)

Related research paper:

Imran Zainuddin, M., M. Yasuda, Y.-H. Liu, H. Maruyama and S. Matsusaka; Development of vibration shear tube method for powder flowability evaluation, Powder Technology, 217, 548-553 (2012)

International conferences:

(1) Liu, Y.-H., H. Maruyama and S. Matsusaka; Formation of agglomerated dry ice particles, Proceedings of APT2009, New Delhi, India, 42 in CD, September (2009)

(2) Liu, Y.-H., H. Maruyama and S. Matsusaka; Surface cleaning by collision of agglomerated dry ice particles, Proceedings of The 13th Asia Pacific Confederation of Chemical Engineering Congress, APCChE 2010, Taipei, Taiwan, in CD, October (2010)

(3) Liu, Y.-H., G. Calvert, C. Hare, M. Ghadiri and S. Matsusaka; Size measurement of dry ice particles in a jet flow using laser diffraction method, Abstracts of European aerosol Conference, Manchester, UK, 250 in MS, September (2011)

(4) Liu, Y.-H. and S. Matsusaka; Characteristics of dry ice particles produced by expanding liquid carbon dioxide and its application for surface cleaning, Proceedings of the 9th International Conference on Measurement and Control of Granular Materials, Shanghai, China, in CD, October (2011)